Order Number 9218248

Nuclear magnetic resonance studies of water in polyimide films

Li, Shizhe, Ph.D.

City University of New York, 1992

U·M·I
300 N. Zeeb Rd.
Ann Arbor, MI 48106

NUCLEAR MAGNETIC RESONANCE STUDIES OF WATER IN POLYIMIDE FILMS

by

Shizhe Li

A dissertation submitted to the Graduate Faculty in Physics in partial fulfillment of the requirements for the degree of Doctor of Philosophy, The City University of New York.

1992

This manuscript has been read and accepted for the Graduate Faculty in Physics in satisfaction of the dissertation requirement for the degree of Doctor Philosophy.

1/28/92
Date

Professor Steve G. Greenbaum
Chair of Examining Committee

1/28/92
Date

Professor Joseph Krieger
Executive Officer

Professor Arthur Nowick

Professor Robert Marino

Professor Frank Owens

Professor Miriam Rafailovich

Supervisory Committee

The City University of New York

Abstract

NUCLEAR MAGNETIC RESONANCE STUDIES

OF WATER IN POLYIMIDES

by

Shizhe Li

Advisor: Professor Steve G. Greenbaum

Polyimide films containing water (H_2O, D_2O and $H_2{}^{17}O$), methanol and acetic acid have been studied by dielectric relaxation (DR) and nuclear magnetic resonance (NMR) spectroscopies. Two types polyimides, Kapton (PMDA-ODA) and Upilex-S (BPDA-PDA) are investigated.

The morphology of dry polyimide films has been investigated by X-ray and proton NMR. The polymer backbones of thin Kapton films are slightly more rigid and more oriented than those of thick films. However compared to Upilex films, the polymer structure of Kapton is much more flexible.

Both DR and NMR measurements of Kapton show that water exists in two configurations called γ_1 and γ_2. The γ_1 water corresponds to the high temperature DR loss peak and broad NMR lineshape component, the γ_2 water corresponds to the low temperature DR peak and narrow NMR lineshape component. The γ_1 water molecules are distributed uniformly throughout the volume of the film and bound to the host polymer through hydrogen bonds. The γ_2 configuration corresponds to small

clusters of water molecules where one or more water molecules are linked to the γ_1 water molecules and form a chain-like structure through weak hydrogen bonds. Therefore, the water molecules in γ_2 clusters are more mobile than the γ_1 bound water molecules. The greater degree of anisotropic configuration and molecular motion of γ_2 water molecules lead to a strong orientation effect while the γ_1 water display only a weak orientation effect.

The DR spectra of methanol and acetic acid consist primarily of one loss peak, methanol peak is at low temperature while acetic acid peak is at high temperature. Both CH_3OD and CH_3COOD exhibit a stronger orientation effect compared to D_2O water. It was found that the O-D bond directions of D_2O, CH_3OD and CH_3COOD are averaged by molecular motion about an axis perpendicular to the film plane.

The measurements of water absorbed in Upilex films are also reported.

ACKNOWLEDGEMENTS

I am indebted to Professor Steve Greenbaum, my advisor, who provided me with a broad background and excellent knowledge of current research. His special guidance, patience and encouragement throughout the course of this research are gratefully acknowledged.

I would like to specially thank Professor Arthur Nowick for his guidance throughout this research, DR measurements carried out in his laboratory and valuable discussions.

I am very grateful to Mr. Richard Krumm for his technical assistance in designing and building two NMR probes.

Professor Robert Marino is gratefully thanked for his knowledge, guidance, and helpful discussion, especially his supervision during Professor Greenbaum's sabbatical leave. I am grateful to Dr. Kresimir Adamic for his helpful advisement and discussions.

I wish to thank Professor Frank Owens and Professor Miriam Rafailovich for their friendly participation in the examination committee and reading this manuscript.

I would like to express my gratitude to Dr. Yiusun Pak for his knowledge and great help in NMR techniques, as well as to Mr Rensheng Chen and Mr. Jayakody Jayakody for their help in experiments.

The financial support from IBM Corporation and PSC-CUNY Research Award Program is gratfully acknowledged.

Table of Contents

Chapter 1. Introduction 1

1-1. Polyimides 1

1-2. Microstructure and morphology of polyimides 3

1-3. Water diffusion and permeation in polyimides 7

1-4. Dielectric relaxation of polyimides 9

1-5. Nuclear magnetic resonance 11

1-6. NMR studies of water in polymer 13

Chapter 2. Theoretical Background of NMR 18

2-1. NMR phenomenon 18

2-2. Detection of the resonance phenomenon 22

2-3. Interactions in NMR 25

2-3.1. Dipolar interaction 26

2-3.2. Quadrupolar interaction 30

2-4. Orientation effect 35

2-5. Relaxation 38

2-5.1. Spin-lattice relaxation 42

2-5.2. Spin-spin relaxation 42

Chapter 3. Experiment 45

3-1. Sample preparation 45

3-2. X-ray diffraction photograph 50

3-3. Dielectric relaxation 50

3-4. NMR experiment 52

3-5. NMR pulse sequences 54

Chapter 4. X-ray and DR Results 57

4-1. X-ray diffraction photograph 57

4-2. Dielectric relaxation 62

4-2.1. Thickness effect 62

4-2.2. Relative humidity effect 63

4-2.3. Solvent effect 64

4-2.4. Backbone structure effect 65

Chapter 5. NMR Results 76

5-1. Summary of the NMR parameters of Solvents 76

5-2. Proton NMR 78

5-2.1. Spectra of dry films 79

5-2.2. Spectra of wet films 84

5-2.3. Spin-lattice relaxation time 85

5-3. D_2O in Kapton films 94

5-3.1. Rolled Kapton films 94

5-3.2. Orientation effect of Kapton films 98

5-3.3. Variable temperature measurements 105

5-4. CH_3OD and CH_3COOD in Kapton films 109

5-5. D_2O in Upilex films 117

5-6. $H_2{}^{17}O$ in Kapton films 118

Chapter 6. Discussion and Conclusions 125

6-1. Speculations on the status of water 126

6-2. A microscopic model for solvents in Kapton films 127

6-3. DR results in terms of proposed Model 131

6-3.1. Temperature effect 131

6-3.2. Water concentration 132

6-3.3. Film thickness 132

6-3.4. Other solutes 133

6-3.5. Dipole moment of water molecules 135

6-4. Proton NMR 135

6-4.1. Morphology difference of dry polyimide films 135

6-4.2. Mobility of water molecules in polyimide films 136

6-4.3. Motion of the polyimide macromolecules 136

6-4.4. Proton dipole-dipole interaction of water 137

6-5. Deuterium NMR of Kapton films 138

6-5.1. Correlation of ^2H NMR results and DR results 138

6-5.2. Orientation effects of Kapton films 140

6-5.3. Variable temperature measurements 142

6-5.4. CH_3OD and CH_3COOD in Kapton films 143

6-6. Oxygen-17 NMR 144

6-7. Deuterium NMR of Upilex films 145

6-8. Conclusions 147

Appendix 150

References 162

List of Tables

1.1 The comparison of polyimides and inorganic dielectrics 2

2.1 The spins of the nuclei investigated in the project 18

3.1 The designation of the samples used in the measurements 46

3.2 The solutions for maintaining constant relative humidity at 25 °C 48

3.3 Water content in polyimides at various relative humidities at 25 °C 49

3.4 Physical properties of the solvents used in the measurements 46

4.1 Values of d-spacing for Kapton-H and Upilex-S films 60

4.2 Dielectric relaxation peaks (1 kHz) for water saturated Kapton films 63

4.3 Dielectric relaxation peaks (1 kHz) of spin-coated film as a function of relative humidity. 64

5.1 Room temperature T_1 of the solvents utilized in the investigation 76

5.2 Quadrupole coupling constant (QCC) of D_2O, CH_3OD and $H_2{}^{17}O$ 77

5.3 The apparent linewidth of dry polyimide films 80

5.4 T_1 values of protons for dry and wet (D_2O) polyimide films 86

5.5 Linewidth and T_1 of D_2O in rolled Kapton films at various D_2O content 94

5.6 The linewidth (at 30 °C) and splitting (at 90 °C) for Kapton films 111

List of Figures

1.1 Molecular structure of three types of polyimides 4

2.1 Zeeman energy levels for spin-1/2 and spin-1 nucleus 20

2.2 Magnetization **M** in a static magnetic field 21

2.3 Effect of the rf pulse on magnetization 23

2.4 Fourier transform of f(t) in three different modes 23

2.5 Formation of the dipolar interaction of two spins 26

2.6 Effect of the dipolar interaction on Zeeman energy of two spins (I=1/2) 29

2.7 Effect of dipolar interactions for a three spin-1/2 system 29

2.8 The orientation of the principal-axis frame of EFG (x,y,z) relative to the laboratory frame (X,Y,Z) 32

2.9 Effect of the quadrupole interaction for spin-1 nucleus 33

2.10 Plot of the function $A|3\cos^2\theta-1|$ vs. θ for A=1 36

2.11 Powder pattern lineshape from two spin-1/2 interacting via the dipole-dipole coupling (ref. 65). 37

2.12 Rotating frame diagrams describing for relaxations 40

2.13 T_1 and T_2 as a function of correlation time (θ) and (1/T) 44

3.1 The schematic diagram of X-ray diffraction photograph 50

3.2 Sample mount chamber for the dielectric relaxation measurement 51

3.3 The block diagram of Novex NMR spectrometer 53

3.4 The circuit diagram of L-C network 54

3.5 The illustration of the inversion-recovery method for T_1 measurements 55

3.6 Free induction decay recorded after 90° pulse at different θ in the inversion-recovery method. 56

4.1 The X-ray photographs of Kapton films 58

4.2 The X-ray photographs of Upilex-S films 59

4.3 A zigzag conformation of polyimide PMDA-ODA 61

4.4 DR spectra of spin-coated 15 μm PMDA-ODA film saturated at 100% RH 67

4.5 DR spectra of the saturated Kapton films with different thicknesses 68

4.6 DR spectra of spin-coated 15 μm PMDA-ODA at various humidities 69

4.7 DR spectra of 50 μm Kapton film saturated with methanol 70

4.8 DR spectra of 50 μm Kapton film saturated with acetic acid 71

4.9 DR spectra of 50 μm Upilex-S film saturated in 100% RH 72

4.10 DR spectra of Upilex-S film with various thicknesses 73

4.11 DR spectra of 50 μm Upilex-R film saturated at 100% RH 74

4.12 The comparison of DR spectra for three types polyimides 75

5.1 Two configurations of the sample installation 79

5.2 Proton NMR spectra of stacked dry Kapton films 82

5.3 Proton NMR spectra of stacked dry Upilex-S films 83

5.4 Proton NMR spectra of 125 μm Kapton with various water content 88

5.5 Proton NMR spectra of 125 μm Upilex-S with various water content 89

5.6 Variable temperature NMR spectra of H_2O in 125 μm Kapton film 90

5.7 Arrhenius plot of proton NMR of H_2O 91

5.8 Proton NMR spectra of H_2O in 125 μm Kapton at Ω=30°, 90° 92

5.9 Proton T_1 of two dry polyimides as a function of temperature 93

5.10 ^2H NMR spectra of D_2O in rolled Kapton films (125 μm and 7.5 μm) 97

5.11 ^2H NMR spectra of D_2O-saturated 125 μm Kapton at several angles 100

5.12 Computer simulation of the NMR spectra of 125 μm Kapton film 101

5.13 The angular dependence of the deuteron quadrupole splittings 102

5.14 ^2H NMR spectra of 125 μm Kapton with 1.3 wt% D_2O at several angles 103

5.15 ^2H NMR spectra of 7.5 μm Kapton with 2.4 wt% D_2O at several angles 104

5.16 Arrhenius plot of deuteron T_1 in 125 μm Kapton with 3.1 wt% D_2O 106

5.17 Variable temperature ^2H NMR spectra of rolled 125 μm Kapton 107

5.18 Variable temperature ^2H NMR spectra of stacked 125 μm Kapton 108

5.19 ^2H NMR spectra of 125 μm Kapton 6.8 wt% CH_3OD
at several orientations 112

5.20 Variable temperature ^2H NMR spectra of stacked 125 μm Kapton
with 7.5 wt% CH_3OD 113

5.21 ^2H NMR spectra of 7.5 μm Kapton with 7.3 wt% CH_3OD
at several angles 114

5.22 ^2H NMR spectra of 125 and 25 μm Kapton films containing CH_3COOD 115

5.23 ^2H NMR spectra of 7.5 μm Kapton with CH_3COOD 116

5.24 ^2H NMR spectra of 125 μm Upilex-S at several angles 120

5.25 ^2H NMR spectra of 125 and 75 μm Upilex-S with different D_2O content 121

5.26 ^2H NMR spectra of 50 and 25 μm Upilex-S with different D_2O content 122

5.27 A comparison of ^2H NMR spectra for three types of polyimides 123

5.28 Oxygen-17 NMR spectra of 125 and 7.5 μm Kapton films 124

6.1 The illustration of two configurations of water molecules

in Kapton film 128

6.2 The illustration of anisotropic orientation of water molecules due to molecular rotation 130

6.3 A comparison of the orientation of average H-H axis of H_2O and average O-D bond of D_2O 141

Chapter 1. Introduction

1-1. Polyimides

Polyimide (PI) are polymers containing cyclic imide groups in the main macromolecular chain.

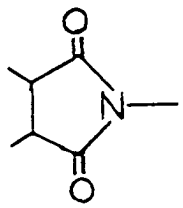

The first synthesis of polyimides was performed as early as the beginning of the 20th century. However, polyimides have been extensively prepared, studied, and utilized only for the last 30 years after DuPont Company established a two-step method for their synthesis. Now DuPont manufactures one very popular kind of polyimide film under the trade name of Kapton.

Polyimides are high-temperature polymers that possess a unique combination of chemical, electrical, and physical properties. They have a high thermal decomposition temperature (up to 500 °C), a high glass transition temperature (>400 °C), high mechanical strength, and a low dielectric constant and dissipation factor. They also have excellent planarization and patterning properties. When fully cured, polyimide are resistent to chemical and physical attack by most acids, common organic solvents, and weak bases. The physical properties of a conventional polyimide are compared to silicon dioxide and silicon nitride in Table 1.1 [1].

Table 1.1 Comparison of Properties Between Polyimide and Inorganic Dielectrics

	Polyimide	SiO_2	Si_3N_4
Process Temperature, °C	300-350	350-400[a]	700-900[a]
Decomposition temperature, °C	450	1710[b]	1900[b]
Dielectric strength, MV/cm	3-7	5-8	5-10
Volume resistivity, ohm-cm	10^{15}-10^{16}	$>10^{16}$	10^{14}-10^{16}
Dielectric constant	3.2-3.8	3.5-4.0	7-10
Expansion coefficient 10^{-6}/°C	20-70	0.3-0.5	4
Thermal conductivity, W/cm-°C	0.0017	0.021	0.12
Density, g/cm^3	1.42	2.2	2.8-3.1
planarization, %	60-100	0	0
Refractive index	1.6-1.8	1.45	2.0
Dissipation factor	0.01-0.02	0.001	-

[a] Deposition temperature

[b] Melting point

Because of their excellent properties, polyimides have been extensively utilized in the manufacture of microelectronics: 1) as fabrication acids; 2) as passivants and interlevel insulators; 3) as adhesives; and 4) as components of the substrate or circuit board [2-4].

Although polyimides have so many advantages in their application, their

reliability is still a broad subject of great interest to many investigators. One specific problem under investigation is the moisture absorption/permeation of polyimides. Moisture absorption in polyimide films raises questions in regard to reliability since absorbed water may cause metal corrosion of devices, change of dielectric properties and decreased electrical resistivity due to motion of impurity ions. Therefore, the studies of moisture absorption of polyimide has become a important investigation for both synthesis and application of polyimides.

1-2. Microstructure and Morphology of Polyimides

Depending on the structure of the radicals attached to the imide group, polyimides can be aliphatic, alicyclic, aromatic; linear or three dimensional. We consider mainly aromatic linear polyimides in the work since they have found wide practical application and are commercially available.

Polyimides are normally prepared in two steps [4,5]. In the first step, an aromatic dianhydride is reacted with an aromatic diamine in N-methylpyrolidinine (NMP) to form an intermediate polyamic acid. Next, the polyamic acid is converted to a polyimide via either chemical treatment or thermal dehydration at high temperature.

The most frequently used kind of polyimides is polypyromellitic dianhydride-oxydianaline (PMDA-ODA), and its commercial analogue, Kapton from Du Pont company. Its molecular structure is shown schematically in Figure 1.1a. The length of a polymer repeat unit is 18.15 Å [6].

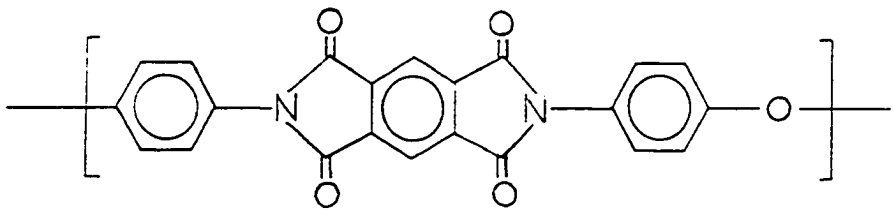

(a) Kapton-H
Poly(pyromellitic dianhydride oxydianaline) PMDA-ODA

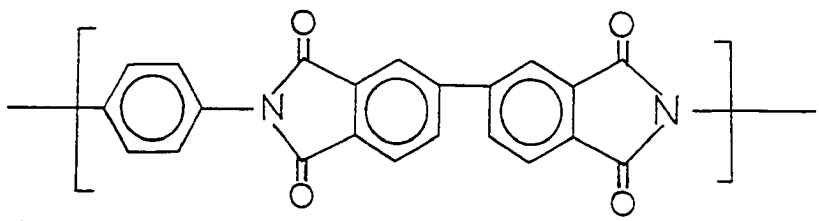

(b) Upilex-S
Poly(biphenyl dianhydride p-phenyl diamine) BPDA-PDA

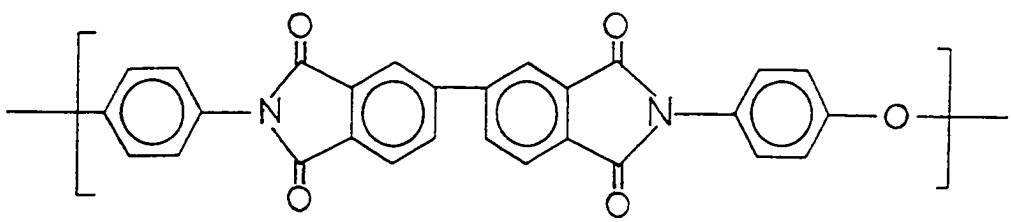

(c) Upilex-R
Poly(biphenyl dianhydride oxydianaline) BPDA-ODA

Figure 1.1 Molecular structure of (a) PMDA-ODA, (b) BPDA-PDA and (c) BPDA-ODA

A new type of polyimide (BPDA-PDA), as shown in Figure 1.1b, is derived from biphenyl tetracarboxylic dianhydride-p-phenylene diamine. Figure 1.1c exhibits the chemical structure of another BPDA-based polyimide - BPDA-ODA. All three of these polyimides are investigated in this project. The mass of the polymer repeat unit for each kind of polyimide (in the unit of atomic mass) is 382 for Kapton, 306 for Upilex-S, and 444 for Upilex-R. The weight-average molecular weight is about 30,000-40,000 [79].

Understanding the morphology of PI films is very important for the investigations of water in the films. Extensive works have been reported on morphology studies, mainly by means of X-ray diffraction technique. However, since morphology of films is highly dependent on the chemical structure of the precursor, film thickness and curing procedure (e.g. curing temperature, free-standing or casted on substrate, etc.), the reported results vary widely. We will, therefore, limit our concern mainly to the morphology of PMDA-ODA or Kapton films.

Some earlier authors reported the crystalline structure of aromatic polyimide fibers and films [7,8]. Kazaryan [7] *et al.* obtained their data by X-ray diffraction studies on PMDA-ODA and indicated that crystallites of orthorhombic symmetry are formed. The chain conformation is that of a planar zig-zag structure with the repeat unit consisting of two monomeric segments bent at alternating ether linkages. Conte *et al.* obtained similar crystal lattice parameters [6]. Gardner described the results of X-ray studies of Kapton films as a function of film thickness: systematic variations of crystallinity(with thickness) exist in commercial films [9]. All Kapton films were semicrystalline; 7.5 μm and 12.5 μm films showed a low degree of crystallinity while

thicker films showed a progressive increase in crystallinity with thickness.

More recent literature on the structure of polyimide has indicated that molecular aggregation of polyimide results in an amorphous configuration [10-14]. DeIasi *et al.* [15] concluded that Kapton film was completely amorphous. However, Isoda *et al.* [10] showed that their SAXS results cannot be interpreted by the amorphous structure model. They proposed a heterogeneous two-phase structure for molecular structure in Kapton films. Kochi *et al.* also concluded a two-phase structure in Kapton [12, 16] that corresponds to ordered and less ordered (or amorphous) phases. The ordered phase was considered to be different from the ordinary crystalline state and intermediate between crystalline and amorphous. It was indicated that Kapton films are basically in an amorphous state with no more than 10% crystallinity [17,18]. Takahashi *et al.* [11] described the structure of PMDA-ODA films in the bulk in terms of a "smetic" ordering. In this model there is a lateral alignment of chain segments where the positions of the phenyl ether linkages are correlated. Russell also cited a smetic-like ordering in his later publications [13].

The X-ray diffraction photographs reported by several authors are quite consistent [10-13,19]. There are basically two diffractional rings for Kapton films: a small ring associated with a d-spacing of ca. 16 Å is attributed to the repeat unit of monomer (18 Å), and a large radius ring corresponding to a d-spacing of 5 Å is attributed to the interchain separation.

Although PMDA-ODA can be prepared in an isotropic form [19], conventionally prepared cast films of PMDA-ODA, including Kapton films, are not isotropic. The X-ray diffraction photographs display an isotropic diffraction ring when

the incident X-ray beam is normal to the film plan; however, the diffraction pattern is anisotropic when the X-ray beam passes through the film edge, parallel to the film plane [10-14]. The conclusion drawn from above experiments is that the polymer chains have an isotropic alignment in the plane of film, but are not isotropically distributed along the normal direction of the film. This in-plane orientation can also be observed by means of integrated optics [14]. This in-plane anisotropy occurs primarily for the thermal-cast imidized polyimide film and Kapton [13,14], and may originate from a reduction in the film thickness upon thermal imidization while the lateral dimensions of the film remain constant [20].

Using SAXS techniques Russell reported the existence of microvoids in PMDA-ODA films [20]. The size of voids varies from a radius of 50 Å to 100 Å. Kapton film was described in terms of a single voids of average size ca. 20 Å [21]. Residual NMP, water formed during the cycloimidization reactions, and carbon dioxide produced via isoimide decomposition are evolved as the temperature is increased. All of these tend to promote microvoid formation. The presence of these microvoids would be in keeping with the known ability of PI to absorb ca. 3 by wt % of water.

1-3. Water Diffusion and Permeation on Polyimides

There have been several investigations of water permeation and diffusion in polyimides. Hubbell *et al.* [22] measured the permeation of water through Kapton-H of 125 μm thickness over a range of 20-55 °C. There was a nonlinear absorption relationship as relative humidity increased above about 60%. This nonlinearity for

Kapton H is attributed to the dependence of the diffusion coefficient on the relative humidity since the material obeys Henry's law as they reported. Sacher and Susko [23,24] investigated the water permeation of Kapton with varing film thickness. The concentration of absorbed water was found to depend on the relative humidity and not on the temperature or sample thickness. The water concentration reaches a ratio of one water molecule per two repeat units. As indicated earlier the interchain distance is about 5 Å while the diameter of the water molecule is about 2.8 Å, thus interchain hydrogen bonding can be precluded and the water must be hydrogen bonded to only one of the chains. However, it is possible that the water molecules hop from point to point and from chain to chain. Further, by analyzing the chemical structure of PMDA-ODA molecule, Sacher and Susko suggested that the water molecule is only associated with the ether linkage, not with carbonyls and imide nitrogens.

Solubility of water in PMDA-ODA and BPDA-PDA films as been investigated by Moylan *et al.* [79]. It was shown that water solubility in these polymers is controlled by chain morphology rather than by differences in chemical affinity. The differences in chemical structure between the polyimides apparently influence the rate of water sorption more than they influence the amount of water sorption.

It was claimed by Denton *et al.* [25] that the absorbed moisture in thin polyimide films (< 7 μm) has a dipole moment nearly equal to that of a free water molecule; inferring that the voids and free volume dominate the absorption phenomena. Their argument is against significant hydrogen bonding, suggested by Sacher *et al* [23].

Yang *et al.* compared the water sorption and diffusion behavior in 50 μm and 7.5 μm Kapton film [26,27]. They found a decrease of diffusion coefficients in both films at higher water concentrations and related this decrease to a formation of water molecular clusters. From the similarity of the water vapor sorption isotherms for two films they suggested that the inherent chemical properties of the two different thickness films are similar. However, the diffusion coefficients for the 50 μm are roughly three times larger than in the 7.5 μm. This difference was explained by the differences in the morphology of the two films rather than from different chemical interaction of penetrants with specific groups in the polymer. This large effect is believed to be related to the presence of small paracrystalline aggregates with large aspect ratios. Iler *et al.* [28] showed the existence of weak physical (hydrogen bonding) and weak chemical interactions between water molecules and PI polymer.

It is generally agreed that moisture uptaken in Kapton is nearly proportional to relatively humidity up to 100 °C, and is a reversible process, e.g. Kapton films will return to their original physical and chemical properties after the moisture is desorbed. Maximum water weight uptaken at 100 % R.H. is in the range of 2-4 % by weight depending on samples.

1-4. Dielectric Relaxation of Polyimides

The mechanism of dielectric relaxation processes in polymers can be summarized by two types of relaxation: dipole-segmental and dipole groups. The dielectric losses due to motion of segments in a polymeric chain are called dipolar segmental losses. The relaxations caused by the localized movement of molecules are

known as dipolar group relaxations. These processes give maxima dielectric loss peaks in the temperature or frequency dependences of ϵ'' and $\tan\delta$, which are the imaginary components of the complex dielectric constant ϵ^* and the dielectric loss tangent, respectively. Usually the dielectric loss peaks in the $\epsilon''=f(T)$ or $\tan\delta=f(T)$ graphs are designated by the Greek letters α, β, and γ etc. The α loss peak corresponds to the relaxation observed at the highest temperature (at a given frequency) or the lowest frequency (at a given temperature). The β and γ symbols then apply to the other relaxation regions in order of decreasing temperature or increasing frequency [29,30]. For polymers in the amorphous state it has been widely accepted that α relaxation results from large-scaled conformational rearrangements of the polymer chain segments (referred as dipole-segmental relaxation previously). In addition to the large-scale relaxation, the amorphous polymer usually exhibit at least one secondary process - the β relaxation. In this state the main chains are effectively 'frozen' so that the relaxations is attributed to the rotation of side-groups contained in the main chains. Both of these are intrinsic properties of the polymer. In contrast, a peak observed near 200 K or below and called γ peak is often found to be due to water or other impurities in the polymer [31]. It is this latter γ-region that we will investigate here.

Since polyimide is a high temperature polymer, some earlier studies emphasized the high temperature dielectric losses in dry Kapton films. The dielectric properties has been reported by Amborski in the temperature range from -60 to 220 °C [32]. Wrasidlo investigated Kapton film (100 μm) in the temperature range from 25 to 500 °C [33,34]. Three dielectric loss regions have been observed. It is believed

that these peaks are associated with intrinsic properties of PI film.

In contrast with high temperature measurements, Sacher measured dielectric properties of Kapton film (125 μm) in the temperature range from -200 to 500 °C with also three loss peaks observed [18]. One of these peaks was found to be water-sensitive, increasing in magnitude with increasing water content.

Yang *et al.* [35] investigated dielectric properties of Kapton in the frequency range from 100 Hz to 100 kHz and in a temperature range from -200 to 25 °C and observed two loss peaks. The heights of the two peaks increased with increasing water content. The same authors [36] later confirmed that the two loss peaks show a pronounced influence of absorbed water on this part of relaxation spectrum. They proposed two different water sites in the polyimide chain where the water could be attached through hydrogen bonding. At the same time G.Xu *et al.* [37] also showed the double loss peak due to water and suggested the existence of two different water sites.

It should be noted here that the relationship between the two dielectric loss peaks and absorbed water content and other factors such as film thickness, will provide crucial input to the interpretation of the NMR data of water in PI films.

1-5. Nuclear Magnetic Resonance

Since the nuclear magnetic resonance (NMR) phenomenon was discovered in 1946 [38,39], it has been extensively studied and utilized as a powerful tool in many different areas.

The NMR methods has been used to study chemical structure because the

NMR chemical shift is sensitive to the detailed electronic environment of the nucleus being observed. NMR can also be used to detect the existence of distinct domains and measure domain sizes in heterogeneous system.

One of the major advantage of NMR is the sensitivity to various types of polymer motions. NMR interactions can be modulated or averaged by molecular motions, greatly affecting the NMR spectrum and NMR associated relaxation times T_1, T_2.

Since some of the NMR characteristics are angular dependent, NMR is widely applied to probe the anisotropy of materials, especially in the solid samples such as singlecrystals, fibers or films.

The NMR facility used in this project is a broadline solid state NMR spectrometer. But in all the data presented here instrumental broadening was not significant. Thus, our attention has been mainly focused on molecular motion and anisotropic properties of our samples, reflected by NMR line shape and relaxation times.

Both polyimide films and water contain hydrogen atoms. As a result of this, proton NMR will detect the mixed proton signal from water and from the polymer matrix. This mixture could result in difficulties in assigning the spectra to water molecules. The simplest technique to acquire NMR signals from water only is to treat polymer films by heavy water (D_2O). This, of course, assumes negligible H-D exchange between the water and the host polymer. Thus, deuterium NMR is major part of this investigation with complementary measurement of proton NMR.

The deuterium NMR experiment and its applications have been

comprehensively reviewed by Smith [40], Spiess [41], and Jelinski [42] and the references therein. Most of their works involve studies of deuterated polymer with the deuterons existing as C-D bonds in polymer chain. Therefore, deuterium NMR for D_2O in polymer and its orientation effects will be a subject discussed in the next section. In addition, proton NMR for unenriched water in polymers will be reviewed.

1-6. NMR Studies of Water in Polymers

To our knowledge there has been no paper published with regard to NMR studies of water in polyimide except for work originating in this thesis [37,80]. However, many NMR investigations have been done on water in oriented polymeric materials such as collagen fibers and cellulose films.

Berendsen [43, 44] investigated water in collagen fiber at different water contents. The spectra exhibited a doublet caused by proton intramolecular dipole-dipole interaction in water molecules. The width of the doublet varies with angle θ according to $(3\cos^2\theta-1)$ where θ is defined as the angle between magnetic field and internuclear vector of protons in a water molecule. A chain-like structure was postulated in such a way that water molecules align in the fiber direction by formation of hydrogen bonds at appropriate sites on fibers, and are free to rotate or reorient about the chain axes. After reinvestigated the same system [45], he proposed an alternative model in which the anisotropy is caused by specific binding of water to the macromolecules. Water molecules are oriented in the direction with their H-H line perpendicular to the fiber axis. Broad-line NMR study of H_2O and D_2O in oriented rayon fiber was performed by Dehl [46]. Both proton and deuterium spectra

showed a splitting feature. The splitting for D_2O is several times bigger than that for H_2O, and the splitting was also angularly dependent. In the model proposed by Dehl, the water molecules do not rotate isotropically, and are slightly biased along the fiber axis. Chapman and Mclauchlan reported NMR results on water in sciatic nerve of rabbit [47] and in collagen fiber [48]. Besides the orientation effect described previously, they calculated the order parameters S_{ii}. In Dehl's latter reports of water in collagen fibers with different water content at room temperature [49], all spectra consisted of a pair of lines, and the separation of the lines also varies according to the factor of $(3\cos^2\theta-1)$. They observed that linewidth and splitting were strongly affected by proton exchange in water molecules, but not by deuteron exchange. Fung *et al.* measured proton spin-lattice relaxation time T_1 in hydrated collagen [50, 51], and suggested two kinds of water may exist in collagen: isotropic water occurring at higher water content, and a hydration layer formed by the water molecules bound to fiber when the water weight percentage is less than 50%. T_1 measurement of D_2O in oriented cellulose [52] also led to the conclusion of the existence of two kinds of water, "bound" water and "free" water. The temperature dependence of T_1 was measured in the range of -10 °C - 35 °C, from which correlation times for water molecular motion could be deduced.

Compared to water in collagen fiber, the studies on water in polymer membranes are more relevant to this thesis because of the similarity of the polymer morphology. Wide-line proton NMR spectra of thick (100 μm) and ultrathin (0.25 μm) membranes of cellulose acetate were obtained in dry and wet film by Krishnamurthy *et al.* [53]. They observed a sharp central peak and a broad outer

doublet in wet thick film, both in the parallel and perpendicular directions. The maximum separation occurs when the plane of the film perpendicular to the dc magnetic field. The differences between spectra of the thick and ultrathin membranes are discussed in terms of "free" and restricted water whose distributions are influenced by the structure of thick and ultrathin films. Shporer *et al.* studied water absorbed at various relative humidities in cellulose ester membranes [54]. Similar to other NMR results, an orientation effect was observed. However, this effect was explained in terms of a geometrical phenomenon due to the bulk magnetic susceptibility of the medium.

A comprehensive investigation on water in cellulose films has been reported recently by Matsumura *et al.* [55-57]. In cellulose acetate film [55], both H_2O and D_2O exhibit splitting due to dipolar and quadrupole interactions. The splitting is angularly dependent and has a maximum when the surface of the film is perpendicular to the magnetic field for both proton and deuteron spectra. This indicated that the motionally averaged axes of the dipole-dipole and quadrupole interactions orient in the direction perpendicular to the film surface. The axis of proton dipole-dipole moment here is referred as the H-H axis in H_2O, and the deuteron principal axis of the quadrupole interaction is the O-D axis in D_2O [56]. In considering molecular motion, if a water molecule rotates around a certain axis fast enough, both motionally averaged dipolar and quadrupolar axes should correspond to the rotational axis [56]. The separation of splitting decreases as the water content increases for both H_2O and D_2O. In variable temperature measurements, the separation of the peaks and linewidth of a single peak in the doublet tend to increase

as temperature decreases.

For cellulose triacetate film, the samples were treated by water (H_2O and D_2O) and methanol (CH_3OD and CD_3OH) [56]. Again, angularly dependent splitting was observed for all solvents except ^{1}H-NMR spectrum of CD_3OH.

It was concluded that the tendency of H-H axis of the water molecules to align perpendicular to the surface of above films is due to the anisotropy in the film [56].

Cellulose film stretched in one direction , so called longitudinal direction, was used to probe the effect of in-plane anisotropy caused by stretching [57]. The significant difference from unstretched film is that the average H-H axes of water molecules were found to be parallel to the longitudinal (stretched) direction in the film plane, instead of perpendicular to film plane in unstretched film. In addition to this, the volume diamagnetic susceptibilities was also found to be anisotropic.

It may be useful to summarized the general behaviors of water in anisotropic fiber and film.

1). The ^{1}H and ^{2}H NMR of H_2O and D_2O and other solvents show a splitting in their spectra. The splitting has the angular dependence of $K(3\cos^2\theta-1)$. In the situation where a clear doublet is not observed, the apparent linewidth varies with the same angular dependence.

2). The quadrupole splitting in deuterated solvents is bigger than the dipole splitting in protonated solvents. For both dipole and quadrupole splitting, the separation with low water content or at low temperature is bigger than that with high water content or at high temperature. The linewidth of a single peak within the doublet becomes broaden as water content or temperature decrease. This

dependence of splitting on water content and temperature is attributed to the molecular motion.

3). For polymer fiber, the maximum splitting was observed when the fiber is parallel to the magnetic field. On the other hand, the separation observed in films reaches a maximum when film plane is perpendicular to the magnetic field. The water molecular orientation effect is attributable to the anisotropy of the polymer material.

Finally, it must be emphasized that, although many orientation phenomena of water have been reported, and the fact that this orientation effect is caused by the anisotropy of the polymer has been well accepted, the question of how the water molecular motion is affected by the anisotropy of the polymer is still unclear. Most of the papers referenced above described water behavior in the polymer from the viewpoint of NMR, but a microscopic model, e.g. the detailed chemical and physical interaction on the molecular level between water molecules and polymer chain or side group, has not been found yet.

Chapter 2. Theoretical Background of NMR

2-1. NMR Phenomenon

According to the principle of quantum mechanics, the magnetic moment μ of a nucleus is proportional to the angular momentum of the nucleus I

$$\mu = \gamma \hbar I \qquad 2\text{-}1$$

where $\hbar$ is Planck's constant divided by 2π and γ is called the magnetogyric ratio of the nucleus. The permitted values of angular momentum I along any chosen axis are described by means of a set of magnetic quantum numbers m, given by the series

$$m = I, (I-1), (I-2), \cdots -I \ ,$$

and I is called the spin of the nucleus.

The nuclei contained in the samples investigated in this project are listed in the Table 2.1 with their spin values.

Table 2.1 The nuclei contained in sufficient abundance in the samples investigated in the project

Nuclei	Spin, I
^{1}H	1/2
^{2}H	1
^{14}N	1
^{17}O	5/2
^{12}C	0
^{16}O	0

Because carbon-12 and oxygen-16 have no spins, we need not consider them at all from the point of view of NMR phenomena.

To consider the bulk or macroscopic magnetic properties of the material, we define the bulk magnetization **M** which is the magnetic moment per unit volume,

$$\boldsymbol{M} = \Sigma \boldsymbol{\mu}_i \quad . \tag{2-2}$$

In a static magnetic field $\mathbf{H}_o$, **M** is proportional to $\mathbf{H}_o$,

$$\boldsymbol{M} = \chi_o \boldsymbol{H}_o \tag{2-3}$$

where χ_o is the static magnetic susceptibility.

The application of magnetic field $\mathbf{H}_o$ produces an interaction energy with the nucleus given by $-\boldsymbol{\mu}\cdot\mathbf{H}_o$. We have, therefore, a very simple Hamiltonian:

$$\mathcal{H} = -\boldsymbol{\mu}\cdot\boldsymbol{H}_o \quad . \tag{2-4}$$

Taking the field along the z-direction, we find

$$\mathcal{H} = -\gamma\hbar H_o I_z \quad . \tag{2-5}$$

Therefore the allowed energy levels, which are also called Zeeman energy levels, are

$$E = -\gamma\hbar H_o m \quad , \qquad m = I, I-1, \cdots, -I \quad . \tag{2-6}$$

It is clear that the difference between two adjacent energy levels is

$$\Delta E = -\gamma\hbar H_o \Delta m \quad . \tag{2-7}$$

For example, Zeeman energy levels of ^{1}H and ^{2}H are illustrated in Figure 2.1.

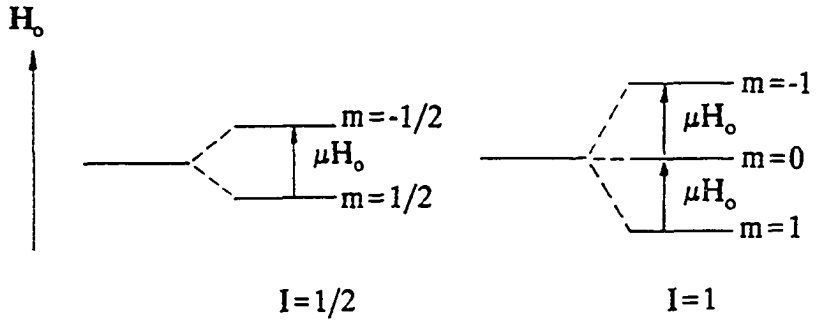

Figure 2.1 Zeeman energy levels for spin-1/2 and spin-1.

In order to induce transitions between the two nuclear spin levels, an alternating magnetic field $\mathbf{H}_1$ is applied to the system. Absorption of energy occurs provided a component of the magnetic vector $\mathbf{H}_1$ is perpendicular to the steady field $\mathbf{H}_0$ and provided the angular frequency ω of the $\mathbf{H}_1$ satisfies $\hbar\omega_0 = \Delta E$, or

$$\omega_o = \gamma H_o \qquad 2\text{-}8$$

The equation 2-8 is called the resonance condition and ω_0 is the Larmor frequency.

So far we have considered the basic magnetic resonance by using quantum mechanical treatment. However, the classical macroscopic treatment is also a useful approach to understand the resonance phenomenon.

When a magnetization $\mathbf{M}$ is placed in a steady magnetic field $\mathbf{H}_0$, it undergoes precession about the static field direction according to the equation

$$\frac{dM}{dt} = \gamma M \times H_o \qquad 2\text{-}9$$

as shown in Figure 2.2.

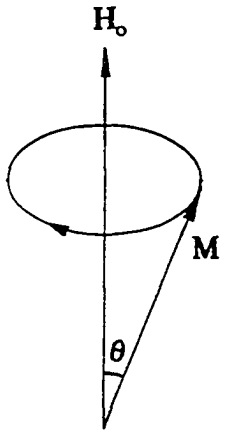

Figure 2.2 Magnetization **M** in a static magnetic field.

Comparing the equation 2-9 with the equation from classical mechanism

$$\frac{dM}{dt} = \omega \times M \quad , \qquad 2\text{-}10$$

we find that the angular frequency of precession is $\omega_o = -\gamma H_o$, and $|\omega_o| = \gamma H_o$, which is same as the equation 2-8.

The magnetization **M** can be made to flip in longitudinal direction away from the direction of $\mathbf{H}_o$ by applying a second magnetic field $\mathbf{H}_1$ at right angle to $\mathbf{H}_o$ and requiring this $\mathbf{H}_1$ to rotate at the precession frequency ν_o, $\nu_o = \omega_o/2\pi$. It can be seen that if $\mathbf{H}_1$ rotates at a frequency close to but not exactly at the precession frequency, it will cause at most only some wobbling or nutation of vector **M**. If $\mathbf{H}_1$ is made to rotate exactly at the precession frequency, it will cause large fluctuations in the angle θ between **M** and $\mathbf{H}_o$. If we vary the rate of the rotation of $\mathbf{H}_1$ through this value, we will observe a resonance phenomenon as we pass through ν_o. If we observe the system in the laboratory frame, the motion of the vector **M** is quite complex: it is

composed of the precession around $\mathbf{H}_0$ axis and the precession around $\mathbf{H}_1$ axis (i.e. changing angle θ) which also rotates around $\mathbf{H}_0$ in x-y plane.

To simplify this situation, we introduce a rotating coordinating frame which rotates with $\mathbf{H}_1$. In the rotating frame $\mathbf{H}_1$ becomes the static field. When $\mathbf{H}_1$ rotates at the resonant frequency, **M** vector is simply tipped from the $\mathbf{H}_0$ axis by an angle θ by $\mathbf{H}_1$ pulse, as we view from the rotating frame. The detail description of motion of magnetization caused by rf $\mathbf{H}_1$ can be found in the references [58] and [59].

2-2. Detection of the Resonance Phenomenon

In the previous section, we have discussed how the nuclear magnetic resonance phenomenon occurs. This section will explain how to detect the resonance signal in pulse NMR.

As we have seen, the field $\mathbf{H}_1$ can make the magnetization **M** tip in longitudinal direction. The tipping angle θ of **M** is given by

$$\theta = \gamma H_1 t_p \qquad 2\text{-}11$$

where t_p is the duration of the pulse $\mathbf{H}_1$. For a simple case, the t_p of $\mathbf{H}_1$ can be set such that the tipping angle θ is equal to 90°, which corresponds the **M** vector being rotated from the vertical direction into the horizontal plane. After this 90° pulse, **M** will precess about $\mathbf{H}_0$ with Larmor frequency ω_0 in the laboratory frame. This situation is illustrated in Figure 2.3.

The rotating magnetization **M** in the coil will induce an electromotive force, which can be detected by electronic means. This alternating signal, a function of time f(t), is termed a free induction decay (FID), referring to the absence of the rf field

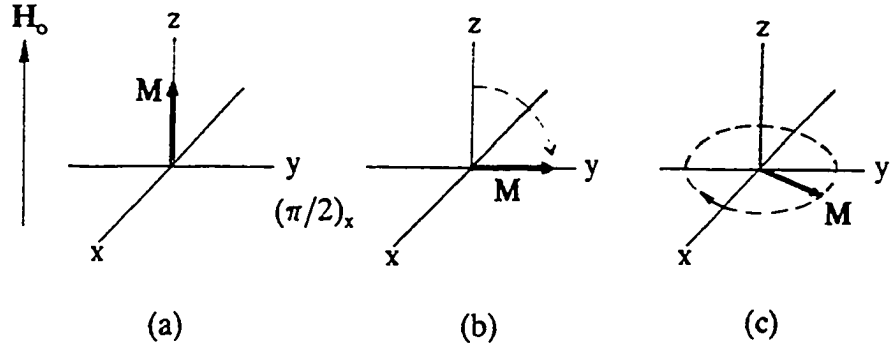

Figure 2.3 Effect of rf pulse on magnetization, (a) before rf pulse, **M** is aligned $\mathbf{H}_o$; (b) at the end of $\pi/2$ pulse applied on x direction, **M** is rotated into xy plane on y axis; (c) after pulse, M precesses in xy plane with Larmor frequency.

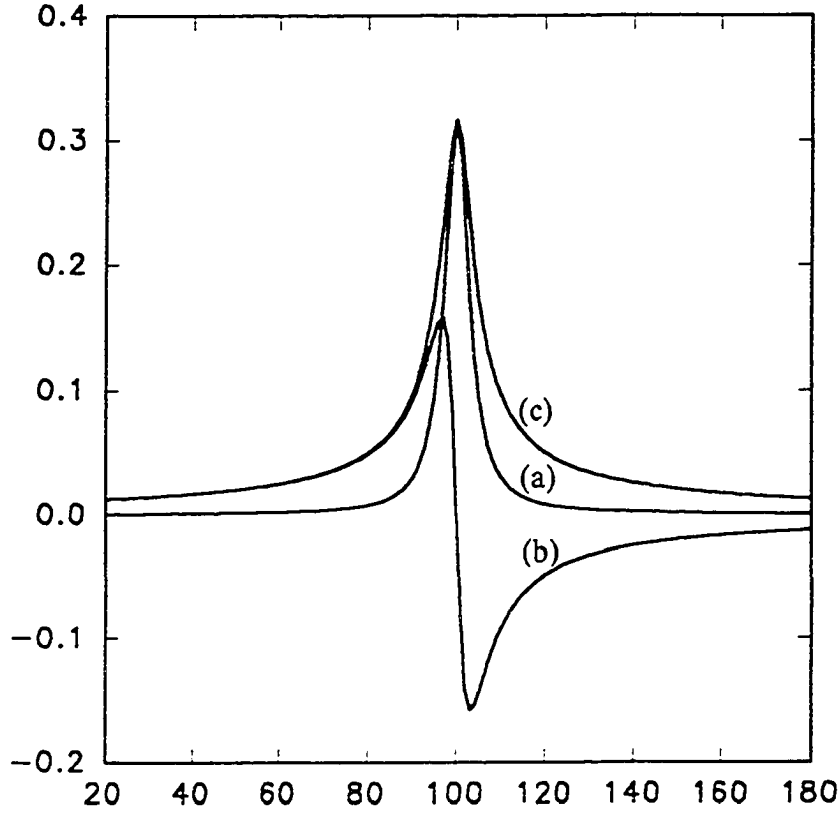

Figure 2.4 Fourier transform of an exponential decay f(t): (a) absorption mode v, (b) dispersion mode u, and (c) magnitude mode M. Note that the linewidth of magnitude mode is √3 times broader than that of absorption mode.

H_1. After Fourier transform (FT), the signal is converted from time domain f(t) to frequency domain spectrum F(ω) or F(ν). Fourier transform is made in terms of the equation

$$F(\omega) = \int_{-\infty}^{\infty} f(t)\, e^{-i\omega t}\, dt = v - iu$$

where v is the real part and u is the imaginary part. For an exponential decay signal f(t)

$$f(t) = A_o \exp^{-t/T_2^*} \quad , \qquad 2\text{-}13$$

its Fourier transform is of Lorentzian shape

$$v = \frac{A_o T_2^*}{1 + \omega^2 T_2^{*2}} \quad , \qquad u = \frac{A_o T_2^{*2} \omega}{1 + \omega^2 T_2^{*2}} \quad . \qquad 2\text{-}14$$

The real part v is termed absorption spectrum and u dispersion spectrum. The spectrum can also be displayed in a magnitude mode defined as

$$M = (v^2 + u^2)^{1/2} \quad . \qquad 2\text{-}15$$

The spectra of v, u and M are shown in Figure 2.4.

It is easy to show that the full width at half magnitude (FWHM), also called linewidth and noted by Δν, for a Lorentzian absorption spectrum v is

$$\Delta \nu_v = \frac{1}{\pi T_2^*} \qquad 2\text{-}16$$

and the linewidth of the magnitude mode spectrum M is

$$\Delta \nu_M = \frac{\sqrt{3}}{\pi T_2^*} = \sqrt{3}\,\Delta \nu_\nu \quad . \qquad 2\text{-}17$$

It is necessary to mention here that many of the NMR spectra shown in this work are displayed in the magnitude mode for the reasons that will be discussed later.

2-3. Interactions in NMR

To analyze the spectrum obtained from experiment, we need to obtain information about two aspects which determine the characteristics of the spectrum: interactions of the nuclei with their environment and the relaxation caused by these interactions and molecular motion. The former is going to be discussed in this section while the latter will be considered in next section.

In terms of quantum mechanism the interactions of the nucleus with its environment are represented by the Hamiltonian of the nucleus. From most NMR literature, the Hamiltonian contains in general case several terms including (1) Zeeman interaction, $\mathcal{H}_Z$, with applied static field $\mathbf{H}_o$; (2) nuclear electrical quadrupole interaction $\mathcal{H}_Q$; (3) dipole-dipole interaction between nuclear spins $\mathcal{H}_D$; (4) chemical shift caused by the shielding electrons around nucleus $\mathcal{H}_{CS}$; (5) scalar J or indirect coupling of nuclear spins $\mathcal{H}_J$; and (6) spin-rotation interaction results from the molecular motion $\mathcal{H}_{SR}$. The total Hamiltonian has the form

$$\mathcal{H} = \mathcal{H}_Z + \mathcal{H}_Q + \mathcal{H}_D + \mathcal{H}_{CS} + \mathcal{H}_J + \mathcal{H}_{SR} \quad . \qquad 2\text{-}18$$

Since the interactions (4), (5) and (6) are more pronounced in liquid or at high temperature [59], their contribution to our solid sample cannot be detected by the

broad line spectrometer. Therefore, we only need to concentrate on the dipole-dipole interaction and quadrupolar interaction.

The Zeeman term has been introduced previously by equation 2-5. Since $\mathcal{H} = \hbar\omega$, the magnitude of the Hamiltonian can also be expressed in the unit of frequency ω which is the ratio of $\mathcal{H}$ to $\hbar$. At 7 tesla magnetic field the Zeeman interaction for protons is about 300 MHz and for deuterons is about 47 MHz.

2-3.1. Dipolar Interaction

The dipolar contribution to the Hamiltonian for two nuclear spins is [58]

$$\mathcal{H}_D = \frac{\boldsymbol{\mu}_1 \cdot \boldsymbol{\mu}_2}{r^3} - \frac{3(\boldsymbol{\mu}_1 \cdot r)(\boldsymbol{\mu}_2 \cdot r)}{r^5} \qquad 2\text{-}19$$

where $\mu_1 = \gamma\hbar\mathbf{I}_1$, $\mu_2 = \gamma\hbar\mathbf{I}_2$ and r is the internuclear vector as shown in Figure 2.5.

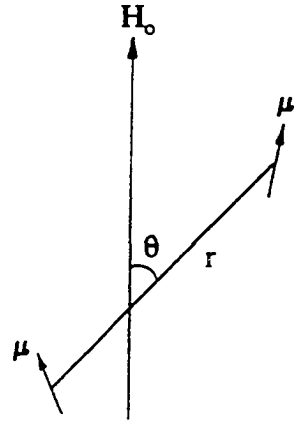

Figure 2.5 Formation of the dipolar interaction of two spins.

It has been shown that we can write $\mathcal{H}_D$ in terms of spherical coordinates:

$$\mathcal{H}_D = \frac{\gamma_1\gamma_2\hbar^2}{r^3}(A + B + C + D + E + F) \qquad 2\text{-}20$$

where

$$A = I_{1z}I_{2z}(1-3\cos^2\theta)$$

$$B = -\frac{1}{4}(I_1^+I_2^- + I_1^-I_2^+)(1-3\cos^2\theta)$$

$$C = -\frac{3}{2}(I_1^+I_{2z} + I_{1z}I_2^+)\sin\theta\cos\theta\, e^{-i\phi}$$

$$D = -\frac{3}{2}(I_1^-I_{2z} + I_{1z}I_2^-)\sin\theta\cos\theta\, e^{i\phi}$$

$$E = -\frac{3}{4}I_1^+I_2^+\sin^2\theta\, e^{-i\phi}$$

$$F = -\frac{3}{4}I_1^-I_2^-\sin^2\theta\, e^{2i\phi}$$

We may estimate the order of the magnitude of dipolar interaction by evaluating the factor of $\gamma_1\gamma_2\hbar^2/r^3$. The separation for protons in a water molecule is about 2 Å, thus the dipolar interaction between this proton pair is approximately equal to (in the unit of frequency)

$$\mathcal{H}_D(\text{H-H}) \approx \gamma_H^2\hbar/r^3 = (2.675\times10^4)^2(1.05\times10^{-27}) \,/\, (2\times10^{-8}) = 95 \text{ kHz}$$

Assuming the deuteron pair in D_2O has the same separation, then

$$\mathcal{H}_D(\text{D-D}) \approx \gamma_D^2\hbar/r^3 = (4.104\times10^3)^2(1.05\times10^{-27}) \,/\, (2\times10^{-8}) = 2.2 \text{ kHz} \ .$$

These values show that the dipole interaction between proton pair is about 50 times larger than that in the deuteron pair. On the other hand, comparison of the magnitude of $\mathcal{H}_Z$ with $\mathcal{H}_D$ shows that the latter is much smaller than the former. We can, therefore, treat $\mathcal{H}_D$ as a perturbation of Zeeman interaction. To first order of the perturbation, only A and B terms are used to calculate the effect of $\mathcal{H}_D$ on the eigenstates of $\mathcal{H}_Z$ [62]. In fact, for unlike or heteronuclear spins I and S, only A term need be used in the calculation while both A and B terms should be used for like or homonuclear spins I and I.

Let us consider the intramolecular dipolar interaction of water first. Since oxygen has no spin (I=0), the dipolar interaction within water molecules can be only the like spins of the proton pair (or deuteron pair in heavy water). One may also consider the dipolar interaction of the protons in one water molecule with spins in other molecules, so called intermolecular dipolar interaction. However, the distance for intermolecular spins is usually considerably longer than that of intramolecular spins. Recalling the dependence of $1/r^3$ of $\mathcal{H}_D$, we may consider that the primary dipolar interaction is contributed by intramolecular nuclei, the intermolecular spins provide a much smaller secondary dipolar interaction. The effect of dipolar interaction of two identical spins (I=1/2) is schemed in Figure2.6 where $\Delta = (1/4)\omega_D(1 - 3\cos^2\theta)$, $\omega_D = \gamma^2\hbar/r^3$ which is called dipolar frequency and line splitting Δ_D is given by

$$\Delta_D = \frac{3}{2}\omega_D(1-3\cos^2\theta) \quad . \qquad 2\text{-}21$$

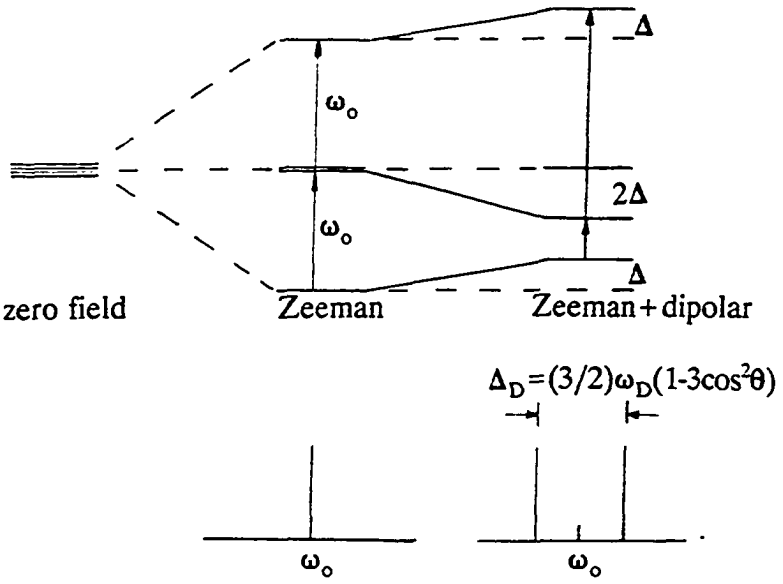

Figure 2.6 Effect of the dipolar interaction on Zeeman energy of two spin-1/2 and the corresponding spectra.

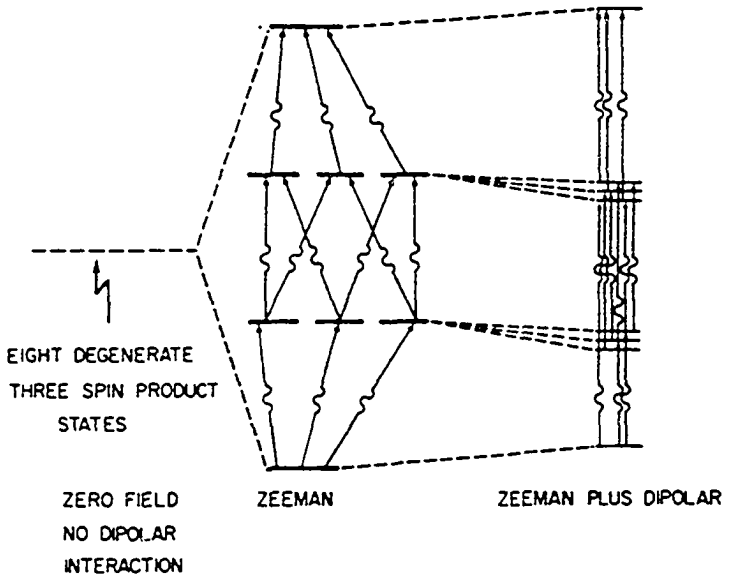

Figure 2.7 Depiction of the effect of dipolar interactions in a three spin-1/2 system. Note the complication of the transition scheme when compared to the system of spin-1/2 interacting in pairs.

The characteristic of the dipolar interaction is spectrum changing from a single peak to a doublet. If we consider three identical 1/2 spins, the effect of dipolar interaction is displayed in Figure 2.7. From this scheme we can see that the transitions are much more complicated than that for two spins and the spectrum is multiple lines instead of two lines as in the case of two 1/2 spins.

With I = 1, two interacting deuterons have nine degenerate states. Thus, the spectrum of two deuterons with the dipolar interaction is also composed of multiple lines.

Up to now, we have considered only an isolated spin pair which is a ideal model for evaluating the dipolar interaction. In a real material, the interaction of the members of each pair dominates, but the interaction between pairs may be not negligible. These many smaller interactions varying with both r and θ, give rise in effect to a multiplicity of lines whose envelope is seen as a continuous curve. This kind of spectral broadening is called dipolar broadening.

In the situation where molecular motion is allowed to take place, the variable r and θ become functions of time. If we assume that r is constant and only θ varies with time, then we need to take the time average of $(3\cos^2\theta - 1)$ during the NMR time scale. Assuming the molecules are moving rapidly, as in liquid, the factor $(3\cos^2\theta - 1)$ will be averaged to zero, and the line will be drastically narrowed compared to its width in the solid state. This effect due to molecular motion is named motional narrowing.

2-3.2. Quadrupolar Interaction

Nuclei with spin I>1/2 have a nuclear electrical quadrupole moment. This quadrupole interacts with the electric field gradient at the position of the nucleus and may have a very strong effect on the NMR spectrum.

We start by considering the classical electrostatic interaction between a charged nucleus with charge distribution ρ(x,y,z) and an external electrostatic potential V(x,y,z)

$$E = \int \rho(r) V(r) dV \quad . \tag{2-22}$$

The potential may be expanded in a series to give

$$V(x,y,z) = V_o + \sum_i \left(\frac{\partial V}{\partial x_i}\right)_{r=0} x_i + \frac{1}{2}\sum_{ij}\left(\frac{\partial^2 V}{\partial x_i \partial x_j}\right)_{r=0} x_i x_j + \cdots \quad , \tag{2-23}$$

then we have

$$E = V_o \int \rho(r) dV + \sum_i V_i \int x_i \rho(r) dV + \frac{1}{2}\sum_{ij} V_{ij} \int x_i x_j \rho(r) dV \quad . \tag{2-24}$$

The first term is identified as the electrostatic potential energy of nuclear charge which is not relevant for NMR. The second integral is the electric dipole moment of the nucleus. It vanishes for nuclei whose ground states have definite parity. The third term is the electric quadrupole term where V_{ij} is a component of the electric field gradient (EFG) tensor at the nucleus. It is convenient to consider the quantities Q_{ij} defined by the equation

$$Q_{ij} = \int (3x_i x_j - \delta_{ij} r^2)\, \rho(r)\, dV \quad . \tag{2-25}$$

In terms of the Q_{ij}, we have the quadrupole energy E_Q

$$E_Q = \frac{1}{6}\sum_{ij} V_{ij}Q_{ij} \quad . \qquad 2\text{-}26$$

The quantum mechanical analog of E_Q can be calculated as [58]

$$\mathcal{H}_Q = \frac{eQ}{6I(2I-1)}\sum_{ij} V_{ij}\left[\frac{3}{2}(I_iI_j + I_jI_i) - \delta_{ij}I(I+1)\right] \qquad 2\text{-}27$$

where eQ is the quadrupole moment of the nucleus.

In the principal axis coordinate system of EFG (x,y,z), $\mathcal{H}_Q$ is reduced to a simpler form

$$\mathcal{H}_Q = \frac{e^2qQ}{4I(2I-1)\hbar}\left[3I_z^2 - I(I+1) + \eta\,(I_x^2 - I_y^2)\right] \qquad 2\text{-}28$$

where eq = V_{zz}, the largest component of EFG and η is called asymmetry parameter defined as

$$\eta = \frac{V_{xx} - V_{yy}}{V_{zz}} \quad . \qquad 2\text{-}29$$

Let us select the applied magnetic field H_o along the Z axis of the laboratory frame and introduce polar angles θ and ϕ between the principal axis coordinate (x,y,z) and laboratory frame (X,Y,Z), as shown in Figure 2.8.

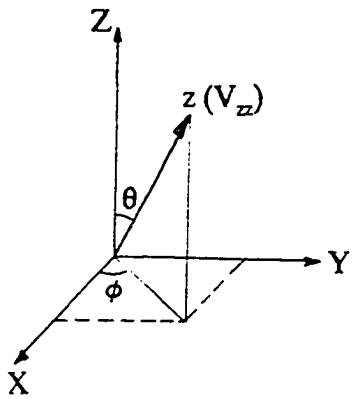

Figure 2.8 The orientation of the principal-axis frame of EFG (x,y,z) relative to laboratory frame (X,Y,Z). The V_{zz} component of EFG tensor is aligned the z-axis.

If we make the simplifying assumption of a electric field gradient with axial symmetry ($I_x=I_y$ or $\eta = 0$), then the equation 2-28 in the lab coordinate system becomes

$$\mathcal{H}_Q = \frac{e^2qQ}{4I(2I-1)}\left[3I_Z^2\cos^2\theta + 3I_X^2\sin^2\theta + 3(I_ZI_X + I_XI_Z)\sin\theta\cos\theta - I(I+1)\right] \quad . \qquad 2\text{-}30$$

Treating $\mathcal{H}_Q$ as a perturbation energy of the Zeeman energy, the energy shift of Zeeman energy level up to the first order perturbation will be

$$E_m = \frac{e^2qQ}{8I(2I-1)}(3\cos^2\theta - 1)\left[3m^2 - I(I+1)\right] \quad . \qquad 2\text{-}31$$

The effect of the quadrupole coupling is shown in Figure 2.9 for the case of deuteron (I=1).

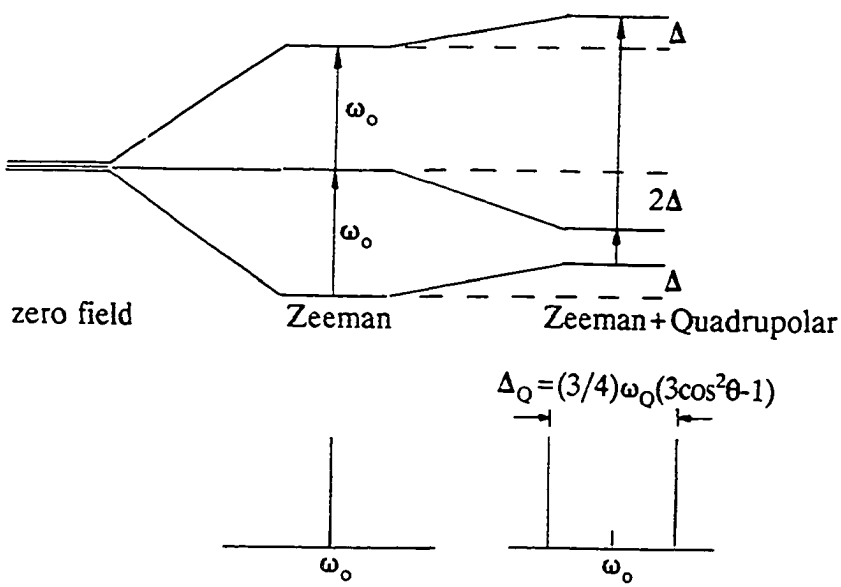

Figure 2.9 The energy levels and spectra for spin-1 nucleus with quadrupole interaction.

In Figure 2.9, $\Delta = (1/8)\omega_Q(3\cos^2\theta\text{-}1)$, $\omega_Q = e^2qQ/\hbar$ named quadrupole frequency and the quadrupole splitting Δ_Q is in the form of

$$\Delta_Q = \frac{3}{4}\omega_Q(3\cos^2\theta - 1) \quad . \qquad 2\text{-}32$$

In the case of a asymmetric field ($\eta \neq 0$), the energy shift E_m has the form [62]

$$E_m = \frac{e^2qQ}{8I(2I-1)}(3\cos^2\theta - 1 + \eta\sin^2\theta\cos 2\phi)\left[3m^2 - I(I+1)\right] \quad . \qquad 2\text{-}33$$

We notice that the quadrupole interaction for a spin I=1 results in a line splitting similar to that caused by dipole coupling for a proton pair displayed in Figure 2.6. Most of the results presented in this work involve ^2H (I=1) NMR.

The previous figure is suitable only for a single spin (I=1) or spins in single crystal in which all the nuclei oriented in the same direction. Recalling the discussion in the dipolar interaction with regard to dipolar broadening and motional narrowing, it is also expected that the quadrupole interaction will cause spectrum broadening and molecular motion will narrow the linewidth.

Of course, for the spin I>1, the quadrupole coupling also creates the multiplicity of line with a more complicate spectrum than that for I=1. Oxygen-17 nucleus (I=5/2) has six Zeeman energy levels in a static magnetic field H_o. The first-order perturbation of the quadrupole interaction results in a ^{17}O NMR spectrum containing five peaks: central transition and four satellites. The intensity of the peaks has the ratio of 5:8:9:8:5 and the satellites are equally spaced by quadrupole splitting. For the solid sample the splitting is in the order of several megahertz.

2-4. Orientation Effect

As we have seen in Figures 2.6 and 2.9, the interactions cause line splitting and the magnitude of the splitting depends on ω_D or ω_Q and orientation factor $(3\cos^2\theta\text{-}1)$. In liquid state, the angular factor will be averaged to zero by isotropic motion of the molecules, therefore, no splitting effect is observed. In solid sample, the line splitting is a characteristic of the molecular orientation. For the isotropically oriented solid nuclei system, for instance powder sample, the total orientation effect contributed by all nuclei results in a special lineshape which is called Pake's pattern or powder pattern. We will discuss this more later.

Let us take the quadrupole splitting as an example for detailed consideration. In the equation 2-32, the variable θ indicates the angle between the applied field $\mathbf{H}_o$ and the principal axis of the EFG tensor, V_{zz}. Since the two peaks in the doublet are symmetric about the Larmor frequency ω_o, we may rewrite the above equation as

$$\Delta_Q = \frac{3}{4}\omega_Q |3\cos^2\theta - 1| \quad . \qquad 2\text{-}34$$

Figure 2.10 schemes the angular dependence of Δ_Q as θ varies from 0° to 180°. It is clear from the scheme that the splitting reach its maximum when the V_{zz} axis is parallel to H_o and its minimum when V_{zz} is 54.7° from H_o. Considering the deuteron as a member of a OD bond, the V_{zz} axis is assumed along the internuclear vector (e.g. connection line between oxygen and deuteron). For the case in which molecules partially orientate, the spatial distribution of OD bond will make peaks broaden and the observed splitting is the average effect of all OD bonds. To describe the degree of molecular orientation a order parameter S_{OD} is introduced, then the equation 2-34

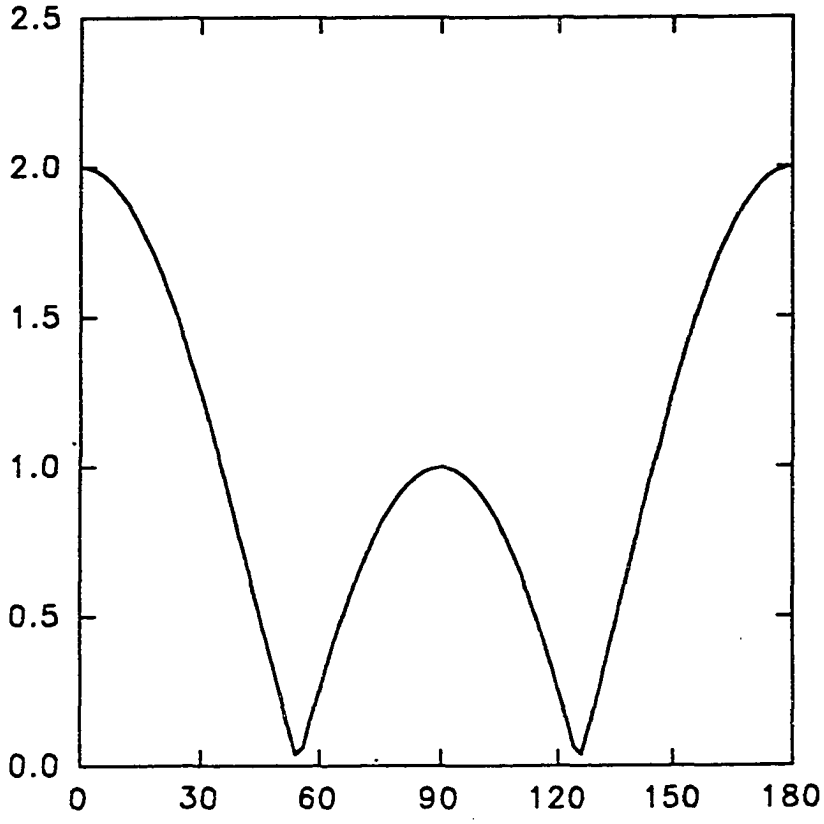

Figure 2.10 A plot of function $A|3\cos^2\theta-1|$ vs. angle θ for $A=1$.

is modified to

$$\Delta_Q = \frac{3}{4}\omega_Q |3\cos^2\theta - 1| S_{OD} \quad . \qquad 2\text{-}35$$

An explicit form of S_{OD} for partially oriented water molecules was derived by Buckingham [63] and Halle [64]. The maximum value of S_{OD} is equal to 1 corresponding to a perfectly aligned system.

Similar conclusion can be drawn from the equation 2-21 for the case of dipolar interaction provided that variable θ is defined as the angle between magnetic field H_o and internuclear vector of the two spins. Since ω_D is generally much smaller than ω_Q, the dipole splitting is quite small comparing with quadrupole splitting.

It is necessary to consider a special situation in which internuclear lines of dipole pairs (or OD bond for quadrupole interaction) are isotropically oriented in all direction without motion and the interaction between different pairs is assumed zero. An example of this kind of system is solid powder sample. A typical spectrum of this system is called Pake's pattern [65] or powder pattern. Pake obtained this kind spectrum first for powder sample of $CaSO_4 \cdot 2H_2O$ which is shown in Figure 2.11.

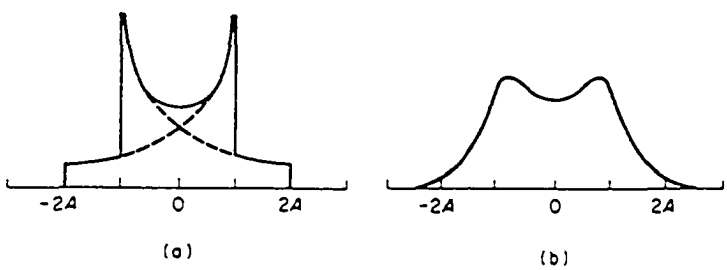

Figure 2.11 Powder pattern lineshape from two spin-1/2 interacting via the dipole-dipole coupling. The lineshape (a) for infinitely marrow component lines reduces to (b) when other broadening mechanisms are present.

If the interaction between a spin-pair and its neighbour is considered, a line broadening is observed and Pake's pattern is smoothed shown in Figure 2.11. In addition, the molecular motion also smoothes Pake's pattern and reduces the separation of the doublet [42,66]. Because Pake's pattern occurs only when molecules are in static state and randomly oriented, we can, in principle, use this feature as a criterion for checking the degree of molecular orientation and motion.

Since the quadrupole interaction of deuterons gives rise to the same angular dependence as the dipole-dipole interaction angular dependence in protons (see Eq. 2-21 and Eq.2-32), a Pake's pattern spectrum is also expected for the isotropically oriented solid deuterons system.

The first-order perturbation theory for oxygen-^{17} nucleus shows that the central transition peak is angular independent while the separations of the satellites are orientation dependent governed by the factor of $(3\cos^2\theta-1)$ if asymmetry parameter η is equal to zero [62]. However, if one considers the second-order perturbation of quadrupole interaction, the central transition is also angular dependent, but this dependence is very weak [62]. Therefore, the orientation effect for the central transition can be ignored.

2-5. Relaxation

The observation of nuclear magnetic resonance requires the absorption of electromagnetic energy (in the radio frequency range) associated with a transition of nuclear spins from lower to upper energy levels. The process by which the spins in the excited state return non-radiatively to the ground state, is called relaxation.

From the view point of thermodynamics the spins may be considered as an isolated system. Incident radiation in the form of an rf pulse transfers "heat" to the spins and raises their "spin temperature". The relaxation mechanisms transfer "heat" to the lattice bath and thus restore thermal equilibrium. The spin-lattice relaxation time T_1 is a measure of the rate of transfer energy from the spins to the lattice. The spin-spin relaxation time T_2 is a measurement of the rate at which the energy can be distributed within the spin system.

Using the classical treatment of magnetization **M** interacting with magnetic field $\mathbf{H}_o$ along Z axis, the contribution of relaxation to resonance phenomena is included in Bloch equations [58]

$$\frac{dM_x}{dt} = \gamma (M \times H_o)_x - \frac{M_x}{T_2} \quad , \qquad 2\text{-}36$$

$$\frac{dM_y}{dt} = \gamma (M \times H_o)_y - \frac{M_y}{T_2} \quad , \qquad 2\text{-}37$$

$$\frac{dM_z}{dt} = \gamma (M \times H_o)_z - \frac{M_z - M_o}{T_1} \quad . \qquad 2\text{-}38$$

From the equations we can see that spin-lattice relaxation is related to recovery of M_z which is parallel to $\mathbf{H}_o$, and spin-spin relaxation is associated with the variation of the components of **M** perpendicular to $\mathbf{H}_o$. The solution of Block equation in rotating frame can be found in many references [e.g. 58,59]. Fig 2.12 exhibits the process of the relaxation corresponding to the variation of magnetization **M** in a rotating frame, i.e. a reference frame that rotates about z at the Larmor frequency.

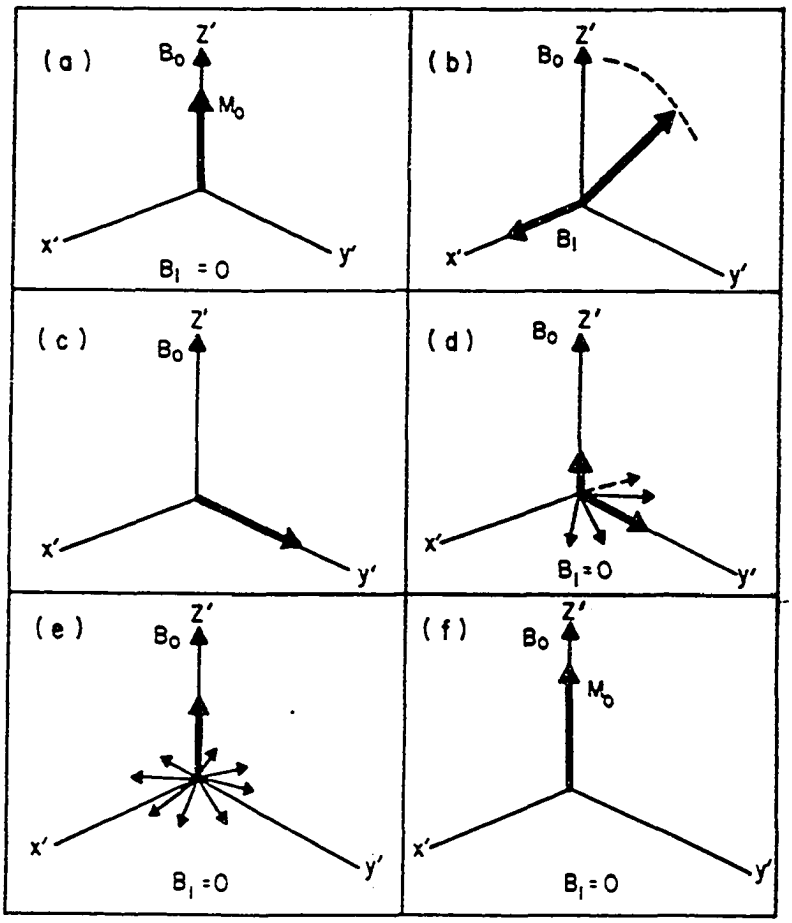

Figure 2.12 Rotating frame diagrams describing for relaxation. (a) The net magnetization M_o is aligned along the magnetic field direction; (b) and (c) An rf pulse B_1 is applied perpendicular to B_o. The duration of B_1 is sufficient to tip the net magnetization by $\pi/2$. (d) and (e) The spins begin to relax in the x-y plane by spin-spin (T_2) processes and in the z direction by spin-lattice (T_1) processes; (f) the equilibrium magnetization is reestablished along B_o.

There are many processes through which the spin system may relax. The equation 2-18 summarizes the possible interactions involved in NMR, each of them can result in a relaxation process. However, as we mentioned earlier, only the quadrupole and dipole interactions dominate in this work, hence we will concentrate our concern on them only.

Before we get into relaxation mechanisms. it is useful to introduce the concept of correlation function and correlation time. In the case of random molecular motion, the correlation time is defined as the time in which a molecule remains in any given position before a collision causes it to change its position or orientation, and the correlation function is given in the form of [67]

$$K(\tau) = K(0)\, e^{-\tau/\tau_c} \quad . \qquad 2\text{-}39$$

This function defines the position of molecule at time τ relative to its position at an arbitrary initial time, K(0). The equation says that the new position , K(τ), is related to the initial position in an exponential manner. The correlation time τ_c is very small for a molecule with a fast average motion. To proceed further, we need to know what ranges of frequencies of motion are present, and this is most easily done by the process of Fourier analysis. We can define a related function of frequency as [67]

$$J(\omega) = \int_{-\infty}^{\infty} K(\tau)\, e^{-i\omega\tau} d\tau = A\left[\frac{\tau}{1 + \omega^2 \tau_c^{\,2}}\right] \qquad 2\text{-}40$$

where J(ω) is called the spectral density function and A is a constant which can readily be calculated.

2-5.1. Spin-lattice Relaxation

For spins I=1, the relaxation rate $1/T_{1Q}$ contributed by quadrupole interaction is [62]

$$\frac{1}{T_{1Q}} = \frac{3}{40}\left(1+\frac{\eta^2}{3}\right)\left(\frac{e^2qQ}{\hbar}\right)^2\left[\frac{\tau_c}{1+\omega^2\tau_c^2}+\frac{4\tau_c}{1+4\omega^2\tau_c^2}\right] \quad . \qquad 2\text{-}41$$

In the extreme narrowing case, $\omega\tau << 1$,

$$\frac{1}{T_{1Q}} = \frac{3}{8}\left(1+\frac{\eta^2}{3}\right)\left(\frac{e^2qQ}{\hbar}\right)^2\tau_c \quad . \qquad 2\text{-}42$$

The relaxation rate resulting from dipole interaction for like spins $1/T_{1D}$ is [62]

$$\frac{1}{T_{1D}} = \frac{2}{5}\frac{\gamma_D^4\hbar^2}{r^6}I(I+1)\left[\frac{\tau_c}{1+\omega^2\tau_c^2}+\frac{4\tau_c}{1+4\omega^2\tau_c^2}\right] \quad . \qquad 2\text{-}43$$

The equations for unlike spins are shown in references [60,62]. For deuteron pair in D_2O, the total relaxation rate is approximately written

$$\frac{1}{T_1}(^2H) = \frac{1}{T_{1Q}}+\frac{1}{T_{1D}} \quad , \qquad 2\text{-}44$$

where quadrupole term is much stronger than dipole term. Protons in H_2O water have no quadrupole moment, thus the dipole interaction is the principal relaxation process for proton NMR.

2-5.2. Spin-spin Relaxation

Similar to equation 2-41, spin-spin relaxation rate for spins I=1 due to quadrupole interaction, $1/T_{2Q}$, has the form

$$\frac{1}{T_{2Q}} = \frac{3}{80}\left(1+\frac{\eta^2}{3}\right)\left(\frac{e^2qQ}{\hbar}\right)^2\left[3\tau_c + \frac{5\tau_c}{1+\omega^2\tau_c^2} + \frac{2\tau_c}{1+4\omega^2\tau_c^2}\right] \quad . \qquad 2\text{-}45$$

Also, the dipole contribution for like spins is

$$\frac{1}{T_{2D}} = \frac{\gamma_D^4\hbar^2}{r^6}I(I+1)\left[\frac{3\tau_c}{5} + \frac{5\tau_c}{1+\omega^2\tau_c^2} + \frac{16}{15}\frac{\tau_c}{1+4\omega^2\tau_c^2}\right] \quad . \qquad 2\text{-}46$$

Again, T_2 for deuteron will involve both mechanisms

$$\frac{1}{T_2}(^2H) = \frac{1}{T_{2Q}} + \frac{1}{T_{2D}} \quad . \qquad 2\text{-}47$$

As mentioned before, $1/T_{2Q}$ is meaningless for proton.

The exponential decay constant T_2^* in eq 2-13 includes all contributions leading to dephasing of the magnetization in the x-y plane.

It has to be emphasized here that the equations 2-41, 2-43, 2-45 and 2-46 are derived from a model of random molecular rotation [62]. Nevertheless, rotation may be the major type of the molecular motion in our sample since translation motion on NMR timescale is assumed relatively minor.

Figure 2.13 gives the plot of T_{1D} and T_{2D} for dipole interaction vs. correlation time τ_c at a fixed frequency ω. The minimum value of T_{1D} curve occurs at $\omega\tau_o \approx 1$. In fact, quadrupole relaxation rate T_{1Q} and T_{2Q} have the similar dependence with the correlation time. In the high temperature region (left side of T_1 minimum), the frequency of molecular motion is faster than the NMR Larmor frequency ω. Therefore, nuclei cannot relax efficiently at the Larmor frequency and results in the long spin-lattice relaxation times. On the right side of T_1 minimum, molecules move

slower than the Larmor frequency, the contribution of nuclei relaxation at Larmor frequency is also small and results in longer T_1 values. When the correlation time of motional molecules close to θ_0 ($1/\theta_0=\omega$), the relaxation is most efficient and leads the minimum of T_1. In general the correlation time is related to temperature (T) and activation energy (E_a) by the Arrhenius equation:

$$\tau = \tau_o e^{(E_a/kT)} \qquad 2\text{-}48$$

where τ_0 is a constant. If molecules freely rotate, the correlation time is approximately inversely proportional to temperature, $\tau \propto 1/T$ [68,69]. For this reason the above curves are usually plotted against 1/T, instead against τ_c (see Figure 2.13).

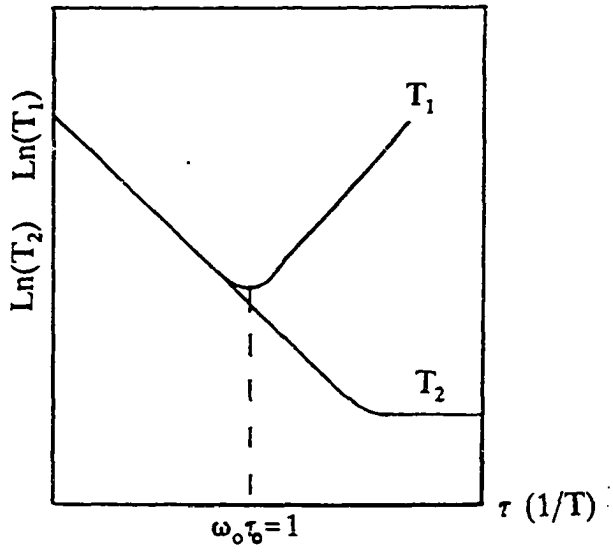

Figure 2.13 Spin-lattice relaxation time (T_1) and spin-spin relaxation time (T_2) as a function of correlation time (τ) or reciprocal of temperature (1/T).

Chapter 3. Experiment

At the beginning of this chapter, the various experimental techniques employed in this research are summarized.

X-ray diffraction photographs have been obtained for both Kapton and Upilex films with the thickness of 125 μm and 25 μm. They provide some information on molecular morphology of the polymer backbone.

Dielectric relaxation measurements were performed in the Department of Material Science and Engineering at Columbia University. Spectra of loss tangent vs. temperature for both types of polyimide films have been obtained for different film thickness (7.5 μm - 125 μm) and at different water content. In addition to water (H_2O and D_2O), the spectra of polyimide films containing other organic solvents such as methanol and acetic acid are also obtained.

NMR measurements were performed on three types of nuclei: proton (^1H), deuteron (^2H), and oxygen-17 (^{17}O). Proton NMR was applied (a) for dry polyimide film to obtain information concerning the polymer backbone and (b) for wet film treated with H_2O to obtain the signal of water which is superimposed on the signal of the protons contained in polymer chain. Deuterium NMR has been studied for three deuterated solvents D_2O, CH_3OD and CH_3COOD in both kinds of films (Kapton and Upilex). Oxygen-17 NMR was employed for water $H_2{}^{17}O$ (^{17}O enriched to 19%) absorbed in polyimide films.

3-1. Sample Preparation

Kapton-H films (PMDA-ODA) were obtained from E.I. DuPont de Nemours, Inc. in thickness ranging from 7.5 to 125 μm. Upilex-S films (BPDA-PDA) and Upilex-R film (BPDA-ODA) were provided by Ube Industries, Ltd. in the range of 25 μm to 125 μm. They are designated by the numerical labels listed in Table 3.1.

Table 3.1 The designation of the samples used in the measurements

Chemical formular	Commercial name	Thickness (μm)	Designation
PMDA-ODA	Kapton 500H	125	K1
	Kapton 300H	75	K2
	Kapton 100H	25	K3
	Kapton 30H	7.5	K4
BPDA-PDA	Upilex 500S	125	US1
	Upilex 300S	75	US2
	Upilex 200S	50	US3
	Upilex 100S	25	US4
BPDA-ODA	Upilex-R	125	UR1

Besides the commercial polyimide films, the self-made spin-coated PMDA-ODA film with 50 μm thickness was also used.

(a). Films for DR measurements

The original film was cut into a rectangular piece in 20 mm long and 15 mm wide. The samples were cleaned by isopropyl alcohol and sputtered with gold on both

sides for electrodes. The coated gold layers gave better electrical contact between films and capacitance bridge and less moisture loss during the loading of wet film into the measurement chamber. Films were dried in a vacuum for several day to remove the residual moisture, then exposed to specific moisture environments for further investigation.

(b). Films for NMR measurements

Since the sensitivity of NMR technique is relatively low and the water absorbed in the films is only a few percent of the dry film weight, a significant quantity of the film (about 1 gram) was used for each sample to get a reasonable signal to noise ratio. The original films were cut into strips with width of 15 mm and rolled up in to 10 mm NMR sample tube. For checking orientation effects, the films were cut into rectangular pieces and stacked (with their planes and cut directions parallel, then put in a 10 mm tube. The tubes were sealed by a cap with rubber O-ring to prevent moisture leakage and exchange with ambient water vapor. Films were pre-treated in vacuum oven for at least three days at 70 °C to remove moisture, although the moisture could be sufficiently removed in about one day. The stacked films in a sample tube ranges from 40 layers for 125 μm film to 700 layers for 7.5 μm film. As a result of the multilayer system, a sharp NMR peak is often observed due to the isotropically free water molecules trapped between layers for the sample with higher water content.

(c). Control of water content

The amount of absorbed water is controlled by the relative humidity (RH) of saturated salt solutions. Table 3.2 lists the relative humidity of different saturated salt

solutions at 25 °C.

Table 3.2 Solutions for maintaining constant humidity at 25 °C

Saturated salt solution	Relative humidity (%RH)
distilled water [H_2O]	100
sodium chloride [NaCl]	75
potassium nitrite [KNO_2]	45
potassium acetic acid [$KC_2H_3O_2$]	25

The water content of the polymer is expressed by weight percentage increase, wt%, relative to the weight of the dry film. The dry samples were put into a sealed bottle containing the appropriate salt solution and suspended above it for several days until equilibrium was reached. The values of water gained by polyimide at different RH are indicated in Table 3.3.

It is clear that the amount of water absorbed in Upilex film is only about one-half of that in Kapton. However, there is no significant difference of water content for different thickness in same kind of film.

Other than water, films treated by CH_3OH and CH_3COOH were measured by dielectric relaxation, and samples containing CH_3OD and CH_3COOD were studied by deuterium NMR. Methanol can be absorbed up to about 7 wt% for all thicknesses of Kapton films and acetic acid content could reach up to more than 10 wt% depending on film thickness. Some relevant physical properties of the above solvents

are presented in Table 3.4.

Table 3.3 Water content in polyimides at various relative humidity at 25 °C

Film	Relative humidity (%)	Water content (wt%) ± 0.1 wt%
Kapton	100	3.1
	75	2.2
	50	1.6
Upilex-S	100	1.7
	75	1.3
	50	0.8
Upilex-R	50	1.5

Table 3.4 Physical properties of the solvents used in measurements

Solvent	Molecular weight (g/mole)	Density (g/cm^3)	Molecular volume ($Å^3$)	Dipole moment ($C \cdot m \times 10^{30}$)
H_2O	18	1	29.89	6.17
CH_3OH	32.04	0.79	67.24	5.67
CH_3COOH	60.05	1.05	95.03	5.80

3-2. X-ray Diffraction Photograph

The experiment of X-ray photograph was undertaken at Rockefeller University on an Enraf Nonius FR590 machine. The X-ray source is Cu$K\alpha$ irradiation at 1.54 Å. The incident beam is perpendicular to the sample film plane and photographic film. The distance between photograph and sample is 10 cm, as shown in Figure 3.1.

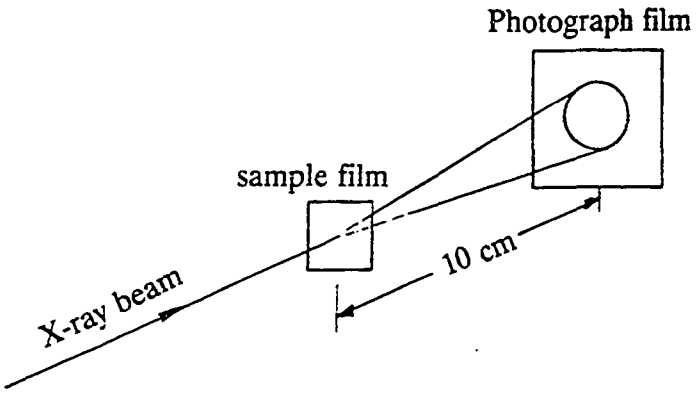

Figure 3.1 The schematic diagram of X-ray diffraction photograph.

3-3. Dielectric Relaxation

The dynamic dielectric measurements of the polyimides have been made at a series of frequencies from 10 to 100 kHz using an Andeen automated AC capacitance bridge controlled by IBM micro computer. The sample film was placed between two pieces of aluminum foil that served as an electrical connection from the sputtered sample electrodes to the capacitance bridge. All measurements are made in the temperature range 55 °K ~ 290 °K using a Janis cryostat. The temperature was controlled by using a Lake Shore Cryotronics Model DRC 81C temperature controller (1°K/min.). During the measurement, seven frequencies (100, 312.5, 1k,

3.125k, 10k, 31.25k, and 10k Hz were applied to take the capacitance and loss tangent data every 2 ~ 3 °K. The experimental apparatus is shown in Figure 3.2. In the dielectric relaxation spectrum, the loss tangent is plotted as a function of temperature or frequency.

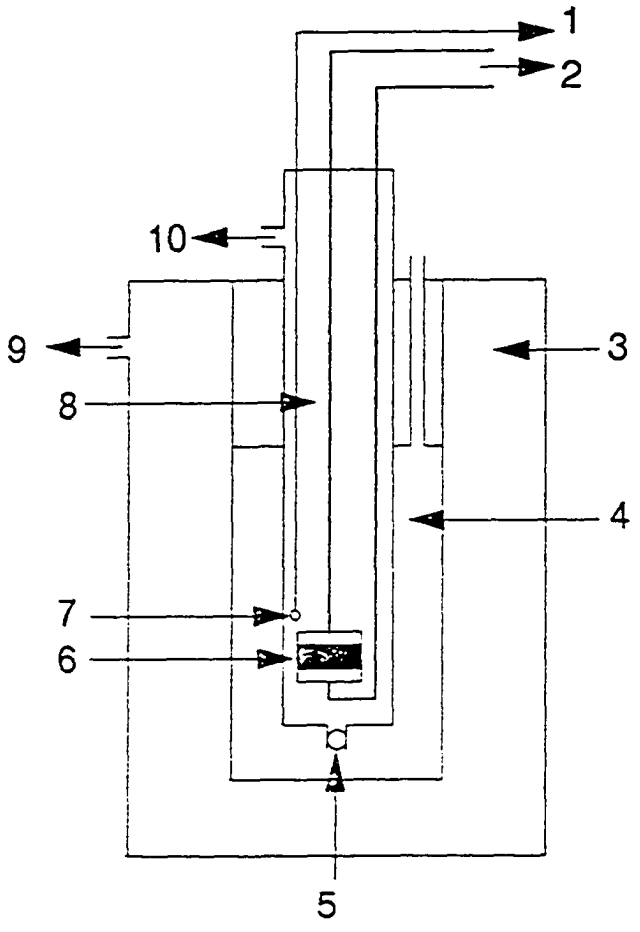

1=Temperature Controller
2=Capacitance Bridge
3=Vacuum Chamber
4=Liquid Nitrogen Chamber
5=Capillary Valve
6=Sample
7=Thermocouple
8=Sample Chamber
9=Vacuum Pump
10=Vacuum Pump and He gas Chamber

Fig. 3.2 Sample mount chamber for the dielectric relaxation measurement.

3-4. NMR Experiment

A Novex broad line NMR spectrometer was used in this study. The rf frequency synthesizer, transceiver, and preamplifier were designed to work in the frequency range from about 10 to 100 MHz. The power amplifier has a maximum output of 1 kilowatt. The free induction decay signal is recorded by either Novex digitizer or LeCroy oscilloscope with built in Fourier transform function. Novex digitizer is equipped with a quadrature detector, but LeCroy is supported by a single channel only. The recorded data were stored in an IBM computer. A block diagram of the spectrometer is shown in Figure 3.3.

Deuterium NMR was undertaken at a frequency of 47 MHz on a Cryomagnet System superconductor magnet at field strength 7.2 Tesla . The homogeneity of the field is about 1 ppm (part per million) for ^2H nuclei (liquid D_2O) at 47 MHz over a volume of 1 cm^3. The linewidth broadening of liquid sample due to the field inhomogeneity is about 40 Hz in 10 mm tube.

The proton NMR measurements have been done at 37 MHz on a Varian electromagnet. The field homogeneity is relatively poor compared to the superconductor magnet. The linewidth of water in 10 mm tube reaches around 180 Hz. Although this poor homogeneity is not sufficient for accurate measurements of narrow lines, it is still sufficient for the broad line signal of protons from polymer backbone.

Both probes used for proton NMR and deuteron NMR are home-made single solenoid probes with the facility of variable temperature measurement in the range of -100 °C - 80 °C. The temperature is controlled by blowing cooled or heated

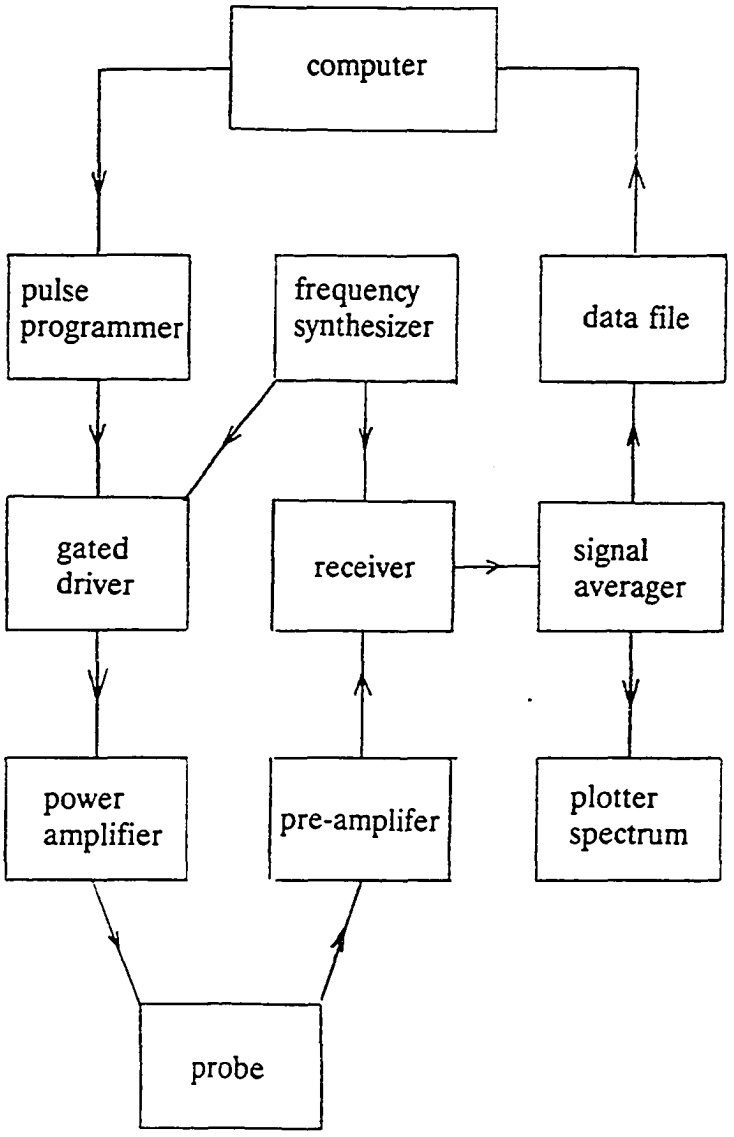

Fig. 3.3 Block diagram of Novex NMR spectrometer.

nitrogen gas through the sample chamber. Temperature regulation of ±2K wasachieved. The impedance matching network is shown in Figure 3.4. The inductance of the coil used for deuterium NMR is 0.47 μH and that for proton NMR coil has a value of ca. 0.5 μH. The quality factor (Q) is in the range of 250-300. The high-voltage variable capacitors in the matching network were obtained from Polyflon company, in the range of 0.8-10 pf.

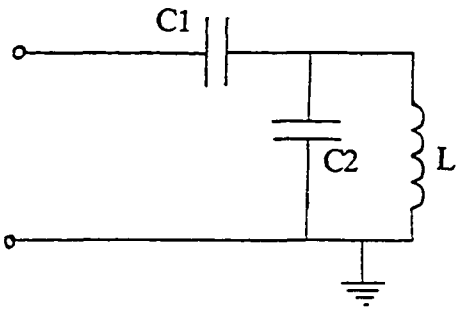

Figure 3.4 The circuit diagram of L-C matching network.

3-5. NMR Pulse Sequences

Three pulse sequences were employed in the NMR measurements. Most of the spectra were acquired by a single pulse sequence in which the free induction decay signal is acquired right after a 90° pulse. T_1 was measured by the inversion-recovery sequence [70,71].

The inversion-recovery sequence contains a $180°_x$ pulse followed by a $90°_x$ pulse after a delay time τ, the signal is examined right after 90° pulse, which is noted as

$180°_x - \tau - 90°_x$ - acquire,

the subscripts indicate the axis on which the rf pulse is applied. The idea is to invert

the z magnetization with a π pulse, then wait for it to relax back towards the +z axis, and finally apply a $\pi/2$ pulse and measure the signal. The relaxation process of z magnetization M(z) is described by the following equation.

$$M(z) = M_o(1-2e^{-\tau/T_1}) \qquad 3\text{-}1$$

T_1 can be calculated by curve fitting of the above equation. Note that when the interval τ is less than $T_1/\ln 2$ the magnetization is along the -y axis after $90°_x$ pulse (according to the convention of +y corresponding to the magnetization following a single 90_x pulse); this corresponds to an apparent negative peak, corresponding to M along -z. When τ is longer than $T_1/\ln 2$, the sampled signal corresponds to an apparent positive peak. The result of such an experiment with varying τ is shown in Figure 3.5.

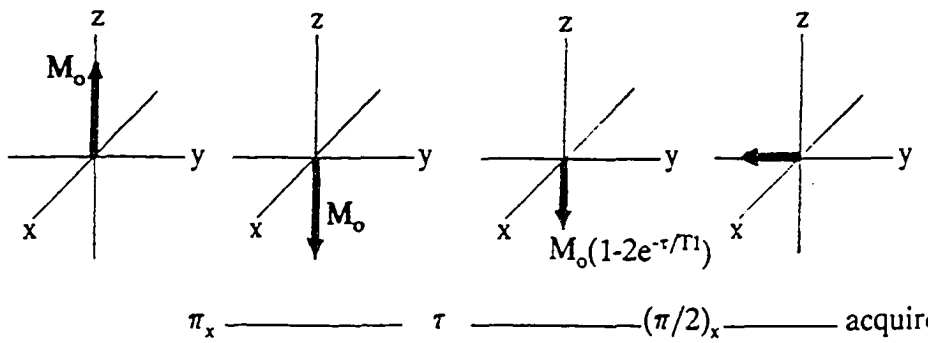

Figure 3.5 The inversion-recovery method for measurement of T_1.

Figure 3.6 illustrates an example of the free induction decay signals in D_2O at different value of τ. The phase of the signal is inverted as τ passes through τ_o, $\tau_o = T_1/\ln 2$.

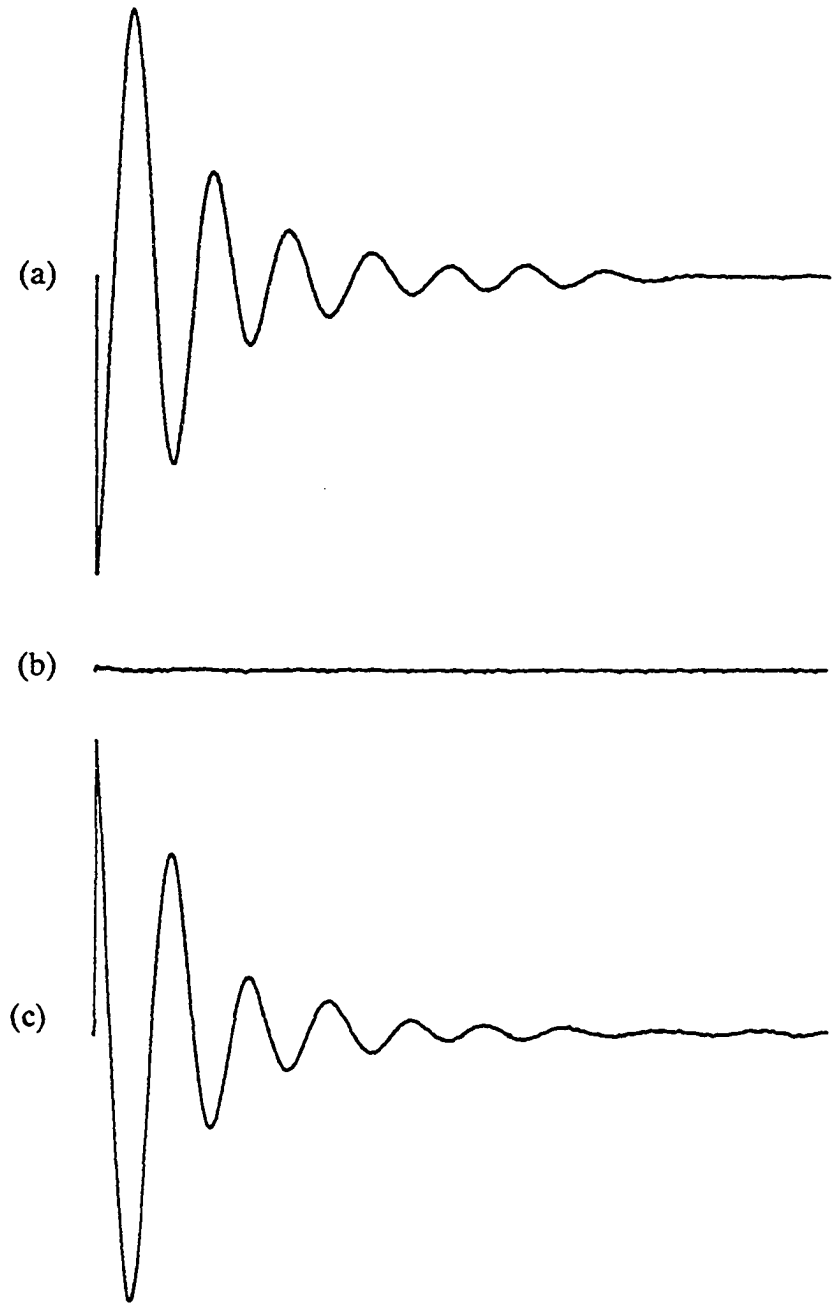

Figure 3.6 Free induction decay signals of D_2O water recorded after 90° pulse when (a) $\tau \sim \tau_o/2$, (b) $\tau = \tau_o$, and (c) $\tau \sim 2\tau_o$, where $\tau_o = T_1/\ln 2$ corresponding a null signal.

Chapter 4. X-ray and DR Results

4-1. X-ray Diffraction

Photographically recorded X-ray diffraction patterns of Kapton-H films of 25 μm and 125 μm as well as those for Upilex films 25 μm and 125 μm are shown in Fig. 4.1. and Fig. 4.2, respectively. There are basically two diffraction rings for each kind of film. Since only a single layer of film was used, the contrast between bright ring and black background is not very good. For each kind of film the diameter of the rings for different thickness sample are almost the same. On the other hand, the size of rings of BPDA-PDA films is significantly bigger than that of PMDA-ODA. To obtain more information from diffraction profile, we need to introduce Bragg's equation

$$\lambda = 2d\sin\theta \qquad 4\text{-}1$$

where λ is the wavelength of X-ray beam, d is defined as the spatial distance between two adjacent atomic layers for ideal crystal structure, and θ is angle between the incident beam and a specific atomic layer. Referring to the schematic diagram of the X-ray experiment set up, Fig. 3.1, it is clear that the angle θ can be calculated from the diameter of the diffraction ring and the distance between the sample and the photographic film which is equal to 10 cm. As consequence of this the distance d can be easily figured out from Bragg' equation. Table 4.1 shows the calculated d-spacing values corresponding different rings and films.

(a)

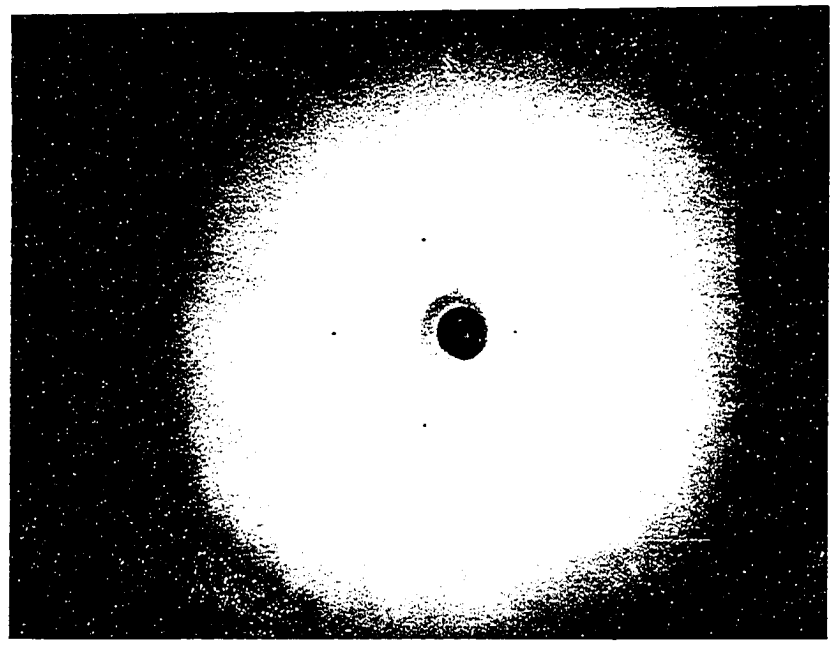

(b)

Figure 4.1 The X-ray diffraction photographs of Kapton films of (a) 125 μm and (b) 25 μm.

(a)

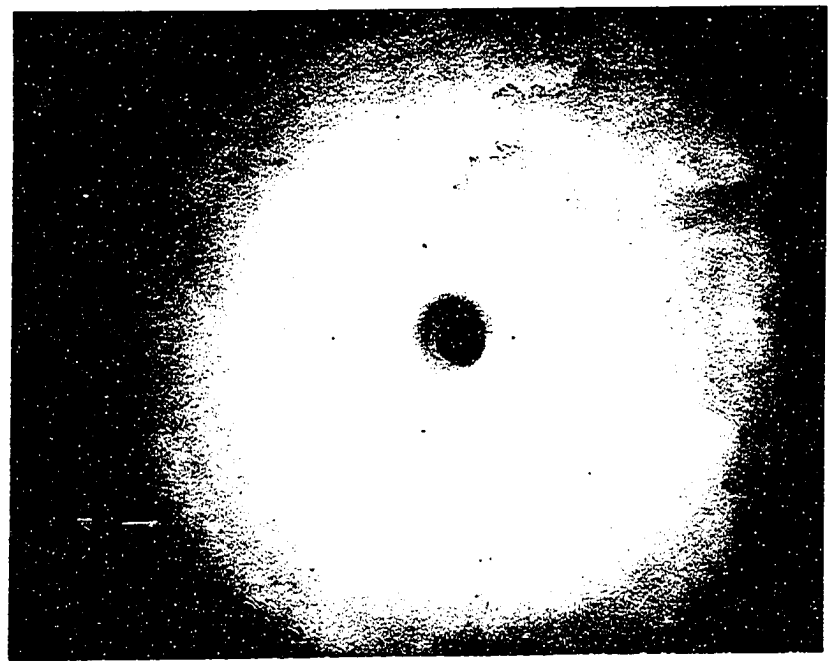

(b)

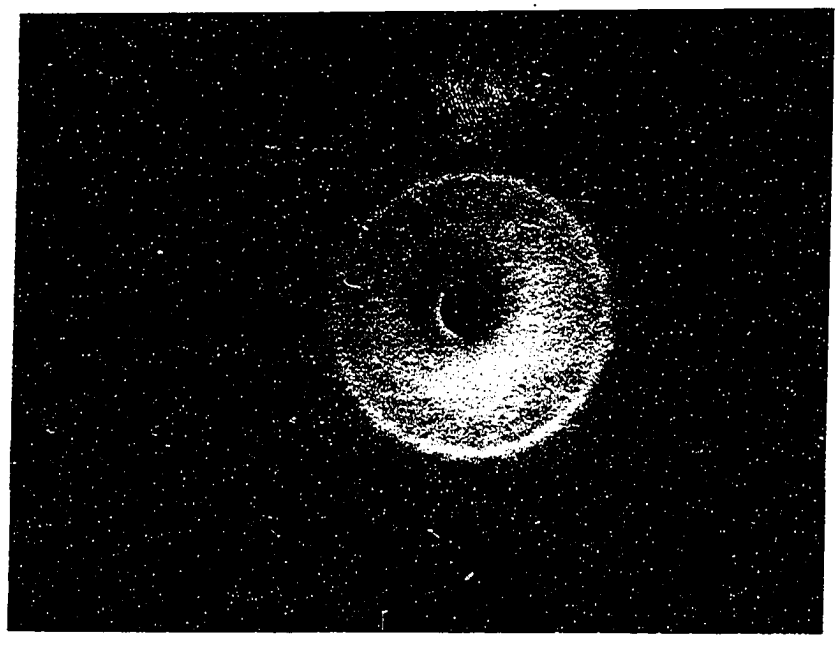

Figure 4.2 The X-ray diffraction photographs of Upilex films of (a) 125 μm and (b) 25 μm.

Table 4.1 Values of d-spacing for Kapton-H and Upilex-S films

Film	Ring diameter (mm)	D-spacing (Å)
K1 (125 μm)	19	16.3
	50	6.3
K4 (25 μm)	19	16.3
	*	*
US1 (125 μm)	39	8.0
	64	5.0
US4 (25 μm)	38	8.2
	63	5.1

* The intensity of this ring is too weak to be seen.

Our results for Kapton films are very close to that reported by Russell [13] and Kochi [12]. In their works the d-space of ca. 16 Å is attributed to polymer repeat units of polyimide and shorter d-spacing is attributed to the interference of adjacent polymer chains. Note that the length of the repeat unit of PMDA-ODA is ca. 18 Å [6,13], the difference between the real length ca. 18 Å and the d-space of ca.16 Å was explained by a zigzag conformation of polyimide [13]. It is well accepted that the PMDA-ODA molecular chains bend at ether oxygen linkage with a bending angle of 118°. Figure 4.3 shows the zigzag conformation of PMDA-ODA. Based on the bending angle 118° and monomer length of ca. 18 Å, the projection of the monomer along the polymer chain direction is calculated at 16.8 Å, which is almost the same as the value in Table 4.1.

For Upilex-S film, the smaller ring corresponds to a repeat unit with a length of ca. 8 Å which is only half that of Kapton film. On the other hand, the intermolecular distance (about 5 Å) is of the same order of that of Kapton film. The significant shortening of monomer length and slight reduction of interchain spacing (relative to Kapton) are quite consistent with the fact that the BPDA-PDA films are much stiffer than PMDA-ODA films.

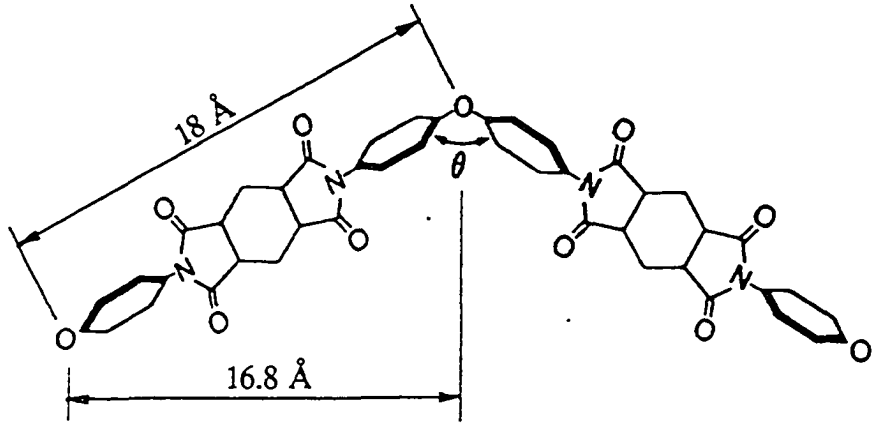

Figure 4.3 A zigzag conformation of polyimide PMDA-ODA. The bending angle θ is 118°.

4-2. Dielectric Relaxation

The dielectric relaxation measurements were performed by Dr. B.S. Lim in Professor Nowick's laboratory at Columbia University. Here we present a summary of the results. The polyimide films which were exposed to moisture exhibit a double peak in the γ relaxation region (near 200 °K). Typical dielectric relaxation loss spectra of 15 μm thickness film, after saturation with moisture at 100 %RH, are plotted against temperature for several fixed frequencies in Fig. 4.4. In contrast to a dry film which showed no dignificant dielectric loss in the temperature range of 50 - 300 °K, the sample treated in a moisture environment shows a main relaxation peak, referred to as γ_1, at 210 °K, as well as an auxiliary peak called γ_2 at 140 °K (the peak temperatures are quoted for a 1 kHz frequency). These two peaks may reflect the existence of two different sites of water molecules, hereafter labeled γ_1 site and γ_2 site. In fact, the behaviour of water molecules at the two sites is the major object of this research.

4-2.1. Thickness Effect

The intensities of the dielectric relaxation peaks due to moisture were monitored as a function of film thickness for Kapton film, as shown in Fig. 4.5. It is interesting that the intensity of γ_2 peak increases with increasing film thickness, however, the intensity of γ_1 peak does not show any systematic relation with film thickness. These results are summarized in Table 4.2.

Table 4.2 Dielectric relaxation peaks (at 1 kHz) for water saturated Kapton films.

Films	γ_2 Peak (low temp.) $\tan\delta_{max.}\times10^5$	T_p	γ_1 Peak (high temp.) $\tan\delta_{max.}\times10^5$	T_p	γ_2/γ_1 (%)
K1(125μm)	1520	155	1470	214	103
K2(75μm)	1225	145	1220	211	100
K3(25μm)	1015	143	1175	218	86
K4(7.5μm)	670	140	1165	225	58

4-2.2. Relative Humidity Effect

Other than the thickness effects, the water content in the sample also has a strong effect on dielectric relaxation spectrum. Figure 4.6 shows the spectrum of the spin-coated film (15 μm) at a frequency of 1 kHz after equilibrium water uptake in various relative humidities. There are still two γ peaks. The γ_2 peak is very sensitive to the total moisture absorbed. It falls off sharply after treatment at lower relative humidity of 75 %RH and almost disappears when processed at 23 %RH. However, the γ_1 peak over the same range of relative humidity decreases only a small amount. Table 4.3 shows the intensities of dielectric relaxation peaks of spin-coated 15 μm film as a function of various relative humidity equilibration.

The dielectric constant ϵ was also measured for the same film at different relative humidities. From the results of ϵ, the dipole moments of water at γ_1 and γ_2 sites are calculated (the detailed calculation is not shown here). The dipole moment of water in γ_2 site is 7.3×10^{-30} C·m and that for γ_1 site is 5.5×10^{-30} C·m. Note that

the value for γ_2 site is bigger than that of free water in liquid. This enhanced dipole moment will be discussed later in Chapter 6.

Table 4.3 Dielectric relaxation peaks (at 1 kHz) of spin-coated film as a function of relative humidity.

Relative humidity(%)	γ_2 Peak (low temp.) $\tan\delta_{max.}\times10^5$	T_p	γ_1 Peak (high temp.) $\tan\delta_{max.}\times10^5$	T_p	γ_2/γ_1 (%)
100	919	138	1131	211	81.3
75	595	135	1045	214	56.9
49	130	130	930	217	38.7
23	*	*	728	218	*

4-2.3. Solvent Effect

The intensities of the dielectric relaxation peaks were monitored after saturation by various solvents. The equilibrium concentrations of these solvents in films were mentioned in the Chapter 3. Significant changes that were observed are shown in the following figures. The spectrum of methanol and acetic acid absorbed in 50 μm Kapton film are shown in Figure 4.7 and Figure 4.8, respectively. Acetic acid gives rise only to a high temperature peak, which is quite similar in appearance to γ_1 in water-containing films, while methanol shows only a low temperature peak which is similar to the γ_2 water peak. An observed phenomenon for Upilex-S film is that it does **NOT** absorb methanol or acetic acid. This result tell us that the solvent

absorption is dependent not only on physical morphology but may be also on possible chemical reactions between residuals of polyimide (e.g. unpolymerized polyamic acid, or impurities associated with the polymerization reaction) and solvent. Nevertheless, it is unlikely that any specific chemical interaction may cause the lack of absorption of methanol and acetic acid, thus, it is very likely attributable to the much more compact polymer structure of Upilex film evidenced by X-ray results. As a result of this, the larger volume of bigger solvent molecules cannot fit into the small space between the polymer chains.

4-2.4. Backbone Structure Effect

In addition to study of the PMDA-ODA films, similar work on another types of polyimide are performed. The BPDA-based polyimides have a more rigid backbone structure which should lead to interesting effects on the γ_1 and γ_2 peaks of water-containing films. The effect on permeability of other solvents was discussed above.

The DR spectra of 50 μm Upilex-S (BPDA-PDA) film with of ca. 1.6 wt% water equilibrated at 100 %RH, thus corresponding to saturation, is shown in Figure 4.9. Figure 4.10 diplays the spectra of water saturated Upilex-S films at four different thicknesses. Two distinct peaks were also observed as in Upilex films. Comparing with PMDA-ODA films, the separation of peaks is slightly bigger, especially for thin films, which means that the peak's position is shifted to higher temperature for γ_1 peak, and the lower temperature for γ_2 peak. The strength of dielectric relaxation is much lower than that of the Kapton films due to lower moisture content (see Table

3.3). Figure 4.10 displays the DR spectrum for the Upilex-R (BPDA-ODA) film after saturation with moisture at 100 %RH. Unlike other two films saturated at 100 %RH, Upilex-R film exhibits a strong γ_1 peak but very small γ_2 peak. The comparison of the dielectric relaxation spectra of the three types of films (Kapton-H, Upilex-S and Upilex-R) is shown in Figure 4.11. It is interesting that the Upilex-R film exhibit a γ_1 peak comparable with the γ_1 peak in Kapton film, and its γ_2 peak is comparable with γ_2 peak in Upilex-S film.

Because deuterated solvents were employed for the NMR measurements, dielectric relaxation spectra were also examined for Kapton-H film treated by D_2O, and CH_3OD. The spectra for deuterated solvents were almost identical with those for regular solvents. Therefore, they are not presented in this thesis.

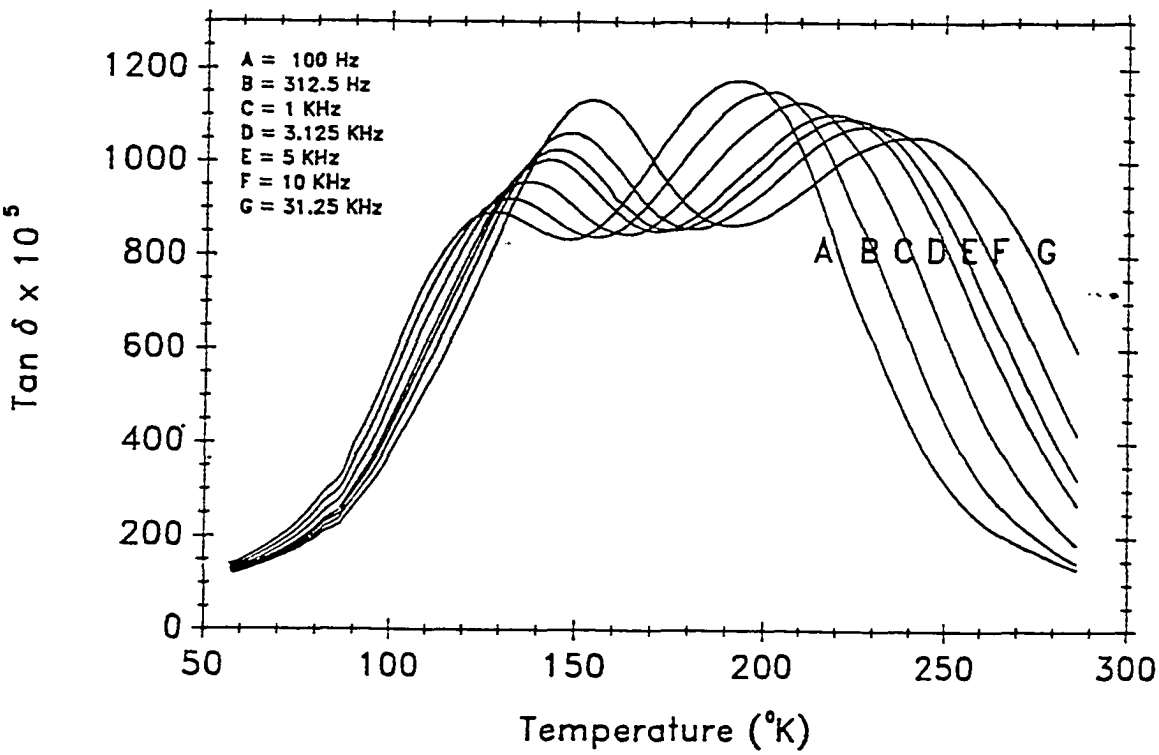

Figure 4.4 Dielectric relaxation spectra of spin-coated 15 μm PMDA-ODA film saturated at 100 %RH as a function of temperature. The individual curves are for various frequencies ranging from 100 Hz to 31.25 kHz.

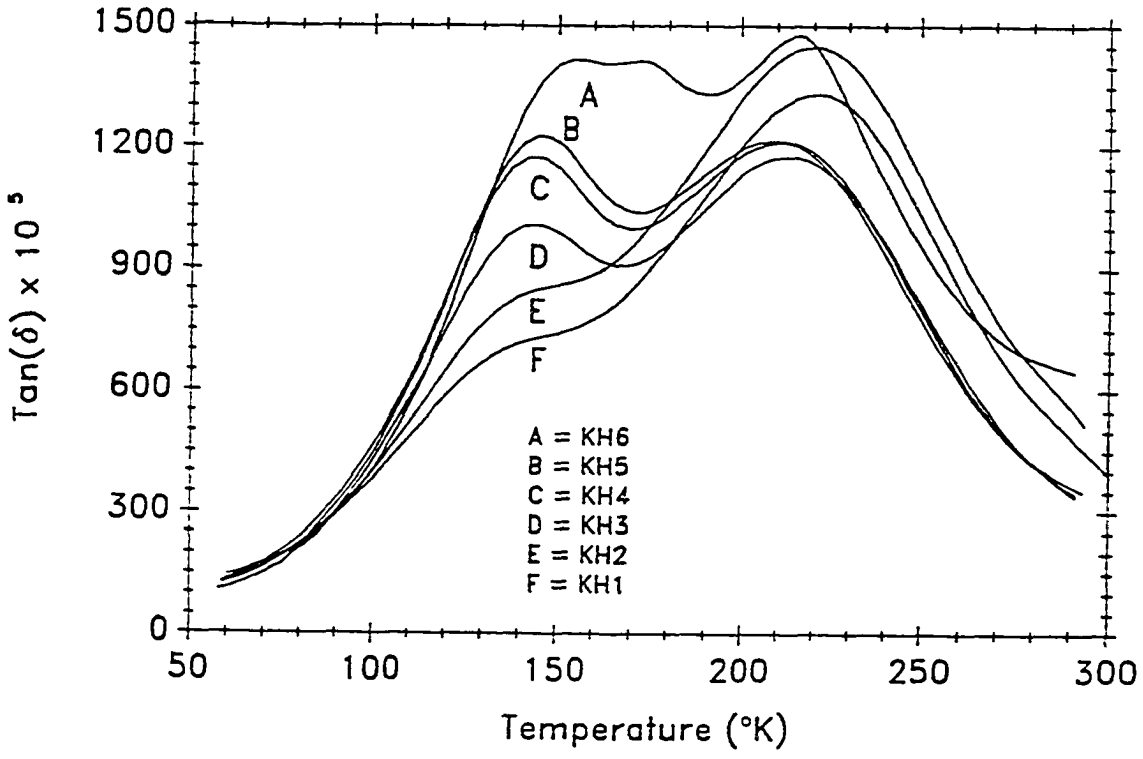

Figure 4.5 Dielectric relaxation spectra of the saturated Kapton-H films at 100 %RH as a function of temperature. The individual curves are for various thickness ranging from 7.5 μm to 125 μm.

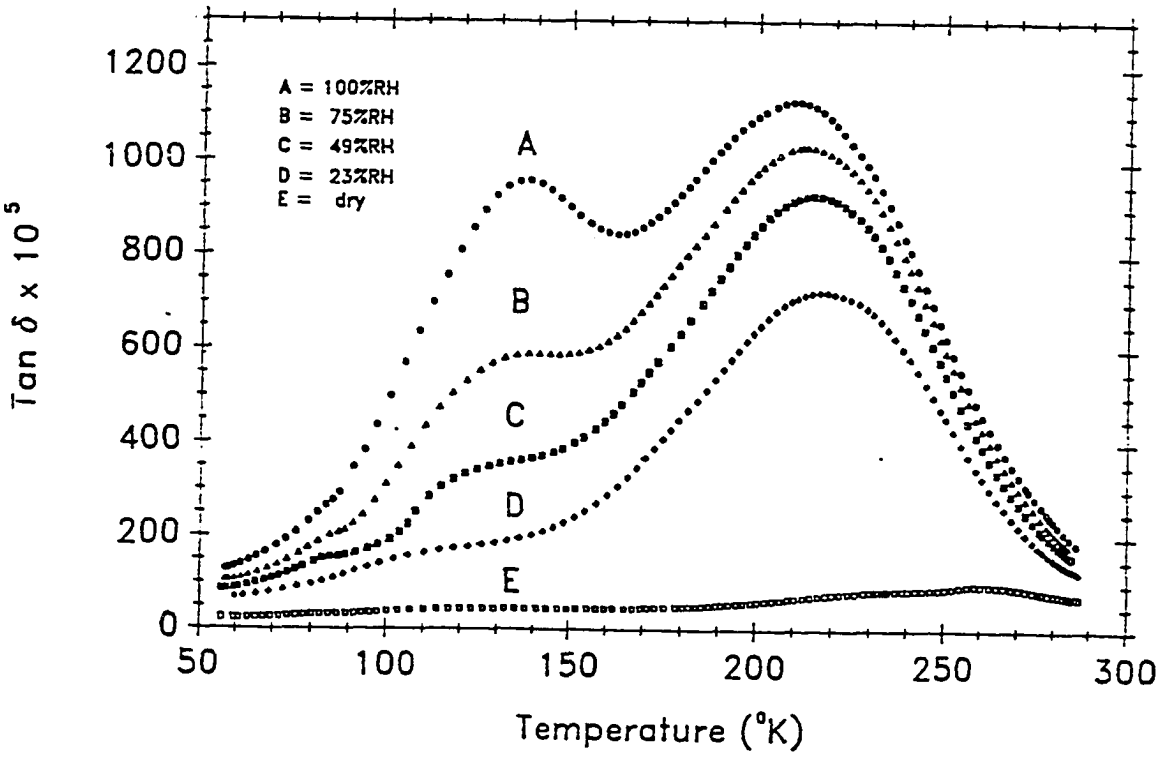

Figure 4.6 Dielectric relaxation spectra of the spin-coated 15 μm PMDA-ODA film saturated in various humidities (at the frequency of 1 kHz): 100, 75, 49, 23 %RH, and dry state.

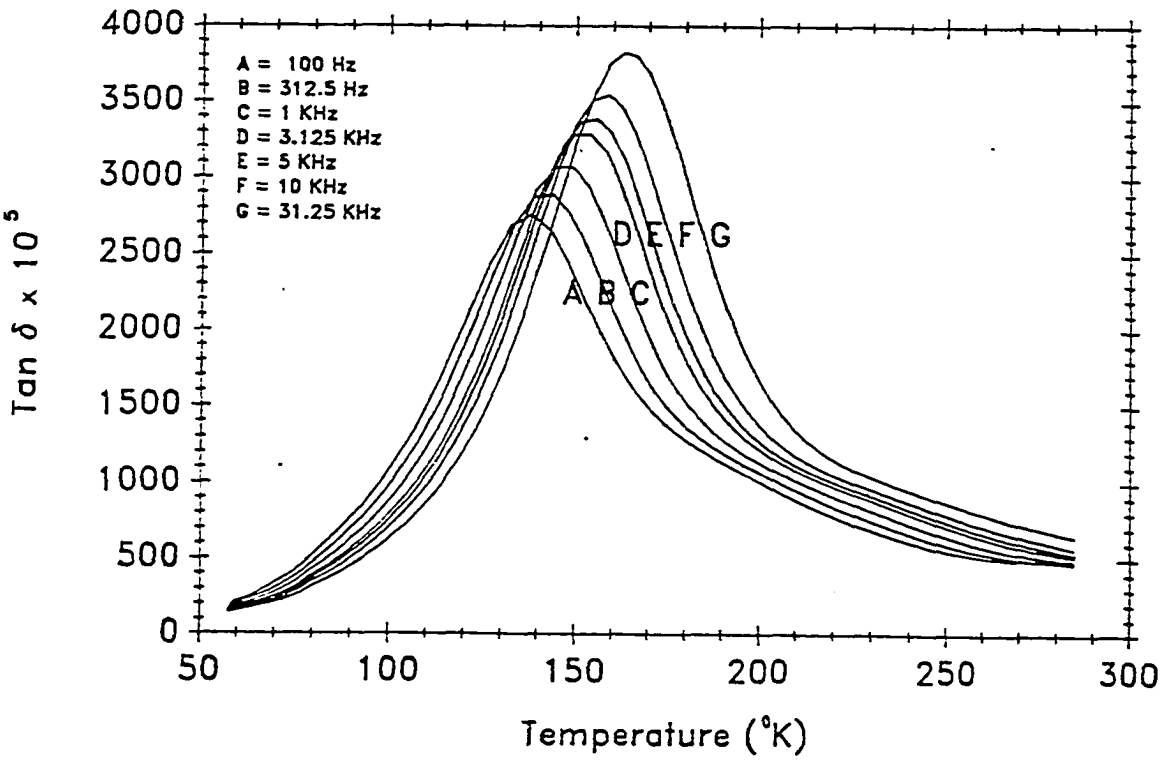

Figure 4.7 Dielectric relaxation spectra of Kapton-H film (50 μm), saturated by methanol (CH_3OH), as a function of temperature.

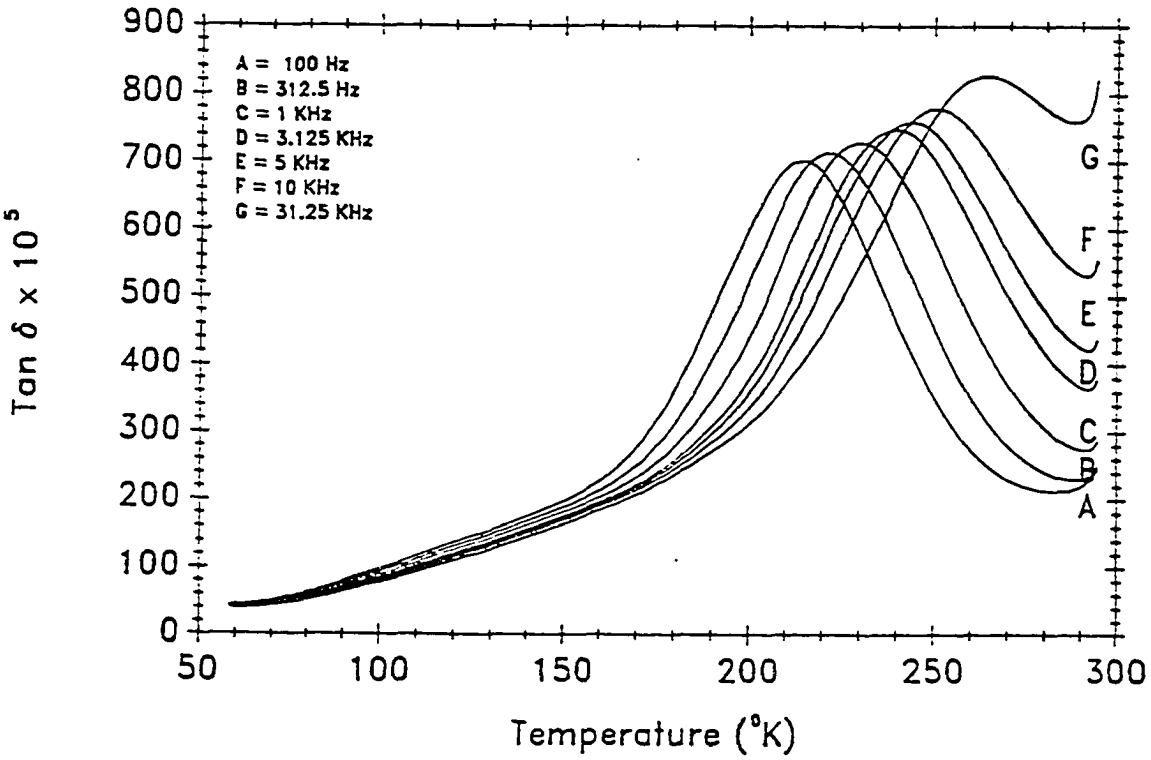

Figure 4.8 Dielectric relaxation spectra of Kapton-H film (50 μm), saturated by acetic acid (CH_3COOH), as a function of temperature.

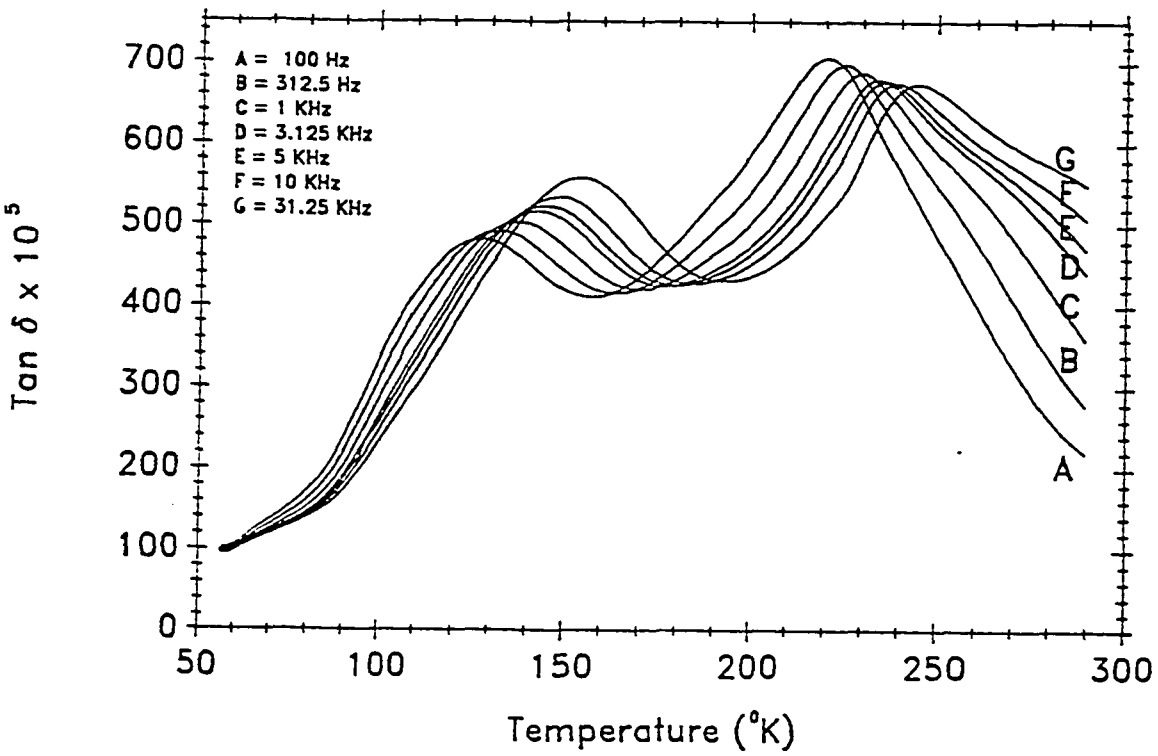

Figure 4.9 Dielectric relaxation spectra of Upilex-S 50 μm film, saturated in 100 %RH of water, as a function of temperature.

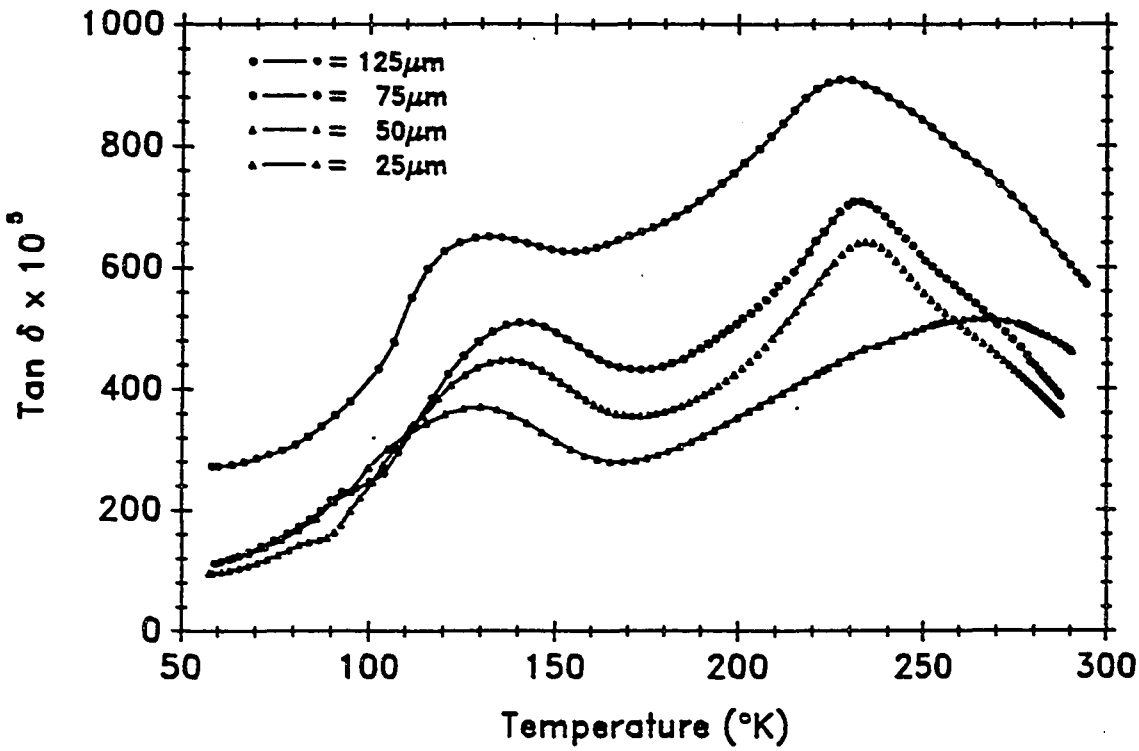

Figure 4.10 Dielectric relaxation spectra (1 kHz) of Upilex films with different film thicknesses, after saturated in 100% RH.

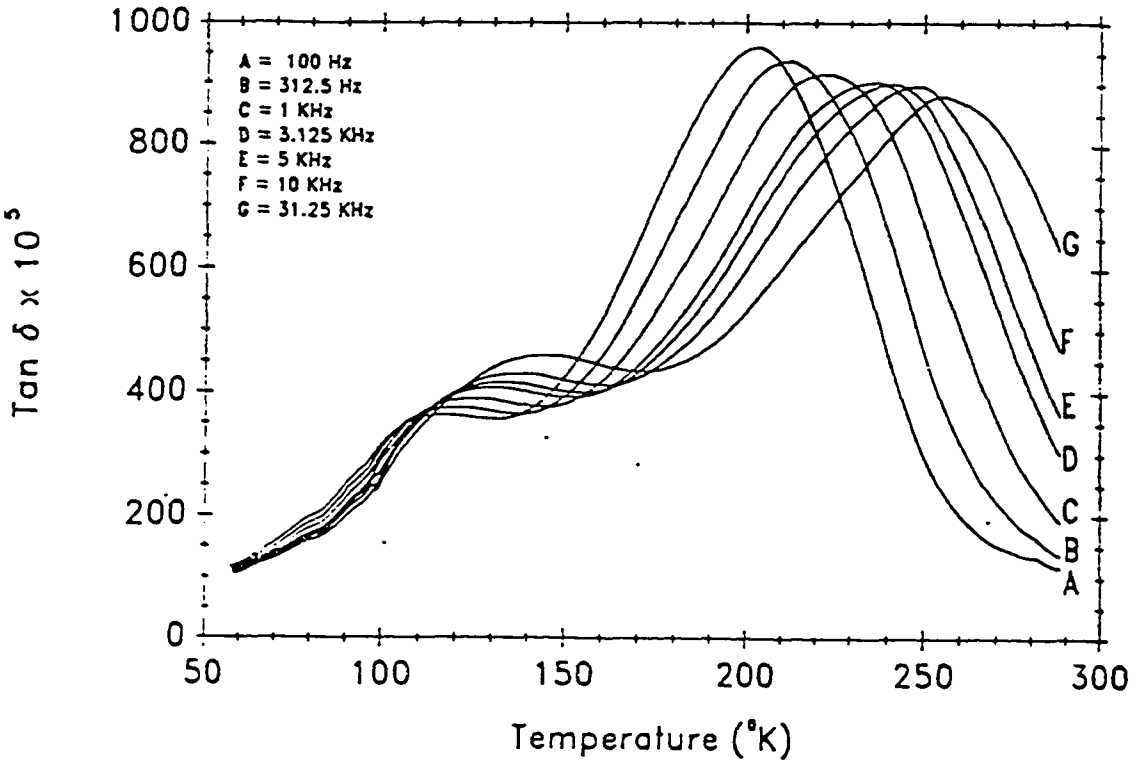

Figure 4.11 Dielectric relaxation spectra of Upilex-R 50 μm film, saturated in 100 %RH of water, as a function of temperature.

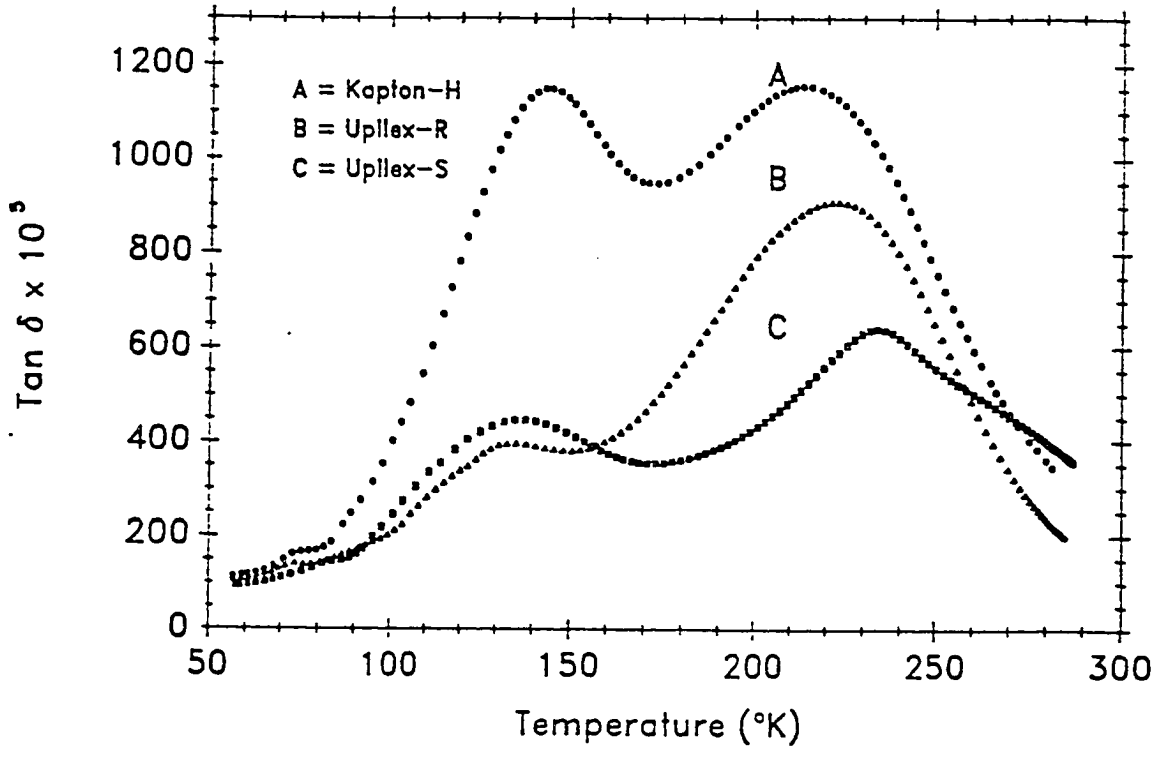

Figure 4.12 Dielectric relaxation spectra of moisture saturated (at 100 %RH) polyimide films (50 μm) at the frequency of 1 kHz. The individual curves are for (a) Kapton-H, (b) Upilex-R, and (c) Upilex-S.

Chapter 5 NMR Results

5-1. Summary of the NMR Parameters of Solvents

It is clear that a comparison of NMR parameters of liquid solvents with those of solvents absorbed in the polymer could provide information about solvent molecular motion and their local environment in the polymer. For this reason some parameters of the solvents including H_2O, D_2O, $H_2{}^{17}O$, CH_3OD and CH_3COOD are summarized in this section.

The values of spin-lattice relaxation time T_1 at room temperature (25 °C) for (1) protons in H_2O, (2) deuterons in D_2O, CH_3OD, and CH_3COOD, and (3) oxygen-17 in $H_2{}^{17}O$ are listed in Table 5.1. The numbers noted by an asterisk (*) are cited from the references indicated there. It is clear that the values obtained in this work agree quite well with the literature values.

Table 5.1 Room temperature T_1 of the solvents utilized in this investigation

H_2O (s)	D_2O (s)	CH_3OD (s)	CH_3COOD (s)	$H_2{}^{17}O$ (ms)
3.6	0.41	0.29	0.13	6.9
3.5*[72]	0.40*[73]	0.29*[74]		6.7*[75]

T_1 values for these solvents at other temperatures can be found in the references cited there. The different T_1 values for various nuclei reflect the

differences of the interaction between nuclei and their surrounding environments. Proton relaxation is attributed to proton intramolecular dipole interaction and intermolecular dipole interaction [72,76]. The intramolecular dipole-dipole interaction is modulated primarily by the molecular rotation; the intermolecular dipole-dipole interaction is affected mainly by translational diffusion [76]. The contribution of the former to the total dipolar relaxation rate is estimated to account for ~60% and the latter for ~40% [76].

Deuteron and oxygen-17 relaxation is dominated by the much stronger quadrupole interaction compared with dipole-dipole interaction. This interaction is characterized by the quadrupole coupling constant (QCC). The values of QCC of deuteron and oxygen-17 in water of different states are listed in Table 5.2, according to the values cited in the references.

Table 5.2 Quadrupole Coupling Constant (QCC) of D_2O, CH_3OD and $H_2{}^{17}O$

Water		QCC	Reference
D_2O	(Gas)	315 (kHz)	77
	(Ice)	215	77
	(Liquid)	222	78
CH_3OD	(Liquid)	192	74
$H_2{}^{17}O$	(Gas)	10.2 (MHz)	75
	(Ice)	6.7	75
	(Liquid)	6.7	78

Values of QCC can be measured directly in the gas and solid phases, but can only be inferred from relaxation behavior in liquid samples. The QCC for deuteron in CH_3OD is also included.

These values indicate that the QCC in the liquid state is very close to that in ice while the value for gas molecules is 50% larger than for ice or liquid. The reason for this difference is that the electric field gradient (EFG) is stronger in gas molecules since molecules are well separated and there is no hydrogen bond between molecules which may affect the EFG at the position of deuteron or oxygen-17.

Another important parameter is the correlation time τ_c of water molecular reorientation. In general, τ_c is on the order of 10^{-12} second for a liquid. The τ_c of H_2O at 20 °C is about 3.5×10^{-12} sec. D_2O has a τ_c of ca. 4.2×10^{-12} sec. and 2.0×10^{-12} sec. at 0 °C and 25 °C, respectively [73].

The asymmetry parameter η for D_2O is of ca. 0.1 [77]. It reaches 0.14 in the gas state and 0.1 in state of ice [73,75]. In oxygen-17 water, η was reported as 0.75 and 0.94 corresponding to gas and ice states [73,75].

5-2. Proton NMR

As we mentioned previously, two types of samples were prepared for NMR measurement: rolled and stacked films. The latter configuration was used to detect the orientation effect. Figure 5.1 illustrates the setup of the two different samples. The angle Ω indicates the angle between the static magnetic field and the plane of the film stack.

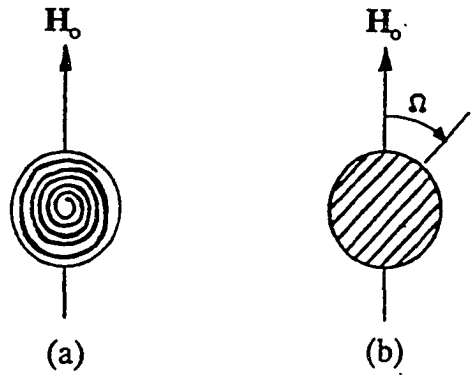

Figure 5.1 Sample configuration of (a) the rolled films and (b) the stacked films

It should be specified here again that all spectra shown in this work are in the magnitude mode. Therefore, the linewidth is bigger than that in absorption mode by a factor of 1.732.

5-2.1. Spectra of Dry Films

Three types of dry films have been measured: Kapton, Upilex-S, and Upilex-R. The proton signals were attributed to the hydrogens in the polymer backbone. The spectra of stacked Kapton films of 125 μm, 25 μm, and 7.5 μm thickness are shown in Figure 5.2, where curve (a) and (b) are the spectra of 125 μm at angle $\Omega=30°$ and $\Omega=90°$, curve (c) and (d) corresponding to 25 μm film at $\Omega=30°$ and $\Omega=90°$, and (e) and (f) corresponding to 7.5 μm film. The small narrow peaks on the top of all spectra may be due to very small amount of water in the films, unreacted monomers

which are not bonded to the main polymer chains, or residual N-methyl pyrrolidinone (NMP) solvent. Comparison of the curves at 30° and 90° gives a small difference in lineshapes: the ones at 90° exhibit a slight doublet while the ones at 30° show a more smooth curve. This small orientation effect tells us that macromolecules are not isotropically or randomly distributed in Kapton films, although the doublet is not very pronounced. It is also observed that the orientation effect for thin films is stronger than for thick films which indicates that the degree of anisotropy for thin films is higher than thick films. The same conclusion has been reaserched by means of optical measurements [14]. As suggested from the X-ray diffraction results [20], the anisotropy may arise from unequal shrinkage in the lateral and normal direction of the film as a result of the curing process.

Figure 5.3 includes the spectra of dry Upilex-S films (a)−(d) and Upilex-R film (e). The curves (a) and (b) correspond to 125 μm BPDA-ODA at 30° and 90°, the curves (c) and (d) refer to 25 μm BPDA-ODA at 30° and 90°. The curve (e) is the spectrum of rolled Upilex-R film of 50 μm thickness. All spectra for Upilex films have a pattern similar to those of Kapton films except the apparent linewidth is broader by about 50%. Table 5.3 shows typical apparent linewidth values of three types of polyimides at $\theta = 30°$.

Since intramolecular ^1H-^1H distances are quite similar for the two types of molecules, the linewidth difference is attributed to different degrees of motion. It is reasonable to assume that the greater broadening observed in Upilex is caused by the morphology difference of the films: the Upilex films are much stiffer than Kapton films. This difference indicates that the motions of protons in rigid Upilex film are

slower than those in the more flexible backbone of Kapton film, the dipole-dipole interaction will experience less averaging, thus leading to a greater linewidth.

In addition to the chemical structure difference, the films also show a linewidth increase as thickness is reduced for same type film. This thickness effect shows that the polymer chains are more rigid in thin films than in thick films.

Table 5.3 The apparent linewidth of dry polyimide films at $\theta=30°$

Film (μm)	Linewidth (kHz)
Kapton 125 μm	34.8 $\pm$0.4
Kapton 7.5 μm	43.6
Upilex-S 125 μm	52.4
Upilex-S 25 μm	62.0
Upilex-R 50 μm	48.8

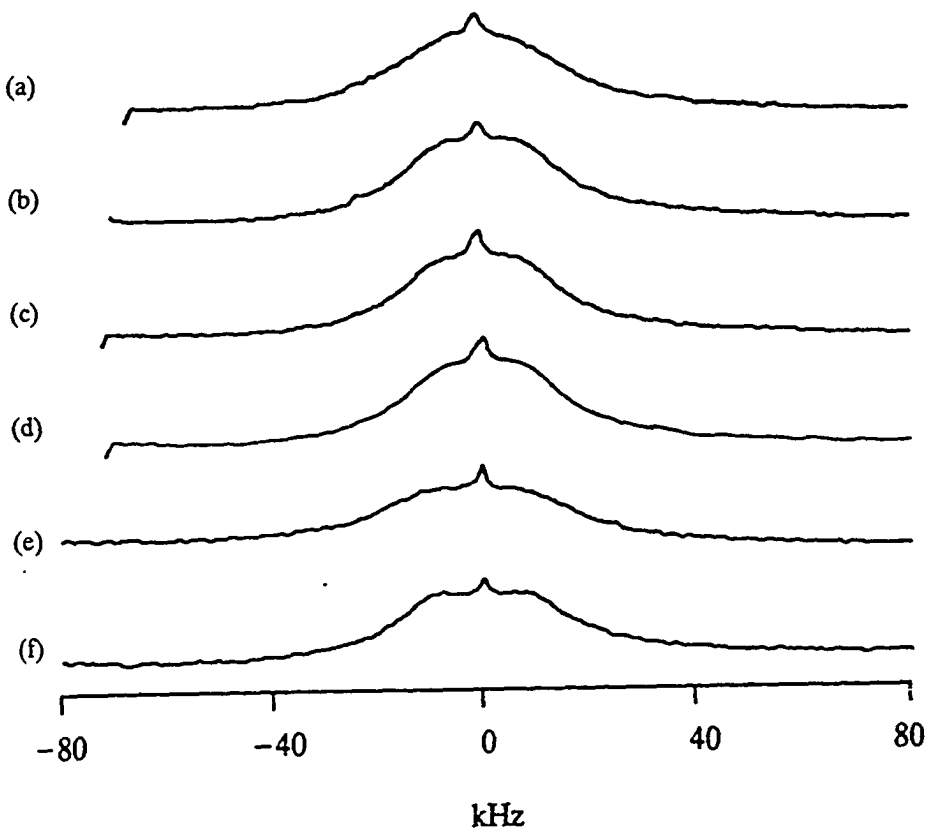

Figure 5.2 Proton NMR spectra of stacked dry Kapton films. 125 μm at (a) 30°, (b) 90°; 25 μm at (c) 30°, (d) 90°; 7.5 μm at (e) 30°, (f) 90°.

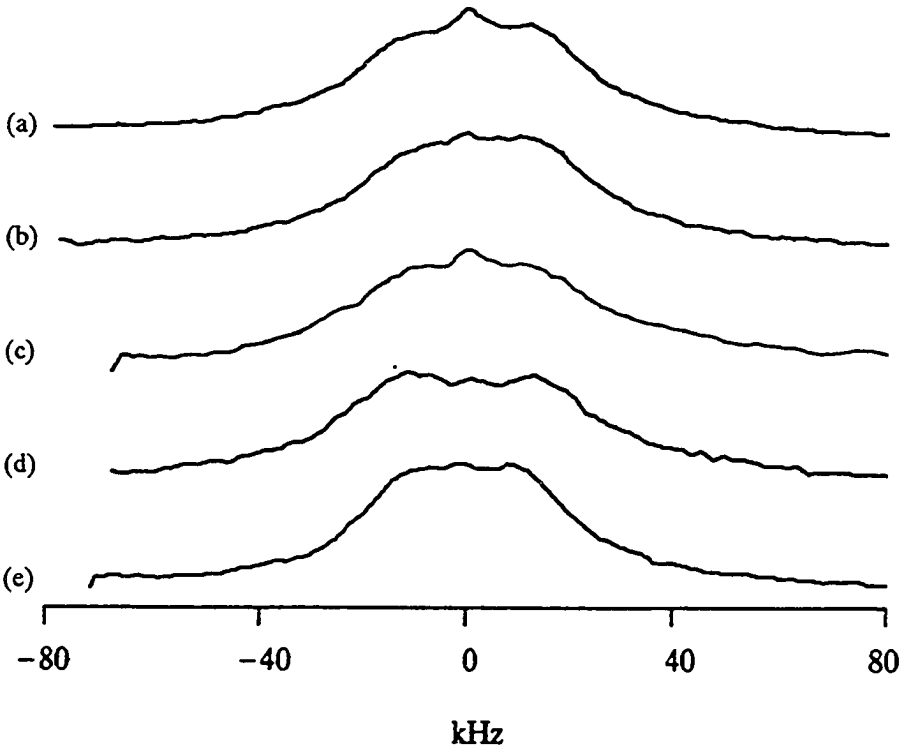

Figure 5.3 Proton NMR spectra of dry Upilex films. (a), (b) Upilex-S 125 μm at 30° and 90°, (c) and (d) Upilex-S 25 μm at 30° and 90°, (e) rolled Upilex-R 50 μm.

5-2.2. Spectra of Wet Films

Figure 5.4 displays the spectra of 125 μm Kapton film at 3.0, 2.2, and 1.8 wt% of H_2O as well as the spectrum of dry film. Each wet film spectrum contains a sharp peak superposed on a broad line. The height of the narrow peak increases as the water content is increased. The narrow peak is thus attributed to water absorbed in the polymer while the broad line is due to the polymer backbone. A similar result is shown in Figure 5.5 for 25 μm Upilex-S film at 1.69 and 1.14 wt% H_2O as well as at dry film condition. It is interesting to note that the linewidth of water molecules is much narrower compared with the polymer backbone, which means that water molecules are quite mobile and they are not strongly chemically bonded to the polymer chains.

Since the linewidth for water is much narrower than for the polymer chain, i.e. the time domain signal of water decays much slower than that for polymer chain, we were able to suppress the signal from the backbone by shifting the beginning point of acquisition behind the fast decayed broad line signal and acquire the rest of the signal of water with an intensity loss less than 15%. In addition, to investigate the dynamic process of water molecular motion in Kapton film, the variable temperature measurements of 125 μm Kapton with 3.0 wt% H_2O waer performed in the range of -40 to 20 °C. The spectra associated with absorbed water at several different temperatures are shown in Figure 5.6.

The linewidth gradually increases from 0.98 kHz at 22°C up to 4.76 kHz at -42°C; the magnetic field inhomogeneity given by the linewidth of the liquid water is about 200 Hz, so that instrument effects are negligible here. As the temperature

falls below -50°C, the water linewidth increased substantially to a value comparable to that of the backbone, so that it was very difficult to separate them. To get the activation energy of the dynamic motion of water in Kapton, the reciprocal of the linewidth was plotted as a function of inserse temperature (standard Arrhenius plot), as shown in Figure 5.7. The curve fitting of the slope of the data yields to an activation energy of ca. 0.14 eV.

The orientation effect was also checked for the narrow NMR line associated with water molecules. Figure 5.8 shows the spectra of 125 μm Kapton at 3.1 wt% H_2O with the angle (a) Ω=90° and (b) Ω=30°. There was no splitting observed for any orientation. However, the linewidth reduced from 1.3 kHz at Ω=90° to 1 kHz at Ω=30°. The same weak orientation effect was observed for Kapton films of other thicknesses. We will discuss this orientation phenomenon later with the orientation phenomena of deuterium NMR.

5-2.3. Spin-lattice Relaxation Time

Although the spin-lattice relaxation time T_1 for protons of water and of polyimide are different, it was found that, unlike their linewidth differences, their T_1 differences are not big enough to separate them presicely. Thus it is not easy to measure T_1 value for protons of water molecules absorbed in polyimide film. However, the T_1 of protons in polyimide films was measured for all dry samples. The T_1 values of Kapton and Upilex films are listed in Table 5.4.

Table 5.4 T_1 values of protons for dry and wet (D_2O) polyimide films

Film (μm)	T_1 dry (s)	D_2O (wt%)	T_1 wet (s)
Kapton 125	0.75	3.0	0.96
Kapton 75	0.74		
Kapton 25	0.46	2.9	0.77
Kapton 7.5	0.37	3.1	0.58
Upilex-S 125	3.49	1.9	2.04
Upilex-S 25	3.39	2.0	2.81

It has been found that, in general, T_1 decreases as film thickness reduces. This T_1 decrease reflects the morphology difference of polyimide film with different thickness. Table 5.4 also shows that the T_1 values of Upilex films are significantly longer than T_1 of Kapton films. This dramatic difference is caused again by the different molecular mobility of macromolecules in two types of films.

To obtain the information of dynamic motion of polymer chains, variable temperature measurements were taken for both kinds of dry films. Arrhenius plots of T_1 are displayed in Figure 5.9 for 125 μm Kapton and for 125 μm Upilex-S. Both types of film show the trend of increasing T_1 as the temperature decreases. According to the spin-lattice relaxation theory summarized in Section 2-5 in Chapter 2, the molecular motion in dry films are slower than the Larmor frequency (37 MHz).

It has been observed that the volume of the film expands by a few percent

after the film was saturated with water. The behavior of the polymer chains may be changed as the result of water absorption. In the strict sense the properties of absorbed water molecules rely on the morphology of swollen films rather than dry films. So, the measurements of T_1 for polymer protons while films are wet could be somewhat useful. In order to avoid the interference of protons from water, we treated the sample with D_2O water, then detected the proton signals from the film backbone. The T_1 values for various films at full saturation of water are also shown in Table 5.4. It is very surprising that T_1 values of the two kinds of film shift in opposite directions for Kapton and Upilex films: T_1 increases for wet Kapton films while it decreases for wet Upilex film. The reason for this seemingly strange result is not clear yet. One possible explanation is that water may have a plasticizing effect on the polymer chains. That would tend to decrease the molecular correlation time. The opposite trends in T_1 for the two types of films could then result if their T_1 minima are below and above room temperature for Kapton and Upilex, respectively. The data in Figure 5.9 are not detailed enough to support or refute this hypothesis.

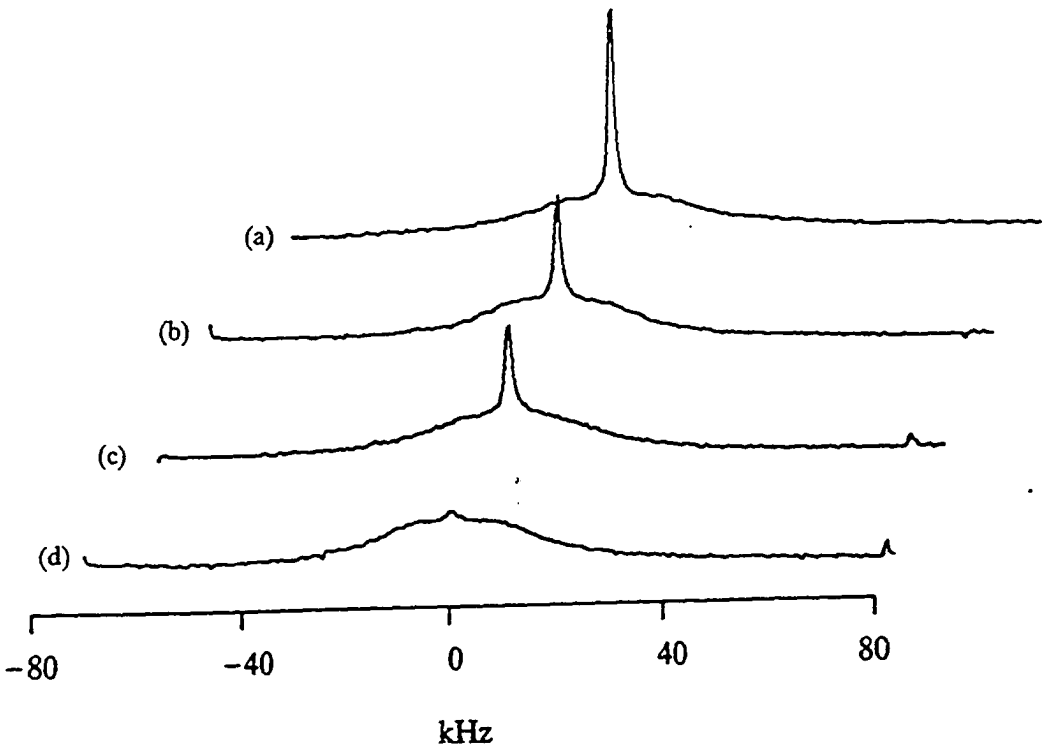

Figure 5.4 Proton NMR spectra of 125 μm Kapton with (a) 3.0, (b) 2.2, (c) 1.8 wt% H_2O, (d) dry film.

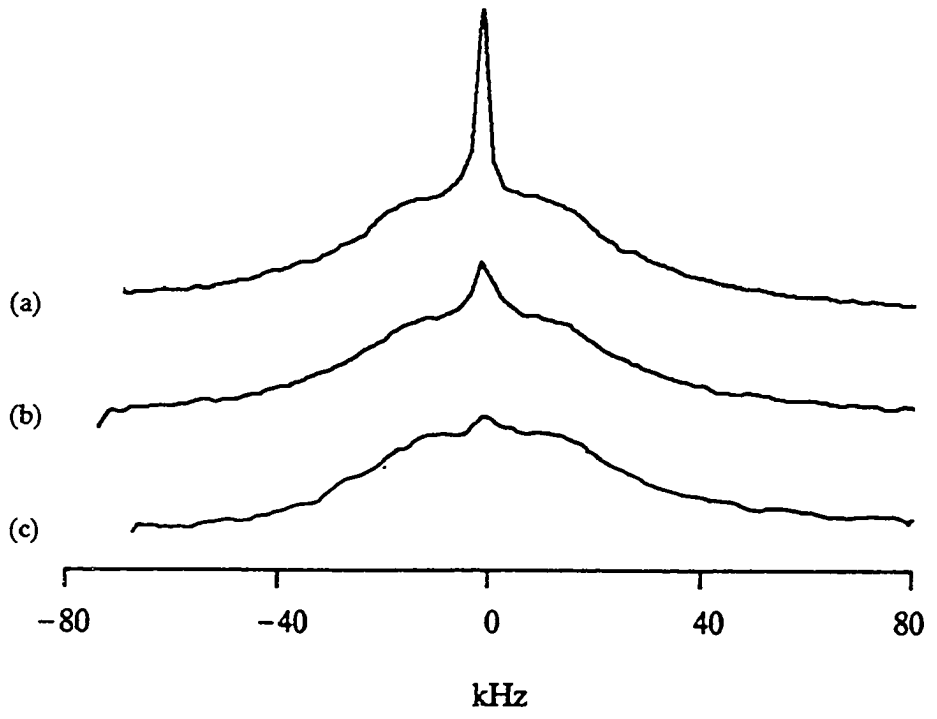

Figure 5.5 Proton NMR spectra of 25 μm Upilex-S with (a) 1.69, (b) 1.14 wt% H_2O. The curve (c) is dry film.

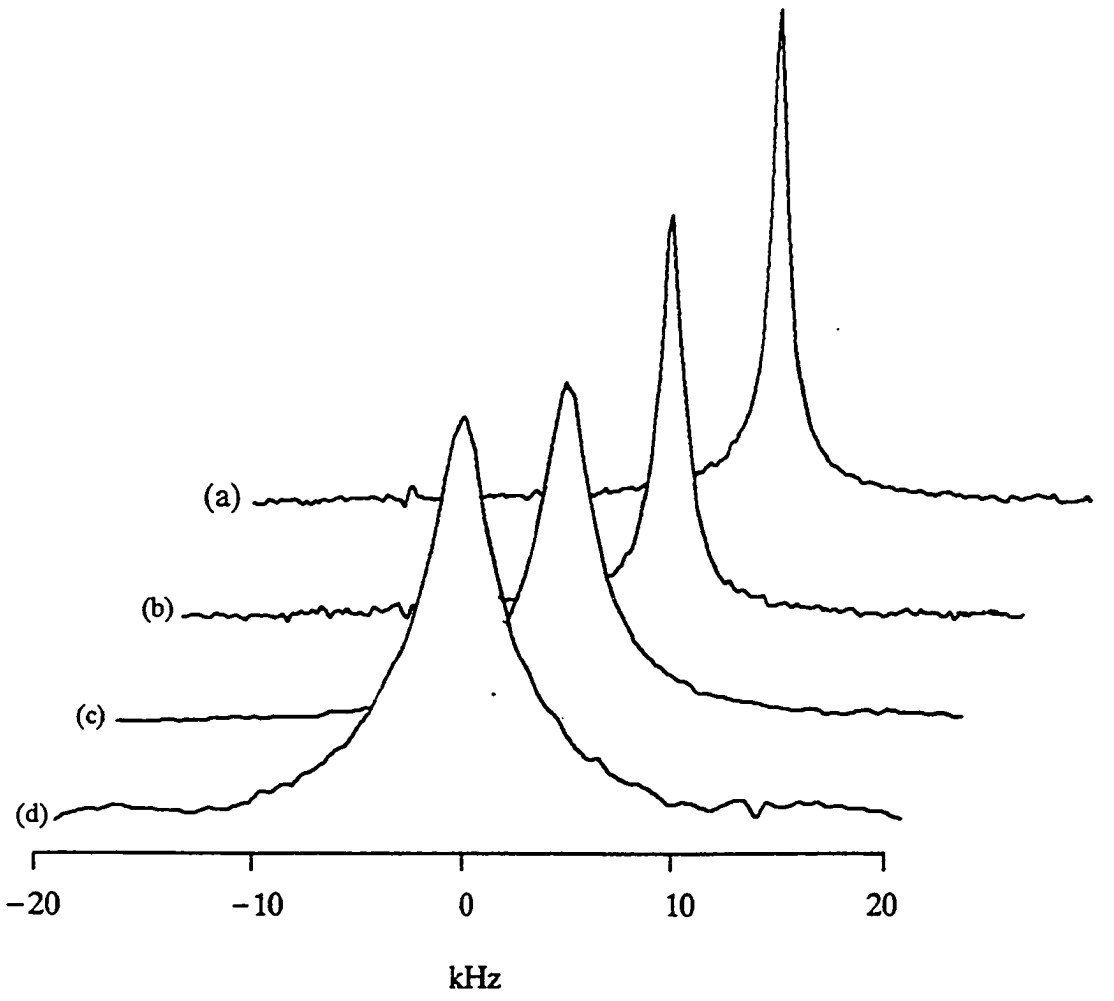

Figure 5.6 Proton NMR spectra of H_2O water in Kapton 125 μm film with 3.0 wt% H_2O at temperature of (a) 22°C, (b) 6°C, (c) −26°C, and (d) −42 °C.

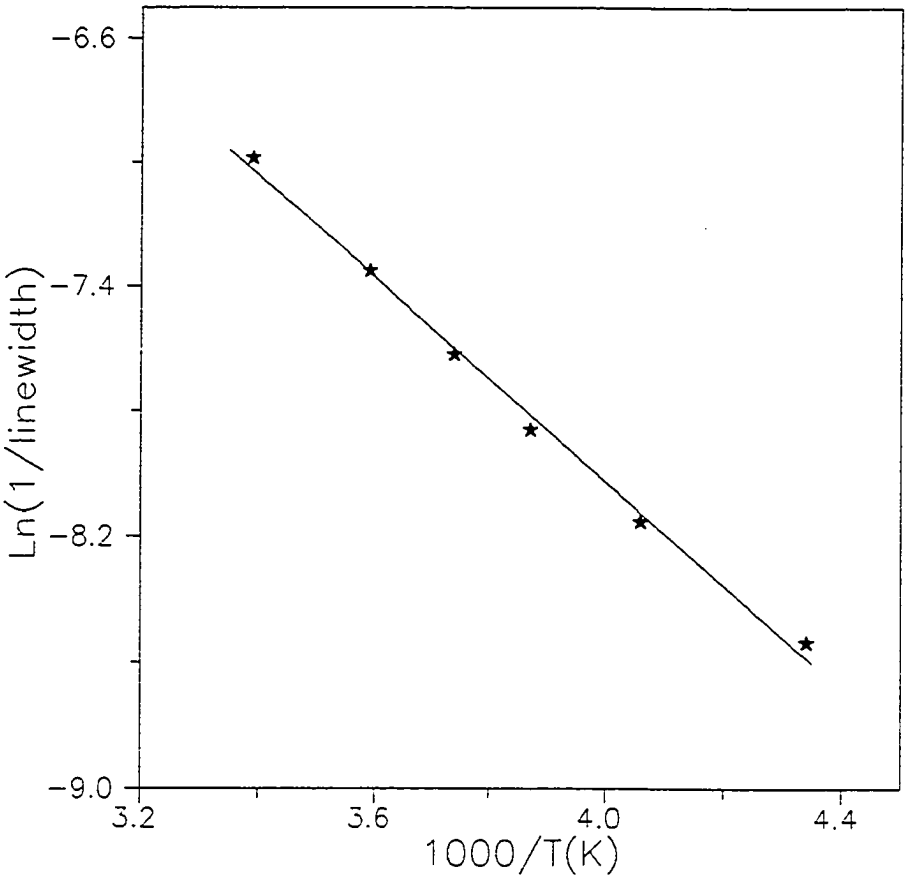

Figure 5.7 The diagram of the reciprocal of linewidth of H_2O in 125 μm Kapton vs. 1000/temperature.

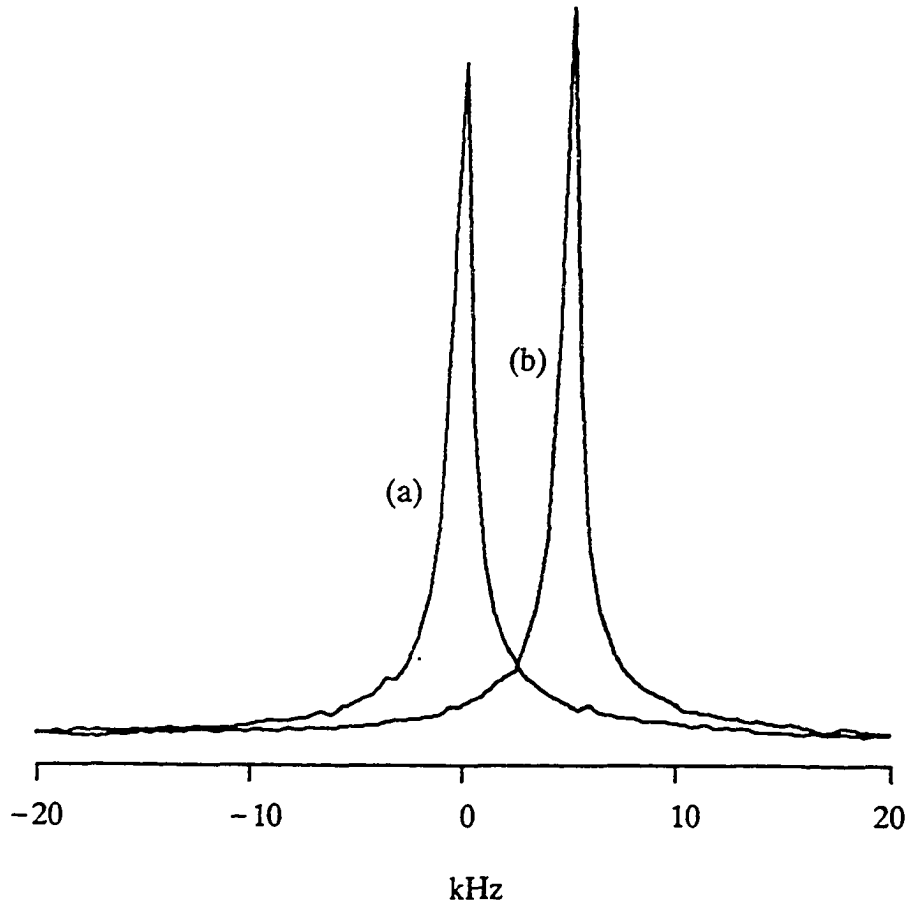

Figure 5.8 Proton NMR spectra of H_2O in stacked 125 μm Kapton while the films orient at (a) 90° and (b) 30°, the latter spectrum is shiftted to the right for display purposes.

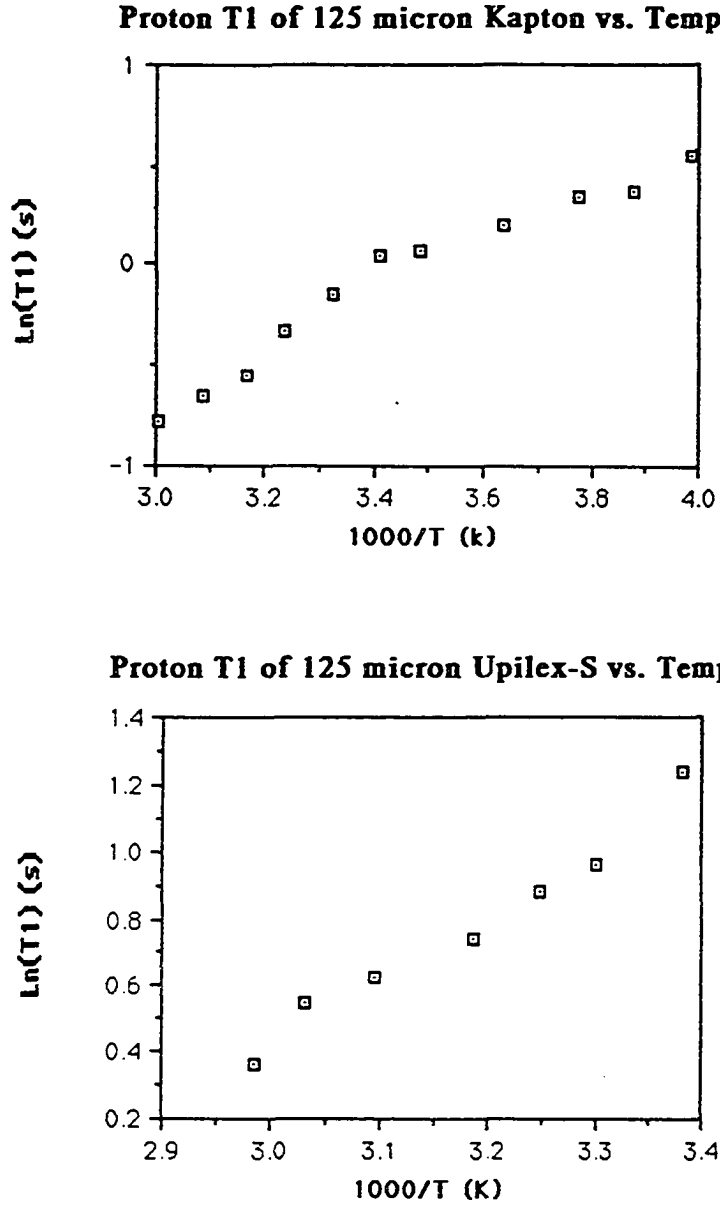

Figure 5.9 Proton spin-lattice relaxation time (T_1) vs. temperature for dry 125 μm Kapton film (top) and dry 125 μm Upilex-S film (bottom).

5-3. D_2O in Kapton Films

Both Kapton and Upilex films have been treated with D_2O water at different relative humidity to obtain films of various water content. Kapton films were prepared in rolled and stacked configurations, Upilex films were prepared in stacked films only.

5-3.1. Rolled Kapton Films

The results of rolled films are displayed as a function of film thickness (125, 75, 25, and 7.5 μm) and water content (100, 75, and 50 %RH) in Table 5.5. Figure 5.10 gives the spectra for Kapton 125 μm and 7.5 μm equilibrated at 100%, 75%, and 50% RH. The small narrow peak in the spectrum of 7.5 μm film at 3.1 wt% D2O is attributed to surface water which is most often observed in thin films at higher water content. For the two extreme cases, 125 μm at 3.4 wt% D_2O and 7.5 μm at 1.6 wt% D_2O, the linewidth increases from ca. 6 kHz to ca. 18 kHz. More data for the intermediate thickness and water content are included in Table 5.5.

Before further analysis of deuterium NMR data, it is noteworthy to compare the linewidth of the proton NMR spectrum of H_2O in polyimide with that of the deuteron NMR for D_2O in polyimide. The linewidth of H_2O in Kapton films is about 1 kHz due to the dipole-dipole interaction of proton pairs in water molecules, including ca. 200 Hz broadening by the magnetic field inhomogeneity. According to the Hamiltonian of the dipolar interaction, the line broadening in D_2O due to the dipole-dipole interaction between the deuteron pair should be 50 times smaller than that in H_2O, see section 2-3 in chapter 2. Therefore, the dipole-dipole interaction of

Table 5.5 Values of linwidth and T_1 of D_2O in rolled Kapton films at various D_2O concentrations

Sample	D_2O (wt%)	Linewidth (kHz)	T_1 (ms, 25 °C)
125 μm	3.1	6.6	20.2
	2.1	9.2	17.0
	1.3	11.0	16.0
75 μm	3.1	7.2	19.4
	2.1	8.4	18.5
	1.3	11.6	17.8
25 μm	2.1	9.8	16.5
	1.4	12.4	15.9
7.5 μm	2.6	12.4	12.5
	1.6	18.0	14.0

deuterons in D_2O could be neglected, and the 7-20 kHz linewidths of D_2O in Kapton films are thus attributable to the quadrupole interaction.

From Table 5.5 it can be seen that the NMR linewidths increase with either decreasing water content or decreasing film thickness. In DR results, the ratio of γ_1 to γ_2 (γ_1/γ_2) also increases with either decreasing water content or decreasing film thickness. Since the existence of two water molecular sites is clearly suggested by the presence of two distinct DR loss peaks, one may also assume that there are two

components of the NMR line for water melecules. However, they are not as clearly separated as in the case of DR. The correlation between DR and NMR results will be discussed more fully in chapter 6.

In order to obtain additional information regarding the nature of the two types of water molecular environments, T_1 measurements were undertaken. Room temperature T_1 values of films with varying thickness and water content are listed in Table 5.5. As in the case of NMR linewidth, one observes a trend in going from thin films with low water content to saturated thick films. The trend is that of increasing T_1. which varies from roughly 13 to 20 ms between the extremes. Again, T_1 measurements of saturated thick films reflect the average relaxation behavior of both sites. In any case the small difference in T_1 values of the two extreme samples makes it difficult to extract an accurate value pertaining to only a single water site.

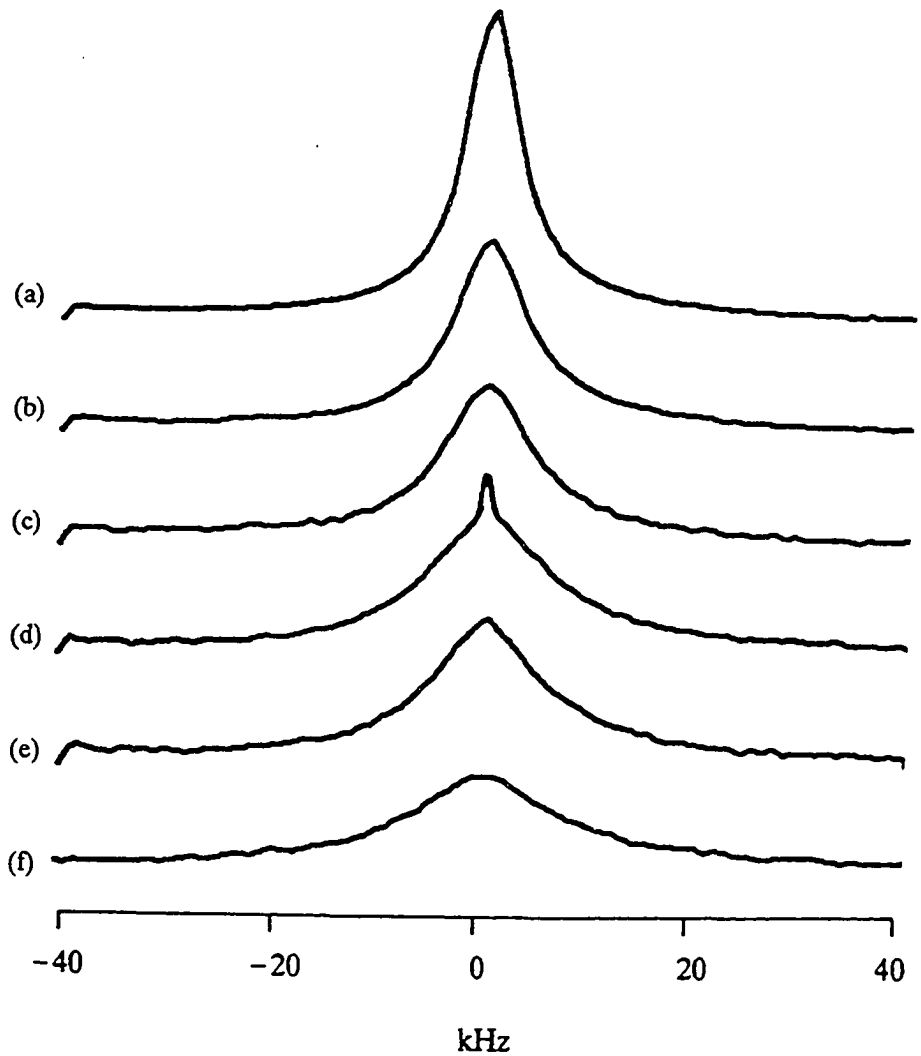

Figure 5.10 Deuteron NMR spectra D_2O in rolled Kapton films. (a)–(c), 125 μm at 3.4, 2.1, and 1.3 wt% D_2O; (d)–(f), 7.5 μm at 3.1, 2.2, and 1.6 wt% D_2O.

5-3.2. Orientation Effect of Kapton Films

The orientation effect was measured by changing the angle Ω between the film plane and the static magnetic field. The spectra of 125 μm Kapton with 3.1 wt% D_2O at various angles at room temperature are shown in Figure 5.11. One can observe that the splitting reaches a maximum value of ca. 4 kHz when the plane of the films is perpendicular to the magnetic field ($\Omega=90°$) and an approximate minimum when Ω is equal to 30°. The doublet in the spectrum is caused by the quadrupole interaction, and the splitting varies with the angle Ω.

To reveal the relation of the splitting to the orientation angle, computer simulation was performed. The simulation program was written in Quick Basic 4.5 computer language, the fitting curve can be chosen as Lorentzian or Gaussian configuration in either absorption mode or magnitude mode. The simulation program is described in the Appendix. The spectra shown in Figure 5.11 are decomposed into two identical components, their intensity, linewidth and separation were chosen in a such way that the superposition of them mostly fit the experiment spesctra. As an example, Figure 5.12 shows the simulation for the spectra of 125 μm Kapton with 3.1 wt% D_2O at orientation of $\Omega=90°$.

The values of the splittings are plotted in Figure 5.13 as a function of Ω, the solid curve representing the curve fitting function $A|\cos^2\Omega-1|$, where A is the constant factor $(3/4)(e^2qQ/h)S_{OD}$, see Equation 2-35. Note that the function $|\cos^2\theta-1|$ in equation 2-35 has a maximum when $\theta=0°$ while the experiment data reach a maximum at $\Omega=90°$. The exact value of Ω corresponding to the minimum is then 35.3°. The comparison results in a correspondence of $\theta=\Omega-90°$ which means that the

averaged quadrupole interaction axes of D_2O molecules are perpendicular to the film plane. The averaged axis here represents the net quadrupole interaction axis contributed by two O-D bonds in D_2O molecule. The order parameter, S_{OD}, represents the degree of orientation of the O-D bonds with respect to a preferred axis fixed in the sample that is not averaged out by translational or rotational motion of the water molecules. For a "rigid" O-D bond, e.g. that which exists in D_2O ice, the quadrupole doublet splitting is approximately 170 kHz. The spectral splitting shown in Figure 5.11 leads to a value of S_{OD} of several percent.

Figure 5.14 shows the spectra of 125 μm Kapton with 1.3 wt% D_2O at several orientations with respect to the external magnetic field. Although the spectral splitting of the kind shown in Figure 5.11 is not observed, there is clearly an angular dependence to the linewidth according to the factor of $|3\cos^2\Omega-1|$. The disappearance of the resolved doublet results from the linewidth broadening at lower water content corresponding to the predominant contribution of the γ_1 sites, as discussed in the previous section.

The measurements of the orientation effects for 25 μm and 7.5 μm at 100% RH and 75% RH were also performed. For the fully saturated 25 μm film a clear doublet was observed like the pattern shown in Figure 5.11. For 7.5 μm sample, there was no resolved doublet observed, even saturated at 100% RH. However, the apparent linewidth varies according to the same angular dependence. As an example of thin film, Figure 5.15 displays the spectra of 7.5 μm Kapton at 2.4 wt% D_2O at several angles. Again, the very narrow peak is due to the surface water molecules. In general, all spectra follow a trend that the linewidth becomes broader with either

decreasing water content or decreasing thickness, which may mask the resolved doublet.

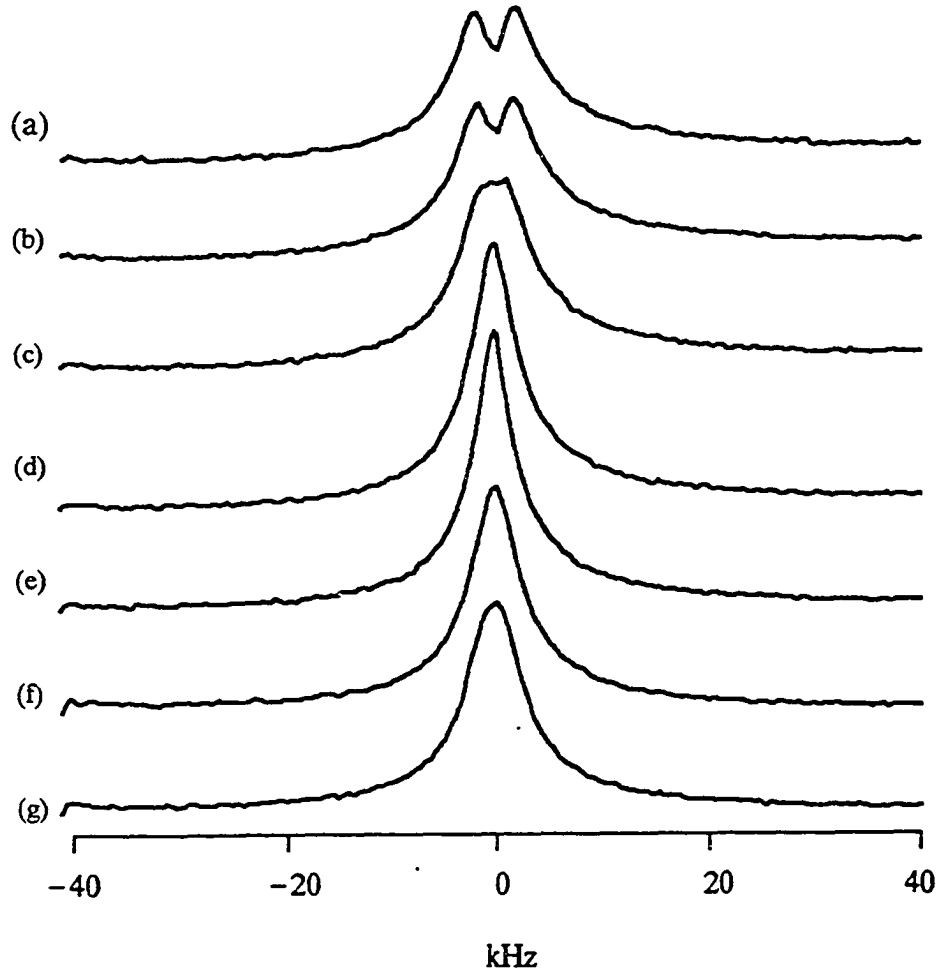

Figure 5.11 Deuteron NMR spectra of D_2O-saturated 125 μm Kapton, taken at several angles between film plane and magnetic field. (a)-(g), $\Omega = 90°$, 75°, 60°, 45°, 30°, 15°, and 0°.

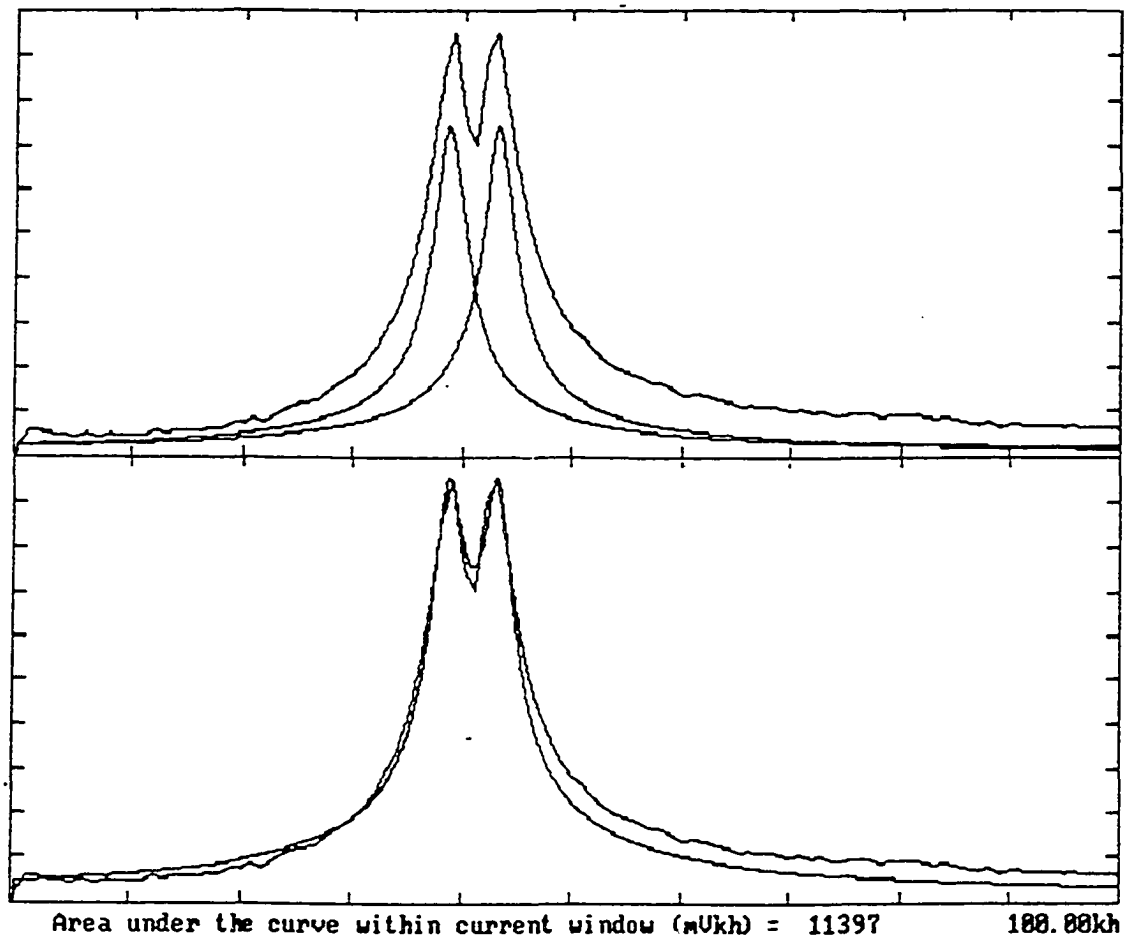

Figure 5.12 The illustration of the computer simulation for the spectrum of 125 μm Kapton with 3.1 wt% D_2O.

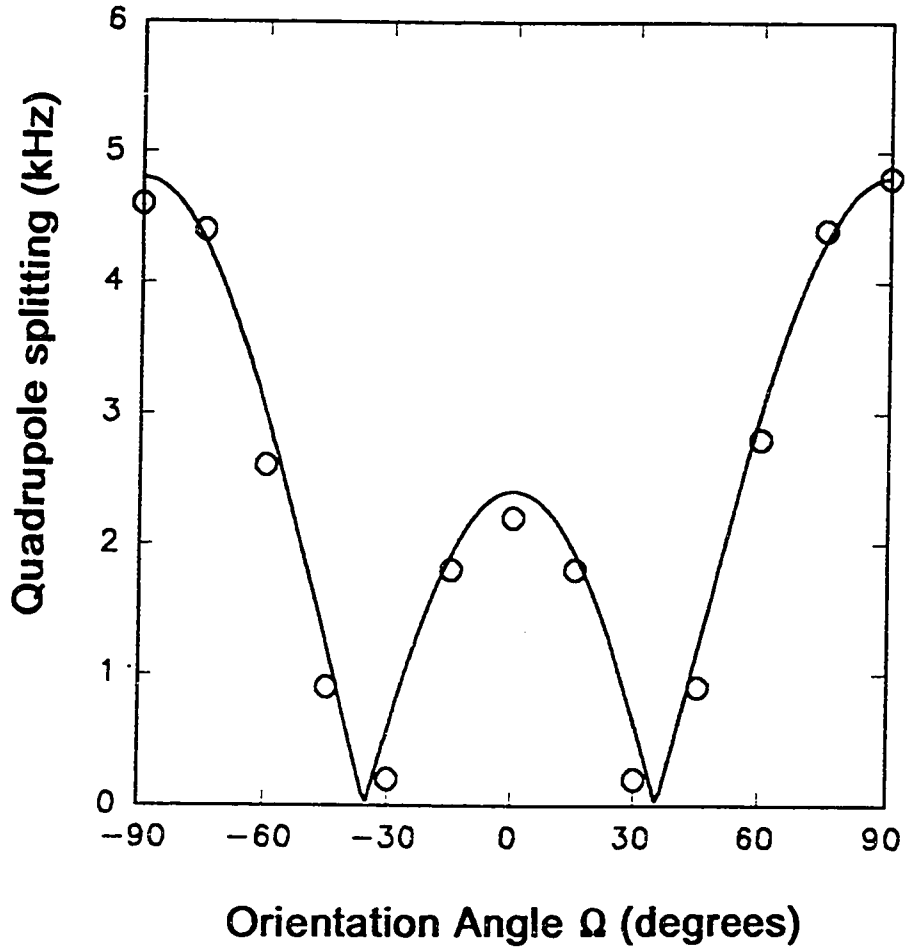

Figure 5.13 The angular dependence of deuteron quadrupole splitting in 125 μm Kapton containing 3.1 wt% D_2O. The solid curve represents the function of $A|3\cos^2\Omega-1|$.

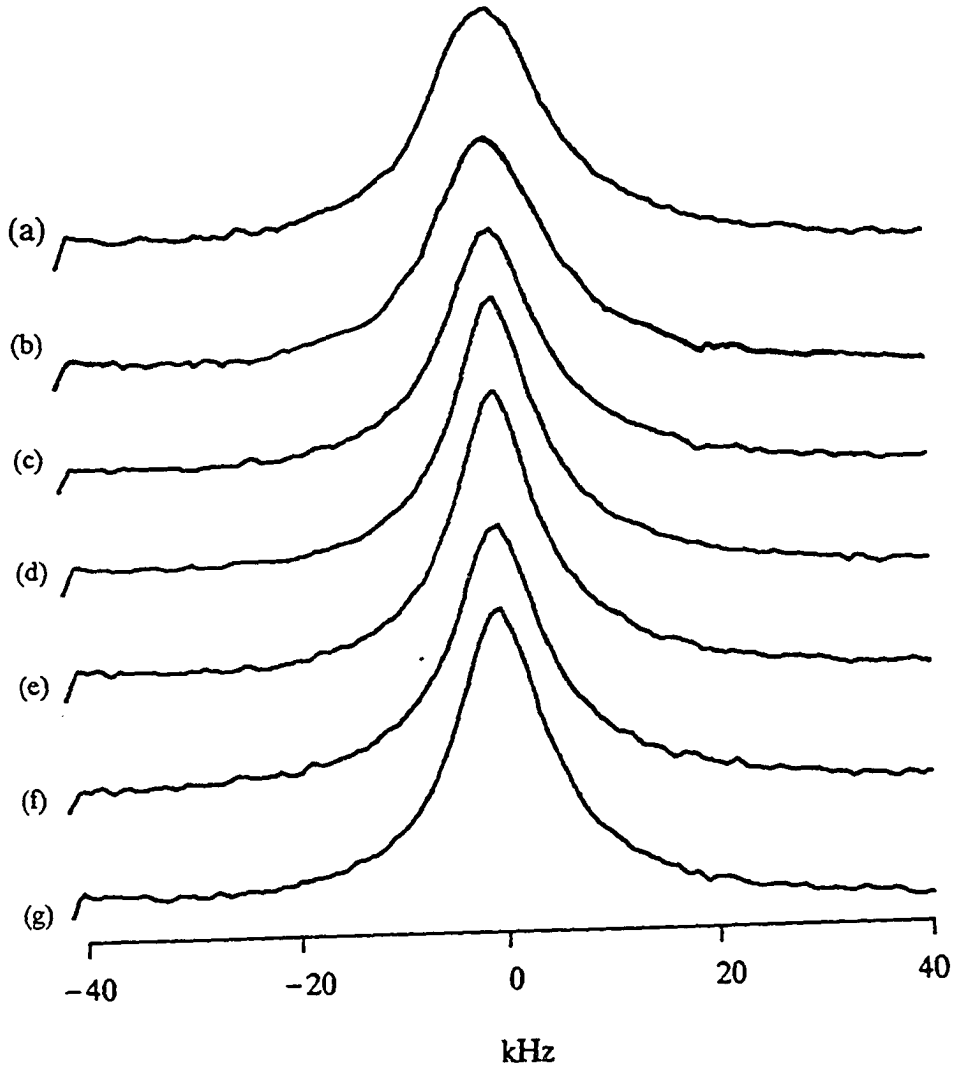

Figure 5.14 Deuteron NMR spectra of 125 μm Kapton with 1.3 wt% D_2O at several angles. (a)-(g), Ω=90°, 75°, 60°, 45°, 30°, 15°, and 0°.

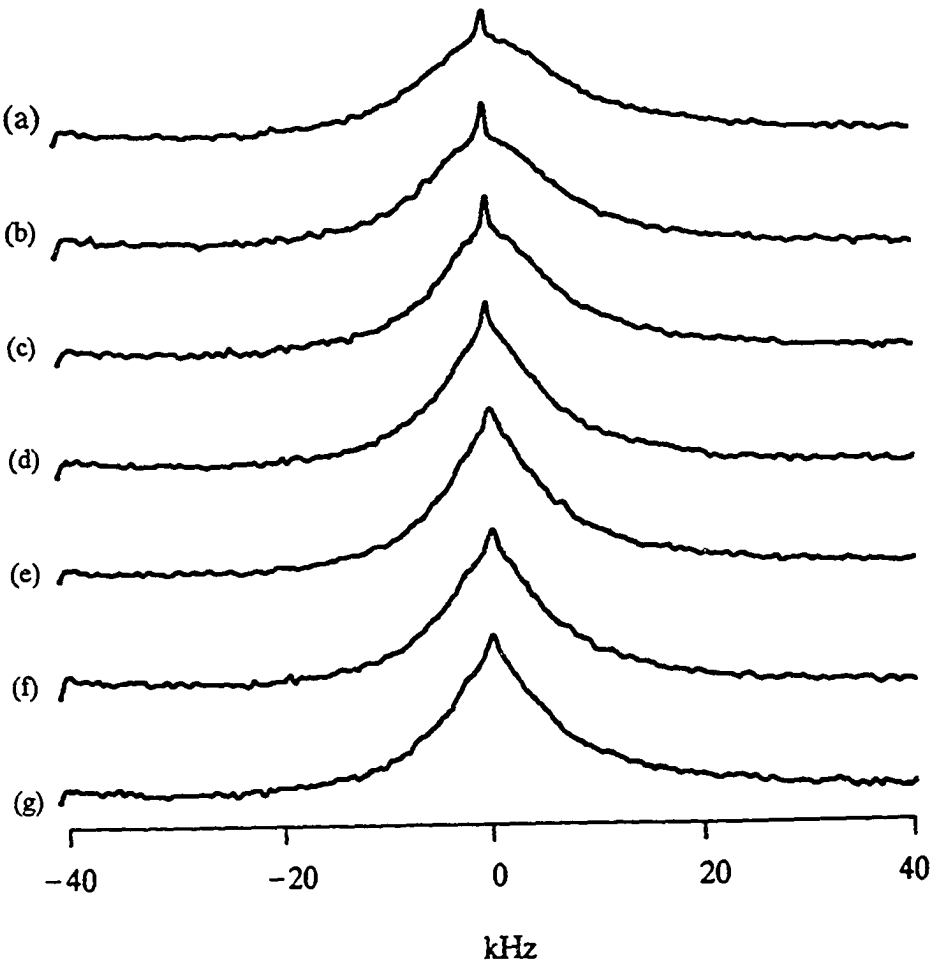

Figure 5.15 Deuteron NMR spectra of 7.5 μm Kapton with 2.4 wt% D_2O at several angles. (a)-(g), Ω=90°, 75°, 60°, 45°, 30°, 15°, and 0°.

5-3.3. Variable Temperature Measurements

Variable temperature measurements of T_1 for 125 μm at 3.1 wt% D_2O were performed in the temperature range of -100°C - 25°C. An Arrhenius plot of T_1 in a saturated (3.1 wt% D_2O) 125 μm film (again, reflecting both sites) is shown in Figure 5.16. The T_1 measurements were restricted in temperature by the value (approximately 175 °K) below which the deuterons become rigid on the NMR timescale, resulting in a broad (~200 kHz) spectrum that is difficult to observe for the D_2O concentrations present. Attempts to determine the T_1 behavior of thin samples with low water content were hindered by poor signal-to-noise ratios. A broad T_1 minimum at about 200 °K was observed in the data in Figure 5.11. From the approximation $\omega\tau = 1$ at the T_1 minimum at about -73 °C (200 °K), where ω is the NMR frequency, one deduces a correlation time of about 3.5 ns for deuteron motion at 200 °K.

The spectra of 125 μm rolled film at 3.1 wt% D_2O were obtained at various temperatures from 20 to -80°C, as shown in Figure 5.17. One can see that the linewidth gradually increases as the temperature decreases. The broadening is clearly due to less efficient averaging of the interaction when the molecular motion is reduced at the lower temperature.

Variable temperature measurements were also carried out for stacked 125 μm Kapton with 3.4 wt% D_2O. Through all temperatures, the sample remained in the orientation of film plane perpendicular to the external magnetic field. The spectra at several temperatures ranging from 20 °C to -70 °C are shown in Figure 5.18. The doublet was smeared out when the temperature decreased. When the temperature

was below than -20 °C, the spectra for the oriented stacked films are almost the same as the rolled films in the same temperature range.

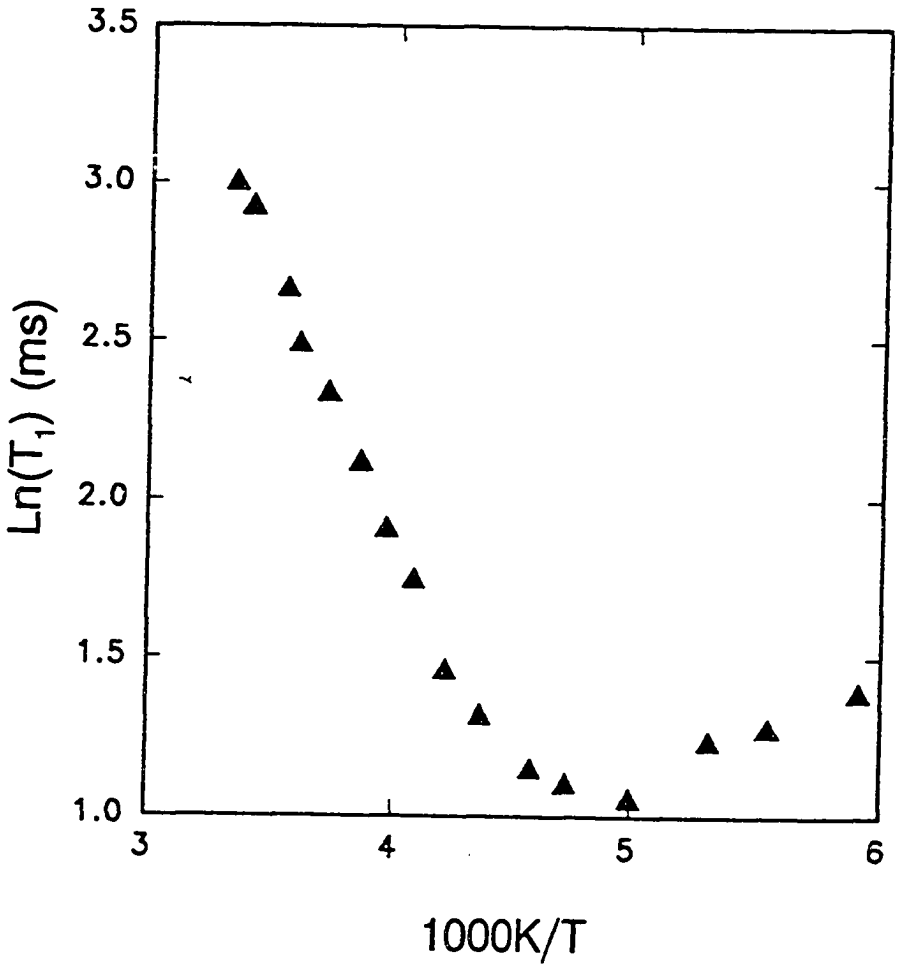

Figure 5.16 Arrhenius plot of average deuteron T_1 in 125 μm Kapton containing 3.1 wt% D_2O.

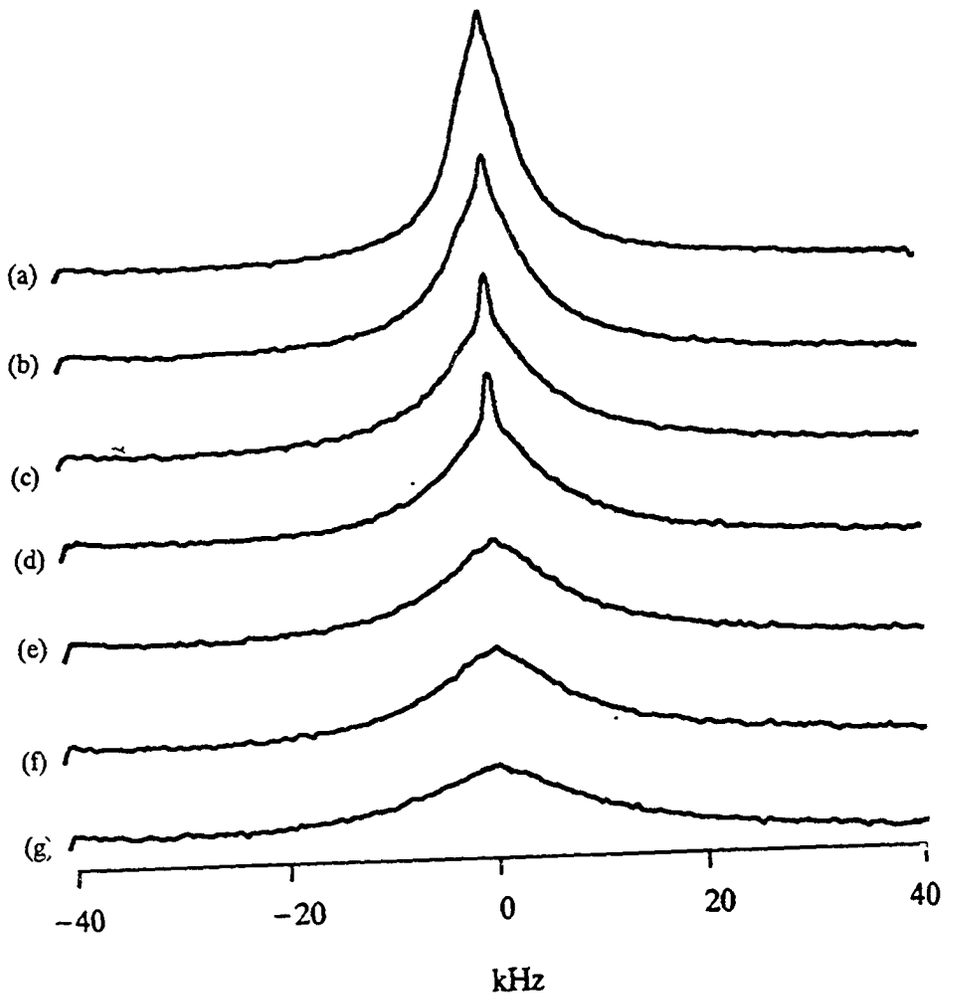

Figure 5.17 Deuteron NMR spectra of rolled 125 μm Kapton containing 3.1 wt% D_2O at several temperatures. (a)-(g), temperature = 20°C, −3°C, −24°C, −35°C, −45°C, −58°C, and −72°C.

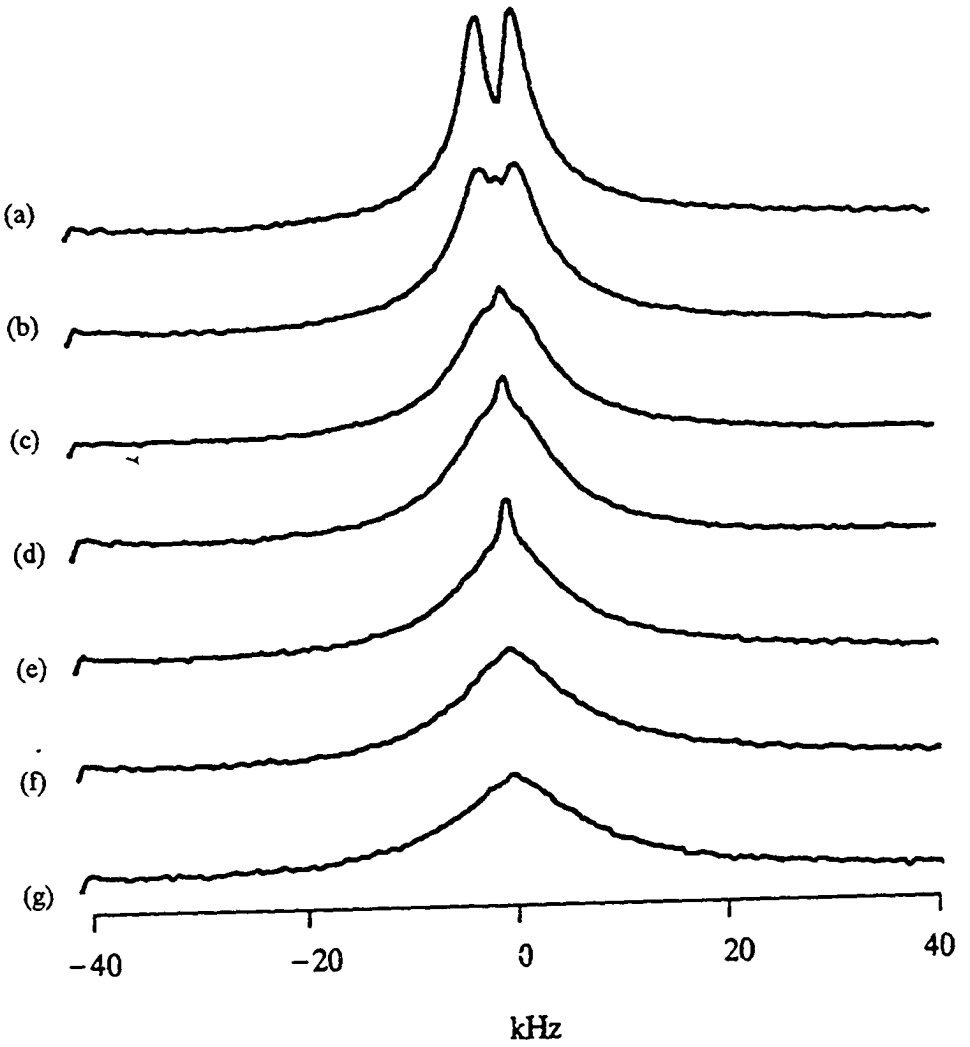

Figure 5.18 Deuteron NMR spectra of stacked 125 μm Kapton containing 3.4 wt% D_2O at several temperature. (a)-(g), temperature = 23°C, 7°C, −13°C, −21°C, −39°C, −53°C, and −66°C.

5-4. CH_3OD and CH_3COOD in Kapton Films

It has been shown in DR spectra that the behavior of methanol and acetic acid in Kapton films are very different from that of water. The loss peak of methanol occurs in the low temperature, γ_2, region, but loss peak of acetic acid appears in the high temperature, γ_1 region. Corresponding to the DR results, deuterium NMR measurements have been taken for deuterated methanol (CH_3OD) and acetic acid (CH_3COOD) in various thickness Kapton films. One of the important differences between the other deuterated solvents and D_2O is that there is only one O-D bond in deuterated methanol and acetic acid molecules while there are two O-D bonds in D_2O molecules. As a result of this, the deuteron in a single O-D bond has a stronger orientation effect than for two O-D bonds molecules (D_2O) for which this effect is reduced by a certain degree due to motional averaging.

Figure 5.19 displays the spectra of stacked 125 μm Kapton films with 6.8 wt% methanol at several orientations. As we expected, the splitting increases significantly from ~4 kHz for D_2O to ~10 kHz for CH_3OD. The same angular dependence as for D_2O is observed, in that the splitting reduces to a minimum as the angle Ω approaches to 35°. The larger splitting of CH_3OD relative to D_2O may indicate that (a) the motionally averaged quadrupole interaction in a single O-D bond is stronger than that in two O-D bonds, i.e. if the D_2O molecule's symmetry axis is oriented perpendicular to the film, the individual O-D bond directions are not, (b) the methanol molecules may be more oriented along a preferred direction than water molecules. The appearance of the maximum splitting at Ω=90° suggests that the averaged O-D bonds of methanol are perpendicular to the plane of the film.

The variable temperature results of the same sample are shown in Figure 5.20 with Ω kept at 90°. Although the linewidth of the individual peaks becomes broader as temperature decreases, the splitting is still noticeable, even at −52 °C. In fact, the splitting also increases from ~10 kHz to ~13 kHz when the temperature decreases.

The orientation spectra of 25 μm Kapton film with 7.6 wt% deuterated methanol are very similar to those of the 125 μm film displayed in Figure 5.19.

In Figure 5.21 the spectra of 7.5 μm Kapton film with 7.3 wt% CH_3OD are plotted. Besides the same angular dependence like other films, the linewidth of the individual peaks is broader and the splitting is increased by 30%, compared with the spectra of 125 μm with 6.8 wt% methanol.

The concentrations of acetic acid in different thickness Kapton films are not as close as in the cases of water and methanol. The weight percentage of acetic acid is 8.6 wt% for 125 μm, 13.6 wt% for 25 μm and 16.0 wt% for 7.5 μm. The spectra of 125 μm and 25 μm films are shown in Figure 5.22, at only two angles, Ω=30° and Ω=90°, for the two extreme values of linewidth. The 125 μm film exhibits a splitting of ~17 kHz while 25 μm sample has a value of ~24 kHz. The splitting for 7.5 μm film gives even bigger splitting of 29 kHz in Figure 5.23. For all three samples the very sharp central peak superimposed on the broad lines is attributed to loosely bound acetic acid molecules on the surface of the films.

As a brief summary of deuterium NMR for Kapton films, one can conclude that (a) the orientation effect generally exists in all thickness films treated by any one of three solvents D2O, CH_3OD, and CH_3COOD, (b) the averaged O-D bond orientation is perpendicular to the film plane, (c) the apparent linewidth becomes

broader with the decrease of solvent concentration, film thickness as well as temperature. One can define the characteristic linewidth of each kind of sample as the apparent linewidth of the stacked films at the orientation of 30°. Then, the values of the characteristic linewidths and the splittings at 90° for most of samples are summarized in Table 5.6.

Table 5.6 The values of the linewidth (at 30°) and splitting (at 90°) for Kapton films.

Solvent	Film(μm)/wt%	Linewidth(kHz)	Splitting(kHz)
D_2O	125/2.9	5.4	4.0
	25/3.0	6.8	4.4
	7.5/3.1	9.2	*
CH_3OD	125/6.8	8.0	10.0
	25/7.6	10.0	10.2
	7.5/7.3	18.2	13.6
CH_3COOD	125/8.6	19.0	17.0
	25/13.6	27.0	24.0
	7.5/16.0	*	29.2

* Data are not available.

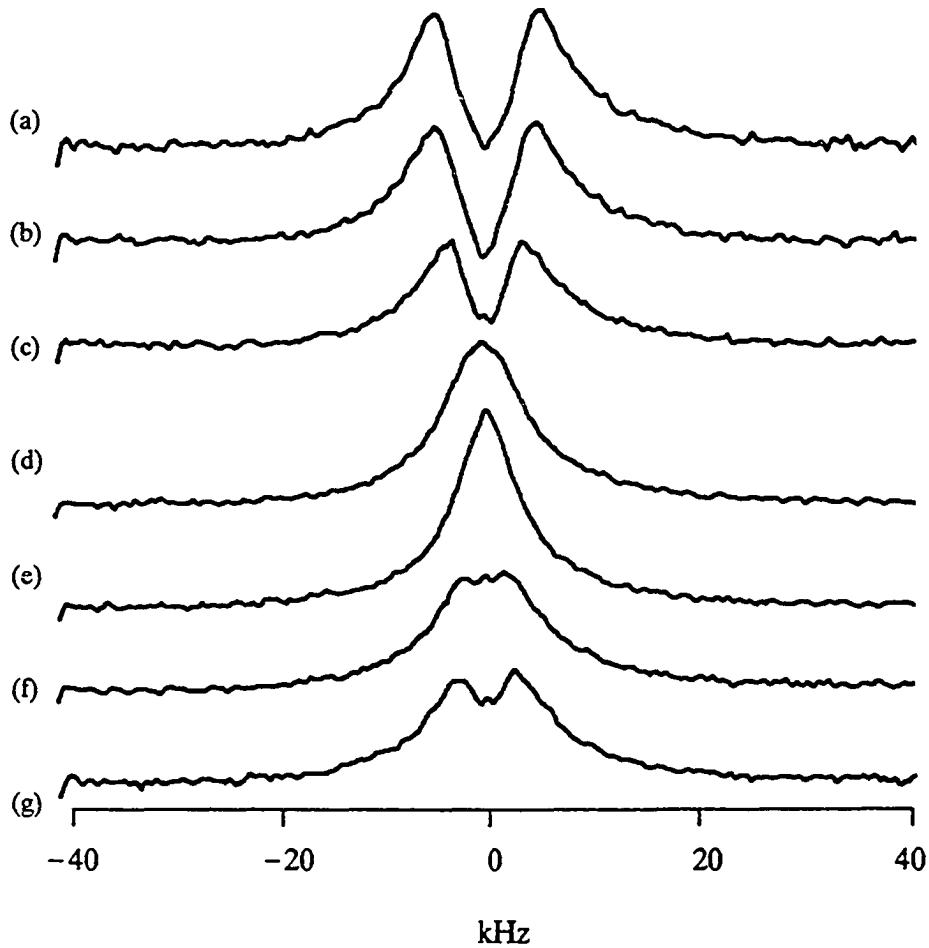

Figure 5.19 Deuteron NMR spectra of stacked 125 μm Kapton containing 6.8 wt% CH_3OD at several angles. (a)-(g), Ω=90°, 75°, 60°, 45°, 30°, 15°, and 0°.

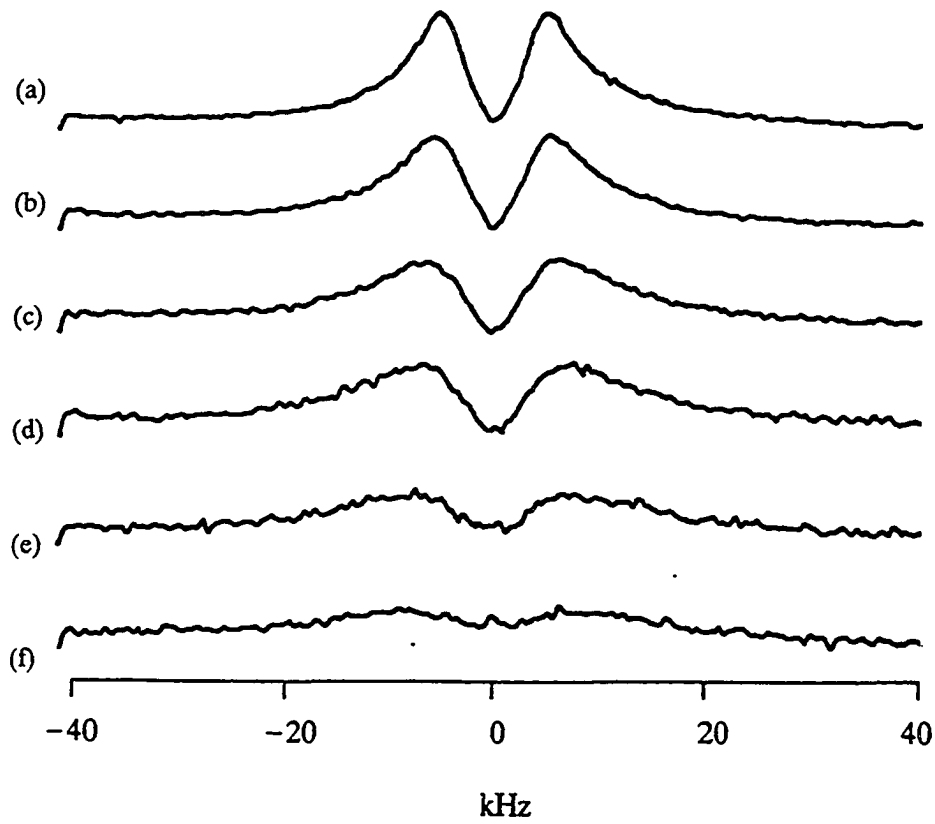

Figure 5.20 Deuteron NMR spectra of stacked 125 μm Kapton containing 7.5 wt% CH_3OD at several temperature. The film is kept at $\Omega = 90°$. (a)-(f), temperature = 20°C, 8°C, −13°C, −24°C, −40°C, and −52°C.

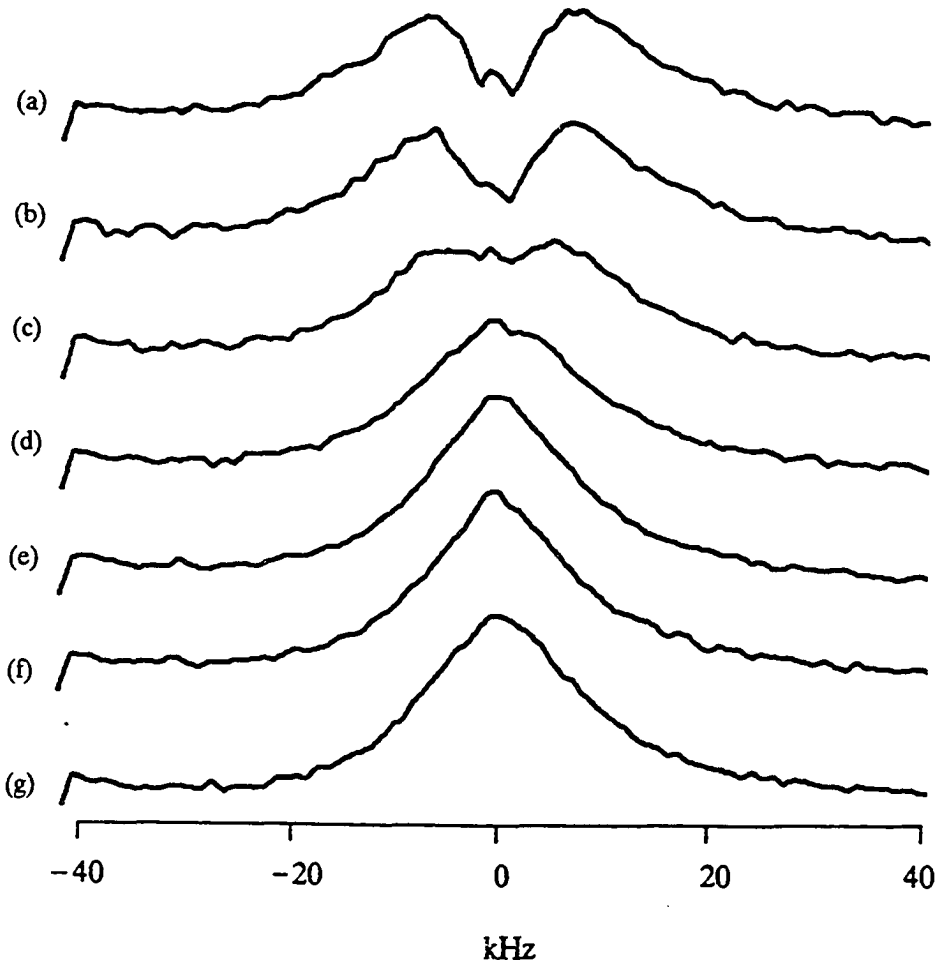

Figure 5.21 Deuteron NMR spectra of stacked 7.5 μm Kapton containing 7.3 wt% CH_3OD at several angles. (a)-(g), Ω=90°, 75°, 60°, 45°, 30°, 15°, and 0°.

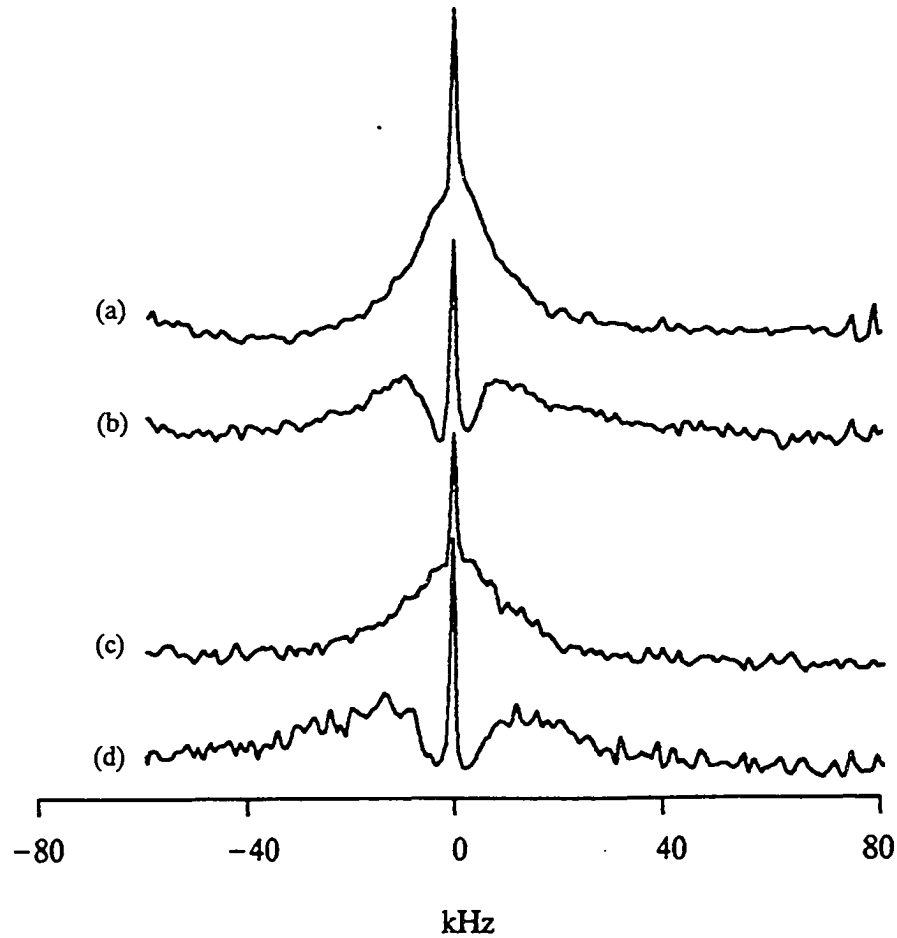

Figure 5.22 Deuteron NMR spectra of Kapton containing CH_3COOD. (a) and (b), 125 μm with 8.5 wt% CH_3COOD at Ω=30° and 90°; (c) and (d), 25 μm with 13.6 wt% CH_3COOD at Ω=30° and 90°.

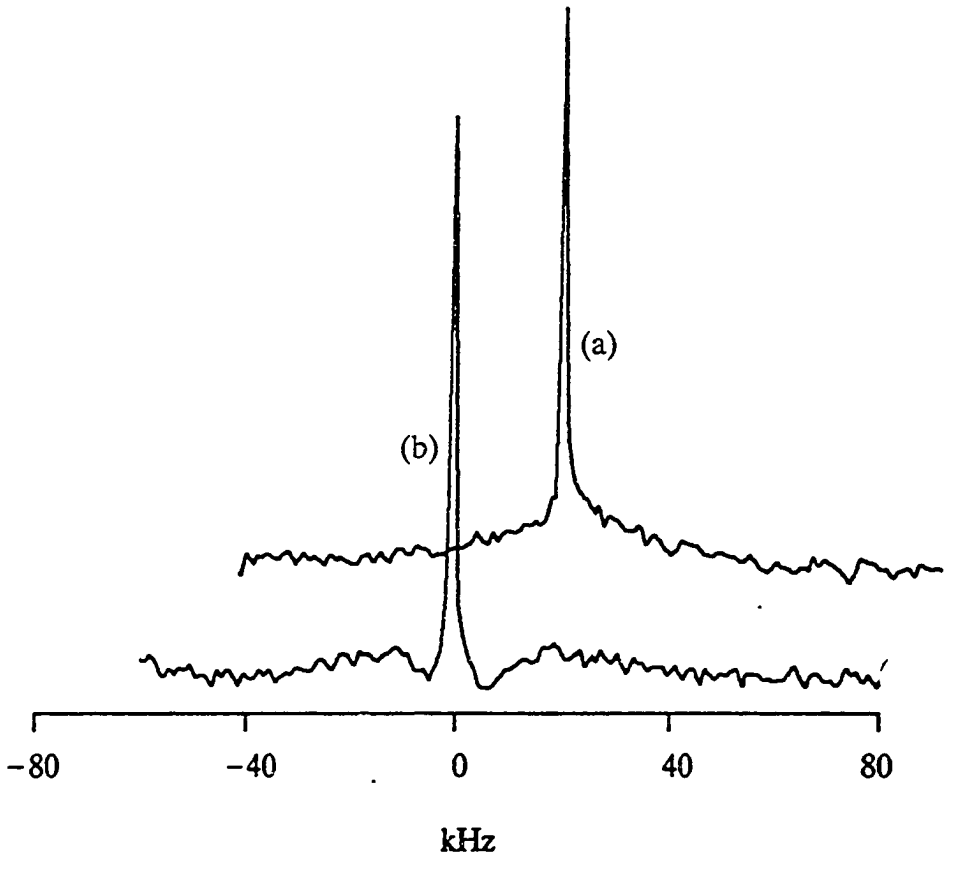

Figure 5.23 Deuteron NMR spectra of 7.5 μm Kapton with 16.0 wt% CH_3COOD at Ω= (a) 30° and (b) 90°.

5-5. D_2O in Upilex Films

Similar work has been carried out for Upilex-S and Upilex-R films. The thicknesses of Upilex-S films are 125, 75, 50, and 25 μm while Upilex-R film has only one thickness of 50 μm. Spectra are plotted in Figure 5.24 for 125 μm Upilex-S film with 1.7 wt% D_2O at four angles.

Unlike Kapton films, where a clear doublet was observed and the splitting was strongly angular dependent, the Upilex-S film did not show a resolved doublet. In addition, the angular dependence is much weaker than in Kapton films. The spectra at all orientations look very similar except the one at 30° is slightly narrower than the one at 90°. For this reason, only one spectrum at 90° is shown for each sample instead of presentation of spectra at several orientations. Figure 5.25 displays the spectra of Upilex-S 125 μm and 75 μm films at 100%, 75%, and 50% RH. Figure 5.26 shows spectra for 50 μm and 25 μm films at the same relative humidities.

The remarkable difference between Upilex-S films and Kapton films concerns the existence of two distinct line components in Upilex films as opposed to the much more subtle difference in the Kapton line components. The narrow one becomes more pronounced for the thinner films. To investigate the origin of the narrow lines, the possibility that it is surface water can be ruled out because (a) the linewidth of the narrow ones is much broader than the linewidth of surface water seen in some saturated Kapton films, (b) the narrow line still exists even at lower relative humidities, especially for thin films (50 μm and 25 μm). Therefore, we can conclude that both narrow and broad line are attributable to the water molecules absorbed inside the polymer matrix. As we have shown in the Chapter 4, all of the DR spectra

of four types of Upilex-S films contain two DR loss tangent peaks and the separations are larger than those in Kapton films. A detailed discussion of the correspondence between two NMR line components and two DR peaks will be given later.

The spectrum of 50 μm Upilex-R film with 1.53 wt% D_2O, saturated at 100%RH, is shown in Figure 5.27 by the curve (c). To compare the differences between the three types of polyimides the spectra of 75 μm Kapton and 50 μm Upilex-S, both saturated in 100% RH, are plotted together in Figure 5.27 by the curves (a) and (b). From this figure one can see that Upilex-S film contains two clearly distinguishable lineshape components, Upilex-R film consists mainly of a broad line, Kapton film may also consist of two lineshape components, but the behavior of the these two components is very close and we are not able to separate them as clearly as in Upilex-S.

Unlike Kapton films, Upilex films do not absorb methanol and acetic acid. A simple explanation of this phenomenon is that macromolecular chains in Upilex films are packed very tightly so that there is no enough space for large volume molecules, such as CH_3OD and CH_3COOD, to fit in.

5-6. $H_2{}^{17}O$ in Kapton Films

The last solvent used to treat the sample is $H_2{}^{17}O$ with 20% ^{17}O enrichment. The quadrupole coupling constant (QCC) of ^{17}O in water is 6.7 MHz, 30 times larger than the deuteron QCC of D_2O, 220 kHz. Hence the NMR signals of ^{17}O water molecules are much more sensitive to their motion and their environments. In other

words, for relatively weak perturbations, like dipole-dipole interactions in H_2O and quadrupole interactions in D_2O, the NMR signals cannot be clearly separated by the small environmental differences of water molecules in γ_1 and γ_2 sites in our samples. Therefore, in the deuteron NMR for D_2O in Kapton, all spectra can be characterized by a single lineshape and the two sites are reflected by the different NMR linewidths of the samples.

After being treated with 20% enriched oxygen-17 water, the spectra of 125 μm Kapton with 2.8 wt% $H_2{}^{17}O$ exhibit clearly two lineshape components: a narrow line superimposed on a broad line, see Figure 5.28 (a) and (b). This is strong evidence of two sites of water molecules in thick film at high water content which was not observed in D_2O at the same condition. The curve (c) and (d) are for 7.5 μm Kapton with 2.6 wt% $H_2{}^{17}O$. It is clear that the thin film contains only one broad line. These results are pretty consistent with the assumption we made before that two water sites water exist in thick films at high water content: γ_1 associated with a broad NMR line and γ_2 with a narrow line. For thin films at low water content, the primary site is γ_1 and the contribution of the γ_2 site is very small.

According to the theory of the quadrupole interaction, the NMR spectrum of oxygen-17 should contain five lines: the central transition and four satellite-lines. Because the intensity of satellite-lines are relative weak and they are often smeared out by the inhomogeneous quadrupole broadening in less mobile molecules, we are not able to observe resolved satellite-lines. Thus the spectra shown in Figure 5.28 are primarily the central transitions, although the satellites may partially contribute to the spectral baseline. Furthermore, since the central transition has a very weak

orientation effect from the second order quadrupole splitting (see section 2-4), it is not surprising that the spectra at $\Omega=30°$ and $\Omega=90°$ show the same lineshape. The intensity of oxygen-17 signal in Figure 5.28 is very small compared with D_2O because, in addition to different "NMR sensitivities" or the two nuclei, the amount of ^{17}O is only about 10% of the deuterons contained in D_2O at the same water concentration.

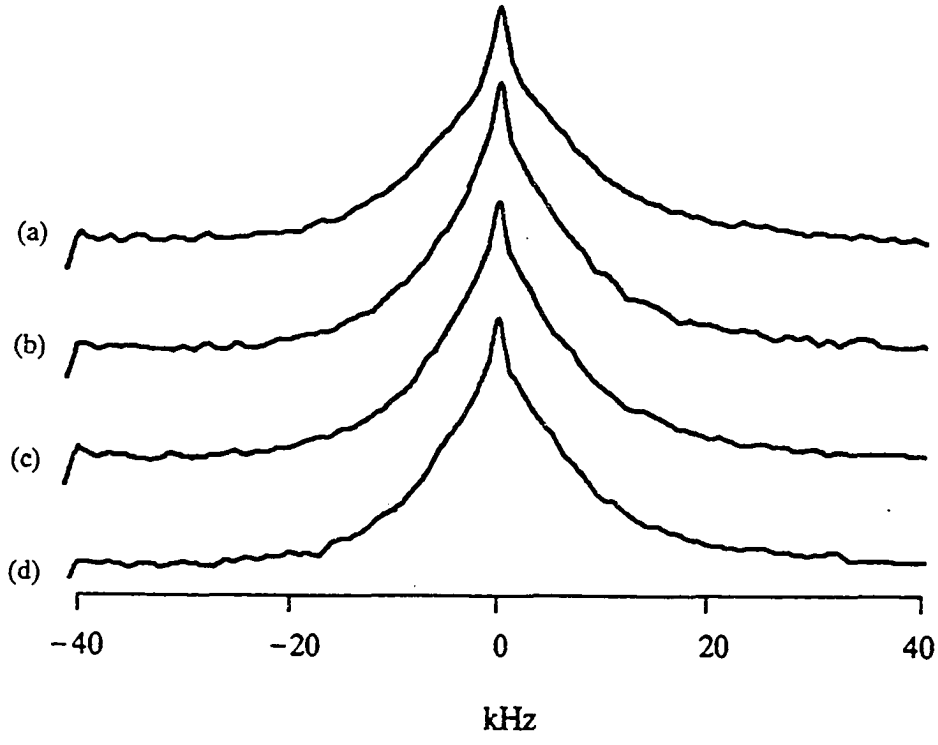

Figure 5.24 Deuteron NMR spectra of 125 μm Upilex-S with 1.7 wt% D_2O at several angles. (a)-(d), $\Omega=90°$, 60°, 30°, and 0°.

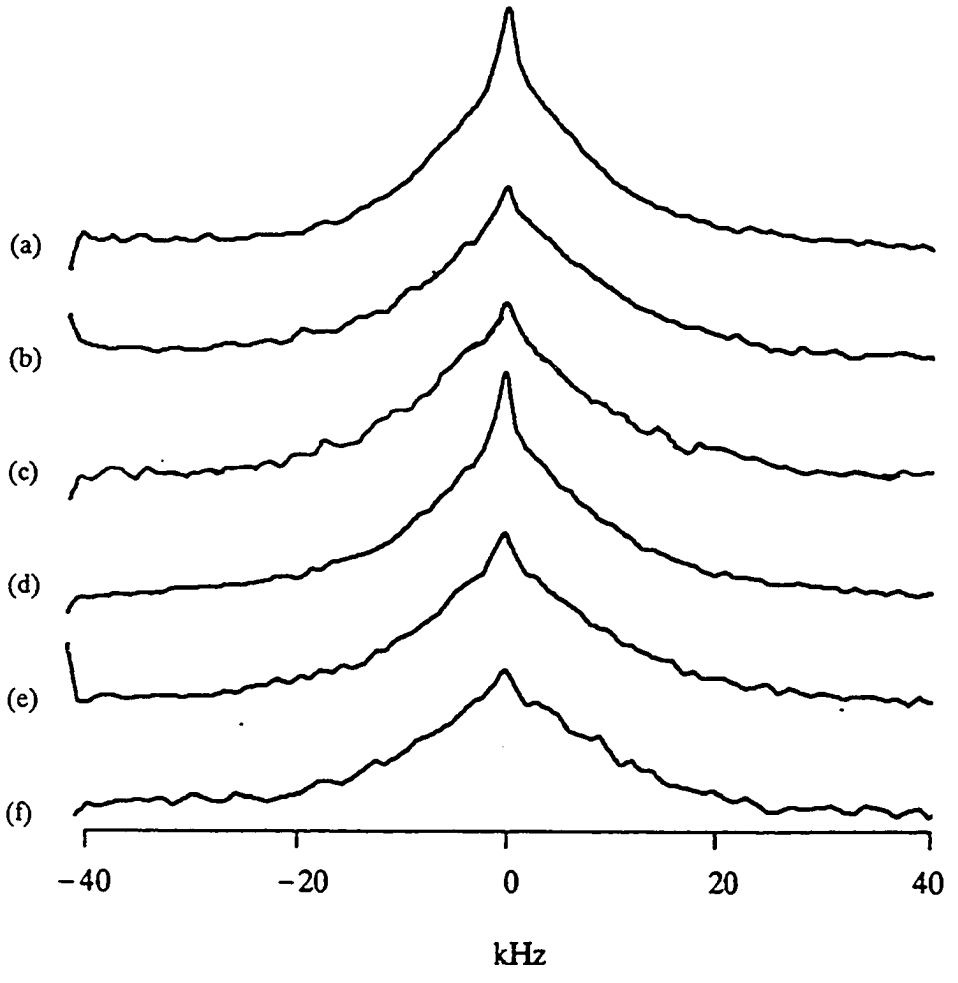

Figure 5.25 Deuteron NMR spectra of stacked Upilex-S films at $\Omega=90°$. (a)-(c), 125 μm containing 1.7, 1.3, and 0.87 wt% D_2O; (d)-(f), 75 μm containing 1.58, 1.33, and 0.97 wt% D_2O.

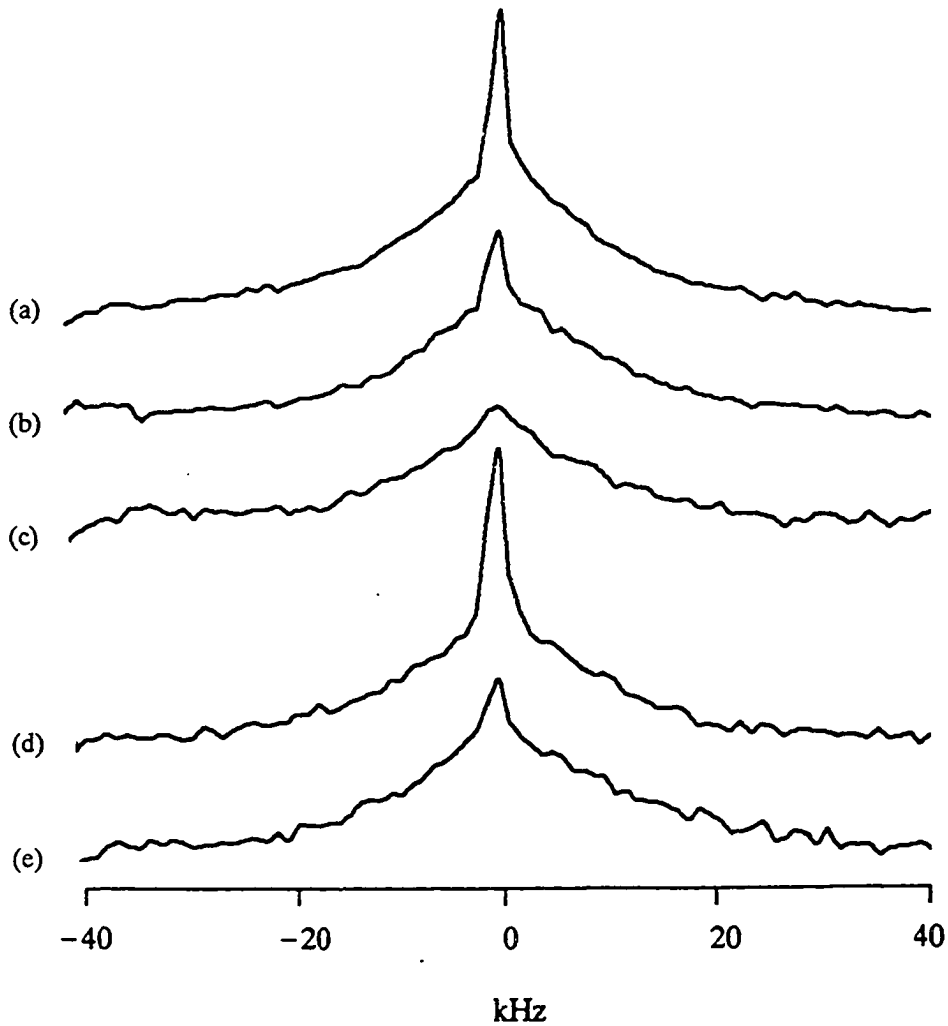

Figure 5.26 Deuteron NMR spectra of stacked Upilex-S films at $\Omega=90°$. (a)-(c), 50 μm with 1.60, 1.35, and 0.84 wt% D_2O; (d)-(e), 25 μm with 1.20 and 0.92 wt% D_2O.

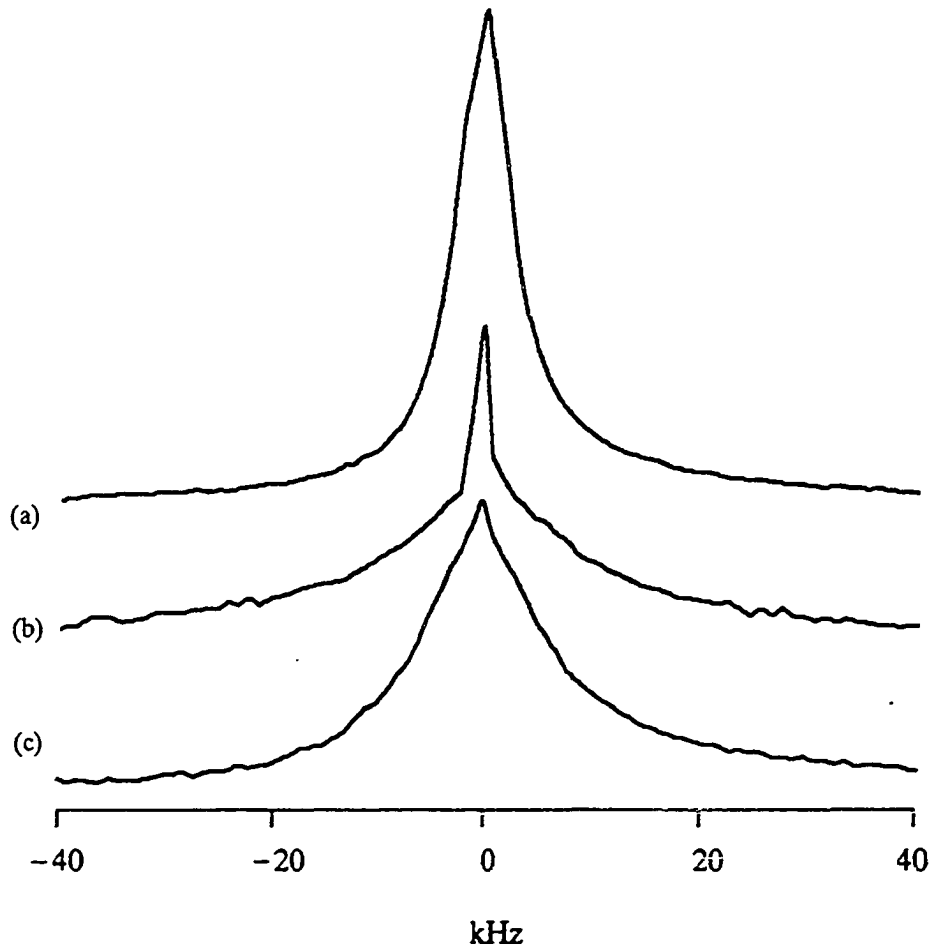

Figure 5.27 Deuteron NMR spectra of polyimide films. (a) 75 μm Kapton with 3.1 wt% D_2O, (b) 50 μm Upilex-S with 1.6 wt% D_2O, (c) 50 μm Upilex-R with 1.5 wt% D_2O.

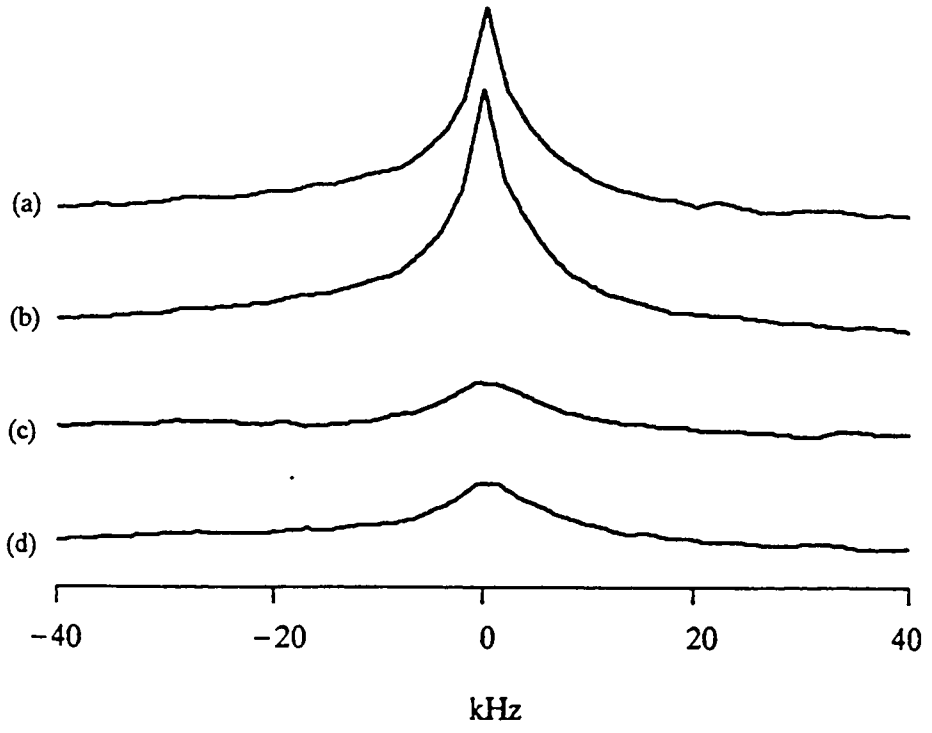

Figure 5.28 ^{17}O NMR spectra of Kapton films. (a)-(b), 125 μm with 2.8 wt% $H_2{}^{17}O$ at $\Omega=90°$ and 30°. (c)-(d), 7.5 μm with 2.6 wt% $H_2{}^{17}O$ at $\Omega=90°$ and 30°.

Chapter 6. Discussion and Conclusions

In the previous two chapters we have shown DR and NMR experimental results. In order to explain those experiment data, we have many questions to be answered or speculated upon. Some of key questions are listed below.

(1) What kind of interactions exist between water molecules and polymer chains? Are water molecules attached to polymer chains through hydrogen bonds? Or do they just stay in the "free space", so called microvoids, in the polymer chains, or a combination of both? If water molecules are bound on polymer chains, which sites are more favorable for water molecules to form hydrogen bonds?

(2) What is the mechanism of two different water behaviors exhibited by the two DR loss tangent peaks at different temperatures? Why does methanol show only one DR peak at lower temperature and acetic acid display one DR peak at high temperature?

(3) How can we match the NMR results to the DR results? Is there a one-to-one correspondence between two DR peaks and features of the NMR spectra?

(4) How do we explain the orientation effects of water molecules in polyimide and why do methanol and acetic acid exhibit stronger orientation effects than water?

In fact, the above questions are not necessarily independent ones. The main purpose of this chapter is to try to analyze our DR and NMR results and search for a reasonable model to fit the experiment results. Since the chemical structure and morphology are different for Kapton and Upilex films and most of investigations

were performed on Kapton, the discussion will be mainly focused on Kapton films. Alternative explanations are presented for Upilex films.

6-1. Speculations on the Status of Water

The formation of hydrogen bonds between water molecules and polyimide chains has been suggested by the authors [23,36,28]. The polyimide molecular structure shown in Figure 1.1 has two kinds of possible sites available for water to make hydrogen bonds: ether linkage oxygens and carbonyl oxygens. Note that Upilex-S has no ether linkage oxygen. The ether linkage oxygens are more favorable for the formation of hydrogen bonds than carbonyl oxygens. According to the water content at full saturation (3.1 wt% for Kapton and 1.6 wt% for Upilex), there are, on average, two water molecules shared by three PMDA-ODA repeat units and only one water molecule per three Upilex-S repeat units. This suggests that water molecules are more favorably bound to ether linkage oxygens than to carbonyl oxygens.

Following the above speculation one may draw the conclusion that the films containing ether linkage oxygens may absorb more water than the films without ether oxygen. However, Upilex-R films contain almost the same amount of water as Upilex-S films although Upilex-R contains ether oxygen but Upilex-S does not. This means that the chemical affinity (e.g. hydrogen bonding) is not necessarily the dominant factor in controlling the absorbed amount of water. The chain morphology is important in determining how much water can be absorbed. The same conclusion has been reported in reference [79]. Since polymer chains in the stiffer Upilex films are packed tighter than the chains in Kapton, which is also reflected by the d-spacing

differences of two kinds of films (Table 4.1), this may explain why Kapton films absorb more water than Upilex films. In addition, Kapton films have larger spacing to fit bigger size solvent molecules like methanol and acetic acid while those solvents are not absorbed in Upilex films due to the tight chain packing.

Although we have suggested water molecules may stay in a restricted state through hydrogen bonds, small water molecular clusters cannot be ruled out in which water molecules are more mobile. In fact, some papers have suggested the existence of water clusters formed inside the microvoids of films [26,27].

6-2. A Microscopic Model for Solvents in Kapton Films

Since there are two clearly separated DR peaks for water in polyimide films, it is reasonable to assume that water molecules in polyimide films are present in two different states: individual water molecules hydrogen bonded on polymer chains and clusters of water molecules. The individual water molecules are distributed throughout all films with different thickness and water content. The cluster water presence is more pronounced in the thick film at high water content.

The individual water molecules may singularly hydrogen bond to the ether linkage oxygens or to carbonyl oxygen, as shown in Figure 6.1a. Since the chemical affinity of ether oxygen to water is stronger than that of carbonyl oxygen, the hydrogen bonds formed between ether oxygen and water are more likely than the bonds between carbonyl oxygen and water molecules. Therefore the configuration of individual water molecules consists primarily of water molecules bonded on ether oxygens. Binding between two adjacent polymer chains is unlikely, because our X-ray

results and reference [12-14] show that the interchain distance is about 5 Å while the dimension of water molecule is only about 1.5 Å.

The formation of a cluster of water molecules is illustrated in Figure 6.1b. Upon the base of the individual hydrogen bonded to the polymer water molecules, additional water molecules may attach via secondary hydrogen bonds between water molecules. These higher level hydrogen bonded water molecules experience few constraints thus are more mobile than the primarily bonded water.

(a)

(b)

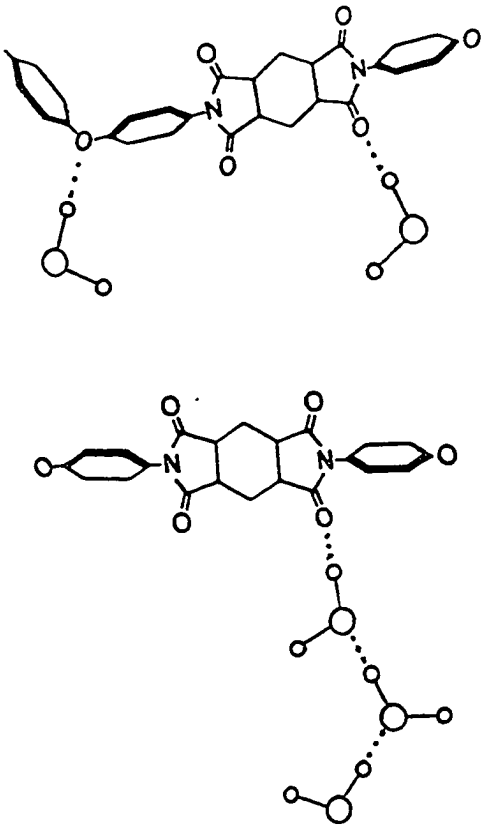

Figure 6.1 The illustrations of two configurations of water molecules in Kapton fims, (a) the individual molecule singularly hydrogen bonded to polymer host, (b) a cluster of water molecules formed with hydrogen bonds.

We propose that the high temperature peak (γ_1) in DR spectra corresponds to water molecules weakly hydrogen bonded to the polymer chain and low temperature peak (γ_2) corresponds to small clusters of water molecules. It is further proposed that a likely scenario involves the formation of γ_2 sites by attachment of one or more molecules to a γ_1 site. Because of chemical (i.e. ether vs. carbonyl oxygen) and morphological constraints, only a certain fraction of γ_1 sites can be converted to γ_2.

As our measurements have detected some anisotropic behaviors of solvents in Kapton films characterized by NMR orientation effects, we need to define our model in further detail with respect to the anisotropic properties. If water molecules in γ_1 sites are more strongly bonded on polymer chains, and polymer chains are only weakly oriented in the amorphous polymer film, then water molecules in γ_1 sites are only weakly oriented and exhibit small orientation effects. The more difficult part is how to interpret the γ_2 sites where the water molecules are more mobile but more oriented. The molecular mobility and degree of orientation are often two oppositing properties of molecules (e.g., in general cases, the more mobile, the less orientation dependence), nevertheless, our experimental results did show that the orientation effects are more pronounced for the less bound water at high water content. To fit our experimental data, an oriented molecular cluster is proposed, the details of which are shown in Figure 6.2a and 6.2b. To simplify the complicated real case, Figure 6.2a shows only one D_2O molecule with a single H-bond and the "free" O-D bond (or O-H bond for H_2O) which can rotate about the hydrogen bond. Supposing that the water molecule rotates about the binding direction O-D_1, where subscripts 1 and 2 represent two different deuterons in the molecule, and the direction of O-D_1 bond

is perpendicular to the film plane, the rotation will not affect the quadrupole interaction for this bond. However, if the rotation about binding axis is faster than the DR time scale or NMR time scale, the contribution of rotating part in the water molecule could be averaged out, which leads to a small effective O-D_2 bond existing in the opposite direction along the rotation axis. The resultant of two bonds gives rise to a net O-D quadrupole interaction along the rotation axis. What is observed in DR is a averaged electric dipole, and in NMR is the averaged H-H direction for proton NMR and the averaged O-D direction for deuteron NMR, along the rotating axis.

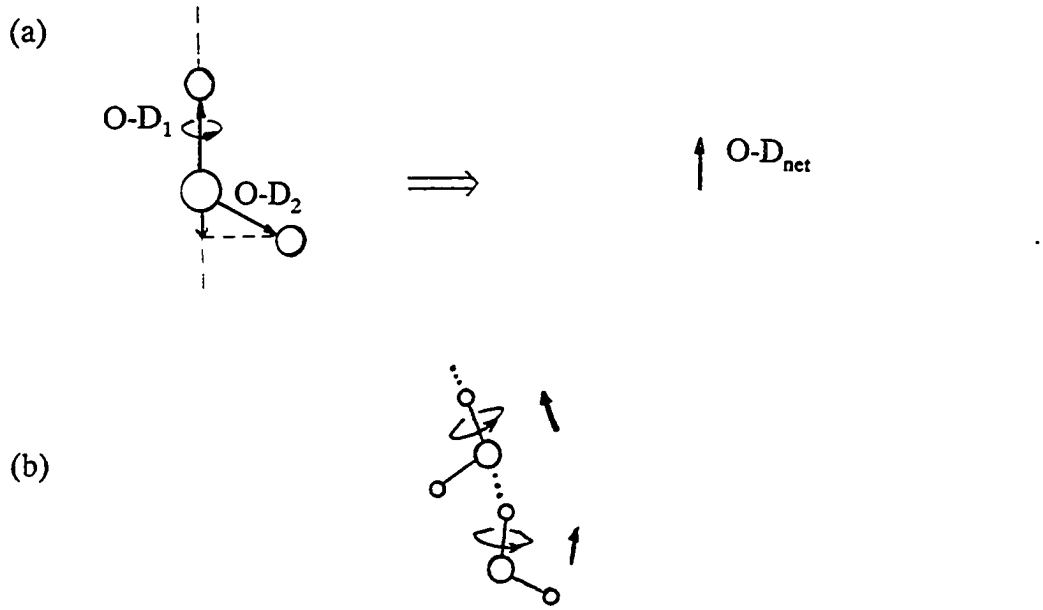

Figure 6.2 The motional average effect of (a) the O-D bonds in a D_2O molecule and (b) several D_2O molecules in a cluster.

Suppose several water molecules are linked together in a chain-like cluster, as in Figure 6.2b, they may form a small anisotropic "cell" in which water molecules are mobile but also more anisotropic. In principle, the configurations formed by the cluster water molecules can be quite different. However, the strong anisotropic feature of γ_2 water suggests that the clusters are more likely to form in the chain-like configuration.

It must be emphasized that the above configurations of two kinds of water are the two extreme cases of the complex water-polymer system. There may be many water molecules which are in some status in between these two configurations.

6-3. DR Results in Terms of Proposed Model

6-3.1. Temperature Effects

Since the γ_1 peak is located at higher temperature than γ_2, this leads to the conclusion that γ_2 water molecules are less bound than γ_1 water molecules, because it requires more energy to force γ_1 molecules to flip following the external alternating electric field than γ_2 molecules. In dielectric relaxation process, the activation energy for γ_1 and γ_2 water are 0.53 eV and 0.47 eV, respectively, according to the measurements from the group at Columbia University. However, the authors in reference 36 reported the activation energy for γ_1 and γ_2 peaks are about 0.5 and 0.25 eV. In spite of some difference between the values for γ_2 water, both sets of results suggest that the γ_2 water molecules are more mobile than the γ_1 water molecules.

6-3.2. Water Concentration

When the water content is decreasing, the strength of γ_2 drastically decreases, but γ_1 decreases only a small amount as shown in Figure 4.6. Actually, since the two curves are overlapped in the intermediate temperature region, the reduction of the γ_1 strength may be caused by the removal of the intensity contribution of γ_2 under the curve of γ_1 curve. The water molecules in a cluster (γ_2) are less strongly bound, therefore, they are more easily removed as water concentration decreases. The stronger hydrogen bonded γ_1 water is still present at lower water concentrations.

6-3.3. Film Thickness

Besides the water concentration dependence, the intensities of the two peaks vary in a similar way as the film thickness is reduced, see Figure 4.5. The drastic decrease of the γ_2 peak as the thickness decreases could be explained by the lack of clusters of water in thinner films due to the tighter polymer packing in thinner films. As we suggested, the γ_2 peak originates from clusters of water molecules, which therefore require larger space than γ_1 water molecules. However, the polymer chains in thinner films are more tightly packed than in thicker films, because polymer chains have to be oriented in the film plane to a higher degree to form the thinner films. This conclusion has been supported by the results of the apparent linewidth of proton NMR for dry films (Table 5.3) where the linewidth for thicker films are smaller than that of thinner films due to the motional narrowing effects. The higher degree of chain packing of thin films has been evidenced by optical studies [14].

An explanation of the difference in morphology between thick and thin films

was suggested in our first publication [37]. It had been noted that even within a given thick film, the inner region (5-10 μm below the surface) has a greater γ_2/γ_1 ration than the entire film. This heterogeneity was postulated to result from the high temperature curing procedure in which imidization occurs under different conditions in the inner and outer regions. In particular, if residual NMP solvent is present in the inner region as the polymerization occurs, the fully cured film will have more volume available for cluster formation in the inner region.

In addition to the changes of the peak intensity, the position of the peaks also shifts as a function of film thickness or water concentration. The trend is that the γ_1 peak shifts towards the higher temperature direction as either the water content decreases (Figure 4.6) or the film thickness decreases (Figure 4.5). This implies that γ_1 water molecules become less mobile when film thickness or water content decreases. It is noteworthy that this γ_1 shift effect will be linked to the line broadening in the NMR spectra because both of them result from the mechanism of reduced motion.

6-3.4. Other Solutes

Since DR spectra of methanol and acetic acid exhibit only a single peak (Figure 4.7 and 4.8), it is reasonable to assume that each kind of solvents exist in a single state rather than two different states as in water. Although methanol and acetic acid exhibit their DR peaks at low temperature and high temperature respectively, we cannot simply claim that methanol molecules are in the same sites as γ_2 water and acetic acid molecules are in the sites of γ_1 water. The dielectric

relaxation technique detects the responses of the electric dipole moments of *molecules* to the external alternating electric field. The flip motion of a whole molecule depends on several factors such as the moment of inertia of the molecule, volumetric constraints and chemical interactions between solutes and polymer hosts. Table 3.4 shows that the dipole moments of both solutes are almost the same, but the molecular weight of methanol is about half of that of acetic acid. The smaller mass and moment of inertia of methanol molecules allow them more easily to flip than acetic acid molecules. In addition, since the volume of acetic acid is about 50% larger than methanol, these larger molecules may experience more constraints from the surrounding polymer matrix. However, the ethanol molecule has a similar volume to that of acetic acid, but its DR spectra (not shown in this thesis) exhibits a γ_2-like lower temperature peak. This result indicates that the volume constraint is not the major factor to control molecular motion of solutes. Another possible factor is the chemical interaction with the polymer host. The oxydianaline (ODA) molecular unit contains two amino end groups. After polycondensation there may be small numbers of amino end groups left. These basic groups will strongly interact with carboxylic groups of acetic acid. Another basic source is the NMP residuals, but their basicity is very weak compared with amino groups. Although the chemical interaction gives the strongest constraint, the amount of those basic groups is very small after the polyimide is fully condensed. Anyhow, it is not easy, at this point, to specify which factors govern the mobility of methanol and acetic acid.

6-3.5. Dipole Moment of Water Molecules

It has been shown in the chapter 4 that the electric dipole moment of γ_2 water is $\sim 10 \times 10^{-30}$ Cm which is bigger than that of free water molecules, 6.20×10^{-30} Cm. This dipole moment increase could be explained in terms of the cluster model. For an isolated static water molecule the dipole moment is along the bisector of the two O-H bonds. In the presence of molecular rotation the averaged dipole moment will be lined up in the direction of the rotation axis. Water molecules in the model illustrated in Figure 6.2b may construct such a cluster in which the average dipole moment of several rotating water molecules is bigger than that for a single free water molecule.

6-4. Proton NMR

6-4.1. Morphology Differences of Dry Polyimide Films

It is concluded from proton NMR results of dry Kapton films (Figure 5.2, 5.3, Table 5.3 and 5.4) that (a) the backbone molecules of Kapton films are more anisotropically structured in thinner films; (b) polymer chains are more rigid in thin films than in thick films; (c) the polymer structure of Upilex-S films is much more rigid than in Kapton films. The last morphology difference results primarily from the chemical structure difference of Kapton and Upilex. In the Kapton molecules there are ether linkage oxygens at which molecular bending can take place. This bending structure has also been verified for Kapton films by the X-ray results (see section 4-1). As a result of this, the polymer structure of Kapton is more flexible and the

existence of microvoids is expected. As mentioned previously, the inner region of thick Kapton films presents additional opportunities for microvoid formation. In contrast to Kapton films, the lack of ether oxygen in the molecules leads to greater rigidity of the polymer chains of Upilex-S. Upilex-R film which also contains ether oxygen has a more flexible structure than that of Upilex-S films.

6-4.2. Mobility of Water Molecules in Polyimide Films

As indicated by the ^1H linewidths of water and polymer backbone (Figure 5.4 and 5.5), water molecules are very mobile compared with the backbone. This means that, because the hydrogen bonds between water and polymer are relatively weak, water molecules can still rotate about binding directions with rotation frequencies greater than the rigid dipolar linewidth (tens of kHz) which efficiently averages the dipolar interaction and thus reduces the linewidth of protons of water molecules.

In fact, three kinds of molecular motions are involved for solutes: translation, flip (as in electric dipole flip as measured by DR) and rotation. After equilibrium is achieved at a particular relative humidity, the translation movement is very slow compared to NMR timescales. Dielectric relaxation frequency is sensitive to molecular flip motion while NMR frequencies are in the range of molecular rotation frequency. Thus, different techniques monitor different motions of the same system which undergo a complex movement.

6-4.3. Motion of the Polyimide Macromolecule

It has been shown at the end of Chapter 2 that the left branch in an Arrhenius

plot corresponds to molecular motion faster than Larmor frequency and the right branch corresponds to motion slower than Larmor frequency. The temperature dependent measurements of proton T_1 for both types of dry films (Figure 5.9) demonstrate that the motion of the macromolecule is quite slow compared to the Larmor frequency. This is consistent with the fact that polyimide films exist in a solid state configuration. Further evidence for this is clear from a comparison between linewidths of backbone and water protons.

6-4.4. Proton Dipole-Dipole Interaction of Water

As mentioned in Chapter 2, the dipole-dipole interaction is the only mechanism to broaden the NMR linewidth for H_2O water molecules. In our systems, the proton NMR linewidths of water in polyimide is about 1 kHz at room temperature (Figure 5.7) including the contribution of about 200 Hz field inhomogeneity. The linewidth really helps us to estimate the contribution of dipole-dipole interaction of deuterons of D_2O in polyimides. Because the dipolar interaction of deuteron pairs is only about 1/50 of that of proton pairs (see section 2-3), we expect that the linewidth broadening caused by dipolar interaction of deuteron pairs will be reduced by the same factor. As a consequence, the 6-15 kHz linewidths of deuterium NMR spectra for D_2O in polyimide films are primarily due to the quadrupole interaction broadening, and dipolar interactions for deuterons can be ignored.

In the measurements of the orientation effects for protonated water in Kapton, no resolved doublet was observed. The absence of a doublet may result from

(a) the weak dipole interaction of mobile water molecules and (b) the field inhomogeneity. However the linewidth changed from 1.3 kHz to 1 kHz as the films were oriented from $\Omega=90°$ to $\Omega=30°$. Although this change is not very large, it does indicate that the motion of the water molecules is anisotropic. Referring to the orientation dependence in section 2-3, one can claim that the residual motionally averaged H-H axes of water molecules are more oriented in the perpendicular direction of the film plane. The proton NMR orientation will be linked to the deuteron NMR orientation later.

6-5. Deuterium NMR of Kapton Films

6-5.1. Correlation of Deuterium NMR Spectral and DR Results

The existence of two water sites is clearly suggested by the presence of two distinct DR loss peaks, γ_1 and γ_2. The manifestation of two sites in NMR results is considerably more subtle since all of the spectra for rolled films are quite similar except for their linewidths, which vary by about a factor of three between the extremes listed in Table 5.5. It is clear that NMR spectra contain contributions from both sites of water, but the spectral components are not as distinct as in DR.

To resolve the problem of correlating the DR and NMR results one should notice that, as mentioned previously, DR and NMR techniques detect different frequencies of molecular motion, or different types of motion. Dielectric relaxation measurements run in the frequency range from 100 Hz to 100 kHz corresponding to flip or reorientation of the whole molecule. NMR T_1 measurements for protons and

deuterons are most sensitive to motion at about 35-50 MHz, corresponding to the rotation or the reorientation of molecules in that frequency range; while linewidth measurements reflect motion on the timescale of hundreds of kHz.

In our model, γ_1 and γ_2 water molecules have different responses to the alternating electric field because of variation of hydrogen bonds and configurations. But, both γ_1 and γ_2 water molecules may rotate at similar frequencies, which are so close that they cannot be separated by deuteron NMR. This rotation does not efficiently affect the dielectric relaxation, but will average NMR interactions and reduce NMR linewidth.

It appears that the D_2O spectra in Kapton films (Figure 5.10 show two extreme cases) can be decomposed into two NMR line components, narrow and broad lines. The narrow one corresponds to γ_2 water and the broad one corresponds to γ_1 water. The spectrum of 125 μm at 100% RH (Figure 5.10 a) has an apparent linewidth of 6 kHz, it could be decomposed into a narrow and broad lines with the linewidths smaller and bigger than 6 kHz. Unfortunately, one cannot define two distinct components since the composition is not unique. This decomposition could be performed for all films at different water content. Following the trend in DR spectra that the ratio of γ_2 peak to γ_1 peak decreases when film thickness decreases or water concentration decreases, the ratio of the narrow component to the broad component decreases similarly. Since the DR spectrum for 7.5 μm film at 50% RH contains only a single γ_1 peak, the NMR spectrum for the same sample (Figure 5.10 f) is characterized by a single broad line with the linewidth of 18 kHz. It is clear that, based on above analysis, the linewidths of the γ_1 component in various samples

become broader when the film thickness is reduced or water content decreases. For example, one cannot identify an 18 kHz broad line component from the spectrum of Figure 5.10a as is found in Figure 5.10f, where only one broad line exists. As mentioned in Chapter 4, the γ_1 DR loss peak shifts to higher temperature when the film thickness is reduced or water content decreases. Both the peak shift in DR and line component broadening in NMR result in the conclusion that the γ_1 water molecules move slower in the thinner films or in the film whth less water content.

With careful comparison of DR and NMR results, one may find that the γ_1 peak shifts by only a small amount, however, the NMR linewidth of γ_1 component changes by a factor 2-3. This comparison demonstrates that the change of high frequency motion (NMR) of γ_1 water in different samples is more significant than the low frequency motion (DR).

6-5.2. Orientation Effects for Kapton Films

The orientation effects have been presented in Figures 5.11-15 for several samples. From the angular dependence of the spectra one finds that the average O-D bond direction of D_2O water is perpendicular to the plane of the films, as mentioned in section 5-3.2. Another striking feature is that the orientation effects are more pronounced at higher water content in thick films. The results seems inconsistent with most of published papers relating the water orientation effect, where the splitting is reduced as the water content increases because water existing at the higher concentration is more mobile and the nuclear quadrupole interactions will be averaged.

Nevertheless, this unusual orientation effect can be adequately explained by our model in terms of anisotropic clusters. The absence of strong orientation phenomena (i.e. spectral doublet) for γ_1 water in thin film at lower water content could be understood from two points of view. Firstly, the γ_1 water molecules are bound to polymer chains and their orientations are highly dependent on the orientation of polymer chains. Since Kapton films consist of an amorphous polymer, that is only weakly anisotropic, the γ_1 water molecules do not have a strong preferential orientation. In fact, this interpretation is equivalent to saying that the order parameter S_{OD} in Equation 2-35 for γ_1 water is very small. Secondly, the stronger quadrupole linewidth broadening due to less motion may smear out the splitting if it is not big enough to be resolved.

As water concentration increases, more water molecules go into clusters in which they can rotate about their weak hydrogen bonds, as shown in Figure 6.2. For the case of cluster in which several water molecules are close together, if they orient and rotate in a similar way as previously described, the average result will be the DR and NMR phenomena we observed in our measurements. Of course, when water concentration is reduced, the oriented γ_2 water are removed causing the disappearance of resolved splitting.

In the orientation measurement for proton NMR, we found that the motionally averaged H-H axes of water are more oriented in the normal direction to the film plane. This configuration is consistent with that for D_2O water, see Figure 6.3.

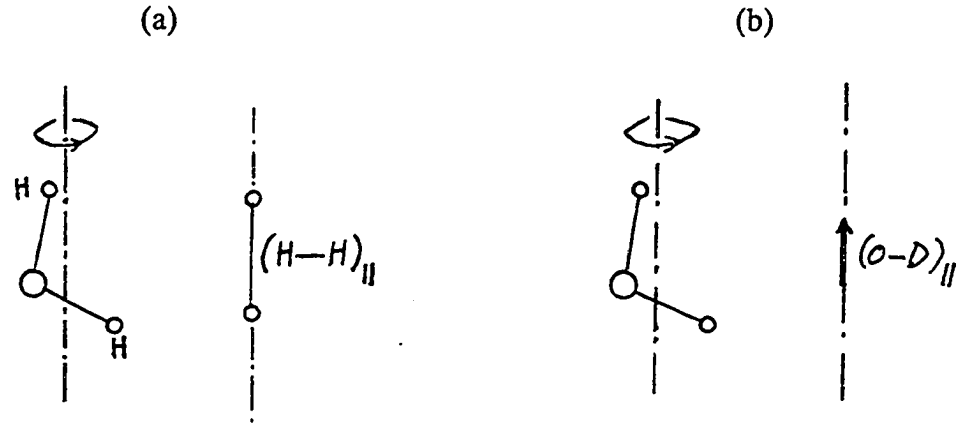

Figure 6.3 A comparison of the orientation of (a) the average H-H axis of H_2O and (b) the average O-D bond of D_2O as a result of molecular rotation.

6-5.3. Variable Temperature Measurements

T_1 relaxation time at low temperature shown in Figure 5.16 has a minimum at about −70 °C. From the condition of $\omega\tau\approx1$ at the T_1 minimum, where ω is the NMR frequency of 47 MHz, one deduces a correlation time of about 3.5 ns for deuteron motion at −70 °C (referring to the average relaxation behavior of both sites). It is noteworthy that the DR loss peak also occurs when $\omega_d\tau_d=1$ where ω_d is frequency of the applied electric field and τ_d is the correlation time of dielectric relaxation. The correlation time from γ_1 peak, occurring at about -60 °C at 1 kHz (Figure 4.5), can be deduced to be of the order of 0.2 ms, which is nearly six orders of magnitude larger than the NMR value. It is thus clear that the mechanism which governs nuclear spin-lattice relaxation of the deuterons is of a localized nature much

different than the molecular electric dipole flips that result in the DR loss peak.

The appearance of T_1 values on the left branch of T_1 minimum in the Arrhenius plot indicates that the NMR correlation times are even shorter, which correspond to faster nuclear motion, at temperatures above the T_1 minimum.

The activation energy derived from the T_1 data in Figure 5.15 gives a value of ca. 0.14 eV (3.2 kcal/mole), which is almost the same as the value for free D_2O water. This again supports the suggestion that water molecules in polyimide are very mobile in the frequency probed by NMR (about 50 MHz).

An unexpected phenomenon was observed in low temperature spectra of rolled and stacked 125 μm Kapton films, shown in Figure 5.17 and 5.18. A narrow peak emerges when the temperature drops from room temperature to ca. -45 °C. It disappears when these molecules freeze out at the temperature below −55 °C. The origin of this narrow peak is still not clear. However it does suggest a rearrangement of at least some of the water molecules to a more mobile configuration as the temperature is lowered.

6-5.4. CH_3OD and CH_3COOD in Kapton

First of all, the angular dependence of both solutes leads to the conclusion that the average O-D bond direction (only one O-D bond per molecule, in contrast to water) is perpendicular to the film plane. Then, compared with D_2O spectra, these two solutes show a considerably larger quadrupole splitting (Figure 5.19-5.23 and Table 5.6). The very sharp lines for samples treated with acetic acid are attributed to mobile acetic acid molecules on the surface of the films.

It has been cited in Table 5.2 that the quadrupole coupling constant of CH_3OD is even smaller than that of D_2O. This excludes the possibility that the larger splitting could result from the difference of QCC. The main reason for such larger splitting is that there is only one O-D bond in the molecules of these solutes while there are two O-D bonds in D_2O. Since two O-D bonds in water orient in two directions with a angle of 104°, the observed doublet is the average quadrupole splitting of two bonds. In terms of the illustration in Figure 6.2, the average quadrupole interaction of two bonds will be smaller than that for a single O-D bond, as in the case of methanol and acetic acid.

Acetic acid spectra display broader linewidths and larger splitting than methanol spectra which, in turn, are broader than D_2O spectra. This trend is consistent with a greater degree of orientation and lower mobility in going from water to methanol to acetic acid.

6-6. Oxygen-17 NMR

Evidence for two distinct ^2H lineshape components corresponding to γ_1 and γ_2 sites is clear only in the comparison of extreme cases, i.e. low water content thin film and high water content thick film. However, from the data shown in Figure 5.28 the assignment of the γ_1 and γ_2 peaks to spectral components of oxygen-17 in 125 μm Kapton film is much clearer. The reason we see two distinct component in oxygen-17 water but not in deuterated water is that the QCC of oxygen-17 is much bigger than that of deuterons, see Table 5.2. The similar environments of two sites cannot be as easily distinguished by the weak quadrupole interaction of D_2O,

however, they could be separated by the much stronger quadrupole interaction of oxygen-17.

6-7. Deuterium NMR of Upilex Films

The discussion on water in Upilex films will be based on the previous discussion of Kapton films. A few differences are pointed out and attempts have been made to give a reasonable interpretation of these differences.

The DR spectra in Figure 4.9 and 4.10 show that two loss peaks are less overlapping, i.e. the separation of two peaks becomes larger as film thickness is reduced. From the point of view of dielectric relaxation, the configurations of the two sites differ from each other more than they do in Kapton. The γ_1 water in Upilex is bound somewhat more tightly than the γ_1 water in Kapton, the γ_2 water in Upilex is looser compared with Kapton, especially for thin film. As a result of this, deuterium NMR shows two separate line components corresponding to two sites, γ_1 site associated with the broad line and γ_2 site associated with the narrow line. The greater resolution of these two spectral components, compared to Kapton, is consistent with the increased resolution of the γ_1 and γ_2 peaks in the DR loss spectrum. The narrow NMR peaks, which are more pronounced in thin films, are attributed to γ_2 sites rather than surface water because the narrow line still appears even at lower relative humidity, although one cannot rule out the possibility that the part of the narrow line is attributable to a very small amount of surface water on the saturated thin films, Figure 5.24 a and d.

It is noticed that the broad line components for various Upilex samples are

generally broader than that for Kapton. This could be interpreted by the greater rigidity and tighter packing of Upilex polymer backbone, where water molecular motion is considerably restrained.

The interpretation of the noticeable narrow lines and γ_2 DR loss peaks in Upilex films is somewhat more difficult than in Kapton. The fact that Upilex films do not absorb methanol and acetic acid solvent implies the microvoid volume in Upilex film is so small that larger molecules cannot go in. With the X-ray results together, one may rule out the possibility of the formation of water cluster in Upilex. Consequently, the narrow line may be attributed to an individual water molecule with a small cavity but binding interactions are weak enough to allow the water molecule to move freely inside. Alternatively, a "cluster" contaning only two water molecules can be envisioned as the source of the γ_2 relaxation and NMR narrow line.

To verify the one-to-one correspondence between the two DR loss peaks and two NMR line components, the DR and NMR spectra of three typical samples have been compared, see Figure 4.12 and 5.27. The two overlapping DR peaks for Kapton film corresponds to a single NMR line in which two line components are not clearly distinguishable; the well separated two DR peaks for Upilex-S result in two separated NMR lines; the primary γ_1 peak and very small γ_2 peak for Upilex-R are associated with a single broad NMR line. As a consequence, the experimental correspondence between DR and NMR results appear to support the model suggested in this thesis.

6-8. Conclusions

(1) As evidenced by proton NMR of dry films, the mobility of the polymer backbone in thin films is slightly smaller than that in thick films. Thin films show more pronounced anisotropic distribution of polymer chains than thick films do. The chain structure of Upilex-S films is much more rigid and tightly packed than that in Kapton films, which leads to a slower motion of polymer chain in Upilex-S than that in Kapton films.

(2) DR and NMR (specially ^{17}O NMR) results show that water molecules absorbed in polyimide are present in two configurations: individual water molecules (γ_1) which are hydrogen bonded to the polymer host and distributed through all samples; small clusters of water molecules (γ_2) which become more pronounced in thick film at high water content. Two kinds of water may be present in the same sites on polymer host, the difference of their behavior is governed by the different configurations.

(3) The γ_1 water molecules are less mobile than the γ_2 water molecules because they experience stronger bonds, however the γ_2 water molecules exhibit stronger orientation effects than γ_1 water. The stronger orientation effects of γ_2 water are mainly attributed to the anisotropic motion of γ_2 molecules while the weak orientation effects of γ_1 water are basically governed by the anisotropic distribution of polymer chains.

(4) Methanol shows primarily a low temperature DR peak while acetic acid exhibits only a high temperature peak. This difference may be caused by several factors such as greater mass of acetic acid, larger moment of inertia, and the special chemical interaction between carboxylic groups of acetic acid and small amount of basic groups in polyimide.

(5) Both proton NMR and deuteron NMR of water indicate that the motionally averaged H-H axes for H_2O molecules and O-D axes for D_2O molecules are more oriented in the direction perpendicular to the film plane. That is, both dipolar (^1H) and quadrupolar (^2H) interactions are partially averaged by anisotropic motion about an axis perpendicular to the plane. The time-averaged single O-D bonds of methanol and acetic acid molecules are also oriented in the normal direction of the film plane. The larger splitting in deuteron NMR spectra of methanol and acetic acid, compared to the splitting for water, is primarily attributed to the presence of single O-D bond in each molecules while each water molecule contains two O-D bonds. In addition, methanol and acetic acid molecules may have a higher degree of molecular anisotropy than water molecules.

(6) For water in Kapton films, the high temperature peak (γ_1) in DR spectra corresponds to water molecules weakly hydrogen bonded to the polymer chain and low temperature peak (γ_2) corresponds to small clusters of water molecules. It is further proposed that a likely scenario involves the formation of γ_2 sites by attachment one or more molecules to a γ_1 site. Because of chemical (i.e. ether vs.

carbonyl oxygen) and morphological constraints, only a certain fraction of γ_1 sites can be converted to γ_2.

APPENDIX

The Program of Computer Simulation for NMR Lineshape

(This program is written in Quick Basic 4.5)

* * * * * * * * * * * *

```
5
DECLARE SUB MENU ()
DECLARE SUB MARKS (FS, VS)
DIM A$(7), X(2520), Y(2520), L1(2520), L2(2520), L3(2520), LT(2520)
DIM G1(2520), G2(2520), G3(2520), GT(2520), LVG(10), GV(10), YC(2520), T(2520)

CLS 0
'ON ERROR GOTO HANDLER
SCREEN 9
COLOR 1, 3
VIEW PRINT 1 TO 25
LOCATE 5, 18
INPUT " TYPE IN DATA FILE NAME (no extension): ", IN1$
LOCATE 8, 24
PRINT "*** LOADING DATA FILE ... ***"

IN$ = IN1$ + ".LCY"
OPEN IN$ FOR INPUT AS #1
OPEN "FIRST" FOR OUTPUT AS #2
OPEN "SECOND" FOR OUTPUT AS #3
OPEN "DATA.PAR" FOR OUTPUT AS #4

FOR I = 1 TO 6
   LINE INPUT #1, A$(I)  ' Store the data on disk file "IN$" into A$(I)
NEXT I

LOCATE 8, 24
PRINT "*** DATA FILE HAS BEEN LOADED ***"

LOCATE 10, 20
PRINT "COMMENT (in data file): "; A$(1)
LOCATE 14, 20
PRINT "PLEASE TYPE IN THE FOLLOWING INFORMATION:"
PRINT
PRINT TAB(25); : INPUT " Frequency per division: ", FPD
PRINT TAB(25); : INPUT " Frequency unit:  ", FU$
PRINT TAB(25); : INPUT " Numbers of division (5 or 6.25): ", DIV
LOCATE 22, 18
PRINT "I am working for you now, just waiting for an hour!"

PRINT #2, A$(4)        ' Data file #1
PRINT #3, A$(5)        ' Data file #2
PRINT #4, A$(3)        ' Parameter information
CLOSE                  ' Close files #1 to #4

'Collecting data
OPEN "FIRST" FOR INPUT AS #1
INPUT #1, L1$
INPUT #1, N1           ' # of items in the data file
OPEN "SECOND" FOR INPUT AS #2
INPUT #2, L2$
INPUT #2, N2
OPEN "DATA.PAR" FOR INPUT AS #3
INPUT #3, L3$
```

```
INPUT #3, N3

' Input the corresponding parameter
FOR I = 1 TO 6
INPUT #3, LVG(I)
NEXT I
RESTORE 6
FOR I = 1 TO 10
  READ GV(I)
NEXT I
6 DATA 5.0, 10.0, 20., 50., 100., 200., 500., 1., 2., 5, ' Exact vertical gain
VOFFSET = (LVG(5) * 256 + LVG(6) - 200) / 25          ' Vertical gain offset
VG = GV(LVG(1) - 21)
IF (LVG(1) - 21) < 8 THEN VGU$ = "mV" ELSE VGU$ = "V"

F = 1: V = 1
FOR J = 1 TO N1
INPUT #1, Y(J)
X(J) = DIV * FPD * J / (N1 + N2)
'Coverting data, refer to LeCroy manual
Y(J) = VG * ((Y(J) - 32768) / 8192 - VOFFSET) * 200 / (LVG(2) + 80)
NEXT J

FOR J = N1 + 1 TO (N1 + N2)
INPUT #2, Y(J)
X(J) = DIV * FPD * J / (N1 + N2)  'data not shown in full screen
Y(J) = VG * ((Y(J) - 32768) / 8192 - VOFFSET) * 200 / (LVG(2) + 80)
NEXT J
CLS 0

GOSUB DISPLAY

10 CALL MENU
ON KEY(1) GOSUB SCALE
ON KEY(2) GOSUB CURSOR
ON KEY(3) GOSUB TWOLORENTZ
ON KEY(4) GOSUB THREELORENTZ
ON KEY(5) GOSUB TWOGAUSS
ON KEY(6) GOSUB THREEGAUSS
ON KEY(7) GOSUB MULTIPLE
ON KEY(8) GOSUB NEWFILE
ON KEY(9) GOSUB QUIT
KEY(1) ON: KEY(2) ON: KEY(3) ON
KEY(4) ON: KEY(5) ON: KEY(6) ON
KEY(7) ON: KEY(8) ON: KEY(9) ON
GOTO 10

DISPLAY:
  FS = DIV * FPD * F: VS = VG * V
  VIEW (10, 15)-(630, 220), , 1
  WINDOW (0, 0)-(FS, VS)
  CLS 1
  CALL MARKS(FS, VS)
  PSET (0, 0)
  AREA = 0
  FOR J = 1 TO (N1 + N2) * F
    LINE -(X(J), Y(J)), 12
    AREA = AREA + Y(J)
  NEXT J

  VIEW PRINT 1 TO 19
  LOCATE 1, 30
  PRINT "Data file – "; IN$;
  LOCATE 1, 2
  PRINT USING "###.##"; VS
```

```
  LOCATE 1, 8
  PRINT VGU$
  LOCATE 17, 5
  PRINT "Area under the curve within current window ("; VGU$; FU$; ") = "; INT(AREA)
  LOCATE 17, 72
  PRINT USING "###.##"; FS:
  LOCATE 17, 78
  PRINT USING "\\"; FU$
RETURN

SCALE:
  VIEW PRINT 19 TO 25
  CLS 2
  LOCATE 19, 10
  PRINT "Frequency:                    Intensity:"
  LOCATE 20, 10
  PRINT "(Ctrl)Right arrow -- Enlarge     (Shift)Up arrow  -- Enlarge"
  LOCATE 21, 10
  PRINT "(Ctrl)Left arrow  -- Reduce      (Shift)Down arrow -- Reduce"
  LOCATE 24, 15
  PRINT "**** Press Enter twice to return the main menu ****"

20 R$ = ""
  DO WHILE R$ = ""
    R$ = INKEY$
  LOOP
  IF LEN(R$) = 1 THEN GOTO 30
    SELECT CASE ASC(RIGHT$(R$, 1))
      CASE 116  'FAST RIGHT
      F = F - 1 / 5
      GOSUB DISPLAY
      CASE 77   'RIGHT
      F = F - 1 / 10
      GOSUB DISPLAY
      CASE 115  'FAST LEFT
      F = F + 1 / 5
      GOSUB DISPLAY
      CASE 75   'LEFT
      F = F + 1 / 10
      GOSUB DISPLAY
      CASE 72   'UP
      V = V - 1 / 10
      GOSUB DISPLAY
      CASE 80   'DOWN
      V = V + 1 / 10
      GOSUB DISPLAY
      CASE ELSE
      BEEP
    END SELECT
  GOTO 20
30 SELECT CASE ASC(R$)
    CASE 56
    V = V - 1 / 5
    GOSUB DISPLAY
    CASE 50
    V = V + 1 / 5
    GOSUB DISPLAY
    CASE 13
    GOTO 40
    CASE ELSE
    BEEP
  END SELECT
  GOTO 20
40 VIEW PRINT 19 TO 25
  CLS 2
```

```
RETURN

CURSOR:
  VIEW PRINT 19 TO 25
  CLS 2
  LOCATE 20, 10
  PRINT "S -->Spectrum (red)"
  LOCATE 21, 10
  PRINT "L1-->1st Lorentz      (blue)      G1-->1st Gauss"
  LOCATE 22, 10
  PRINT "L2-->2nd Lorentz      (magenta)   G2-->2nd Gauss"
  LOCATE 23, 10
  PRINT "L3-->3rd Lorentz      (gray)      G3-->3rd Gauss"
  LOCATE 19, 20
  LINE INPUT "Type in the line code to select the line :"; N$

  CLS 2
  LOCATE 19, 10
  PRINT "Frequency ("; FU$; ") = "
  LOCATE 19, 46
  PRINT "Intensity ("; VGU$; ") = "
  LOCATE 21, 10
  PRINT "Ctrl + <-- : fast left              Ctrl + --> : fast right"
  LOCATE 22, 10
  PRINT "       <-- : slow left                    --> : slow right"
  LOCATE 24, 15
  PRINT "**** Press Enter twice to return the main manu****"

  IF N$ = "S" OR N$ = "s" THEN
    FOR J = 1 TO (N1 + N2) * F
      YC(J) = Y(J)
    NEXT J
    C = 12   'LIGHT RED
  ELSEIF N$ = "L1" OR N$ = "l1" THEN
    FOR J = 1 TO (N1 + N2) * F
      YC(J) = L1(J)
    NEXT J
    C = 9    'LIGHT BLUE
  ELSEIF N$ = "L2" OR N$ = "l2" THEN
    FOR J = 1 TO (N1 + N2) * F
      YC(J) = L2(J)
    NEXT J
    C = 13   'LIGHT MAGENTA
  ELSEIF N$ = "L3" OR N$ = "l3" THEN
    FOR J = 1 TO (N1 + N2) * F
      YC(J) = L3(J)
    NEXT J
    C = 8   'GRRY
  ELSEIF N$ = "G1" OR N$ = "g1" THEN
    FOR J = 1 TO (N1 + N2) * F
      YC(J) = G1(J)
    NEXT J
    C = 9
  ELSEIF N$ = "G2" OR N$ = "g2" THEN
    FOR J = 1 TO (N1 + N2) * F
      YC(J) = G2(J)
    NEXT J
    C = 13
  ELSEIF N$ = "G3" OR N$ = "g3" THEN
    FOR J = 1 TO (N1 + N2) * F
      YC(J) = G3(J)
    NEXT J
    C = 8
  ELSE
    BEEP
```

```
  END IF

  I = 1
50
  P$ = ""
  DO WHILE P$ = ""
    P$ = INKEY$
  LOOP

  FOR M = -4 TO 4
    PRESET (X(I), YC(I) + M * VS / 400), 11
  NEXT M
  PRESET (X(I), YC(I)), C

  IF LEN(P$) = 1 THEN GOTO 80
  SELECT CASE ASC(RIGHT$(P$, 1))
    CASE 116  'fast right
      I = I + 10
      GOTO 52
    CASE 77   'slow right
      I = I + 1
52    IF I > (N1 + N2) * F THEN GOTO 60
      FOR M = -4 TO 4
        PSET (X(I), YC(I) + M * VS / 400), 1
      NEXT M
      LOCATE 19, 27: PRINT USING "###.##"; X(I)
      LOCATE 19, 63: PRINT USING "###.##"; YC(I)
    CASE 115  'fast left
      I = I - 10
      GOTO 54
    CASE 75   'slow left
      I = I - 1
54    IF I < 1 THEN GOTO 70
      FOR M = -4 TO 4
        PSET (X(I), YC(I) + M * VS / 400), 1
      NEXT M
      PSET (X(J), YC(J)), 1
      LOCATE 19, 27: PRINT USING "###.##"; X(I)
      LOCATE 19, 63: PRINT USING "###.##"; YC(I)
    CASE ELSE
      BEEP
  END SELECT
  GOTO 50
60 BEEP: I = I - 5: GOTO 50
70 BEEP: I = I + 5: GOTO 50
80 CLS 2
RETURN


TWOLORENTZ:
100
  CLS 0
  GOSUB DISPLAY
  VIEW PRINT 19 TO 25
  LOCATE 19, 10
  PRINT "Lorentz: I(V) = Io*(T2) / [1+(2*3.14)^2*(V-Vo)^2*(T2)^2] + BL"

  LOCATE 20, 10: INPUT "I1o value :", I1o
  LOCATE 20, 40: INPUT "V1o value :", V1o
  LOCATE 21, 10: INPUT "T2(1) value :", T2(1)
  LOCATE 21, 40: INPUT "BL1 value :", BL1

  LOCATE 22, 10: INPUT "I2o value :", I2o
  LOCATE 22, 40: INPUT "V2o value :", V2o
  LOCATE 23, 10: INPUT "T2(2) value :", T2(2)
```

```
  LOCATE 23, 40: INPUT "BL2 value :", BL2
  CLS 2

  LOCATE 19, 10
  PRINT "Simulation: I(V) = Io / [1+(2*3.14)^2*(V-Vo)^2*(T2)^2] + BL"
  PRINT , "I1o="; I1o, "V1o="; V1o, "T2(1)="; T2(1), "BL1="; BL1
  PRINT , "I2o="; I2o, "V2o="; V2o, "T2(2)="; T2(2), "BL2="; BL2
  J1o = V1o * (N1 + N2) / (DIV * FPD)
  J2o = V2o * (N1 + N2) / (DIV * FPD)

  PSET (0, 0)
  AREA1 = 0
  FOR J = 1 TO (N1 + N2) * F
    L1(J) = I1o * SQR(1 + 39.43 * (X(J) - X(J1o)) ^ 2 * T2(1) ^ 2) / (1 + 39.43 * (X(J) - X(J1o)) ^ 2 * T2(1) ^ 2) + BL1
    LINE -(X(J), L1(J)), 9
    AREA1 = AREA1 + L1(J)
  NEXT J

  PSET (0, 0)
  AREA2 = 0
  FOR J = 1 TO (N1 + N2) * F
    L2(J) = I2o * SQR(1 + 39.43 * (X(J) - X(J2o)) ^ 2 * T2(2) ^ 2) / (1 + 39.43 * (X(J) - X(J2o)) ^ 2 * T2(2) ^ 2) + BL2
    LINE -(X(J), L2(J)), 13
    AREA2 = AREA2 + L2(J)
  NEXT J

  LOCATE 22, 15
  INPUT "Display the total spectrum on same screen ? (Y/N) ", C$
  LOCATE 22, 15
  PRINT "                                                  "
  IF C$ = "y" OR C$ = "Y" THEN GOTO 110
  CLS 1
  GOSUB DISPLAY
  VIEW PRINT 19 TO 25

110
  PSET (0, 0)
  FOR J = 1 TO (N1 + N2) * F
    L3(J) = L1(J) + L2(J)
    LINE -(X(J), L3(J)), 8
  NEXT J

  TOTALAREA = AREA1 + AREA2

  LOCATE 22, 10
  PRINT "Area1 ("; VGU$; FU$; ") = "; INT(AREA1)
  LOCATE 22, 43
  PRINT "Area2 ("; VGU$; FU$; ") = "; INT(AREA2)
  LOCATE 23, 29
  PRINT "Total area ("; VGU$; FU$; ") = "; INT(TOTALAREA)
  LOCATE 24, 25
  LINE INPUT "Another line simulstion? (Y/N) "; Y$
  IF Y$ = "y" OR Y$ = "Y" THEN GOTO 100
  CLS 2
RETURN

THREELORENTZ:
200
  CLS 0
  GOSUB DISPLAY
  VIEW PRINT 19 TO 25
  LOCATE 19, 10
  PRINT "Lorentz: I(V) = Io*(T2) / [1+(2*3.14)^2*(V-Vo)^2*(T2)^2] + BL"

  LOCATE 20, 5: INPUT "I1o value :", I1o
```

```
LOCATE 20, 25: INPUT "V1o value :", V1o
LOCATE 20, 45: INPUT "T2(1) value :", T2(1)
LOCATE 20, 65: INPUT "BL1 value :", BL1

LOCATE 21, 5: INPUT "I2o value :", I2o
LOCATE 21, 25: INPUT "V2o value :", V2o
LOCATE 21, 45: INPUT "T2(2) value :", T2(2)
LOCATE 21, 65: INPUT "BL2 value :", BL2

LOCATE 22, 5: INPUT "I3o value :", I3o
LOCATE 22, 25: INPUT "V3o value :", V3o
LOCATE 22, 45: INPUT "T2(3) value :", T2(3)
LOCATE 22, 65: INPUT "BL3 value :", BL3
CLS 2

LOCATE 19, 10
PRINT "Simulation: I(V) = Io / [1+(2*3.14)^2*(V-Vo)^2*(T2)^2] + BL"
PRINT , "I1o="; I1o, "V1o="; V1o, "T2(1)="; T2(1), "BL1="; BL1
PRINT , "I2o="; I2o, "V2o="; V2o, "T2(2)="; T2(2), "BL2="; BL2
PRINT , "I3o="; I3o, "V3o="; V3o, "T2(3)="; T2(3), "BL3="; BL3
J1o = V1o * (N1 + N2) / (DIV * FPD)
J2o = V2o * (N1 + N2) / (DIV * FPD)
J3o = V3o * (N1 + N2) / (DIV * FPD)

PSET (0, 0)
AREA1 = 0
FOR J = 1 TO (N1 + N2) * F
  L1(J) = I1o * SQR(1 + 39.43 * (X(J) - X(J1o)) ^ 2 * T2(1) ^ 2) / (1 + 39.43 * (X(J) - X(J1o)) ^ 2 * T2(1) ^ 2) + BL1
  LINE -(X(J), L1(J)), 9
  AREA1 = AREA1 + L1(J)
NEXT J

PSET (0, 0)
AREA2 = 0
FOR J = 1 TO (N1 + N2) * F
  L2(J) = I2o * SQR(1 + 39.43 * (X(J) - X(J2o)) ^ 2 * T2(2) ^ 2) / (1 + 39.43 * (X(J) - X(J2o)) ^ 2 * T2(2) ^ 2) + BL2
  LINE -(X(J), L2(J)), 13
  AREA2 = AREA2 + L2(J)
NEXT J

PSET (0, 0)
AREA3 = 0
FOR J = 1 TO (N1 + N2) * F
  L3(J) = I3o * SQR(1 + 39.43 * (X(J) - X(J3o)) ^ 2 * T2(3) ^ 2) / (1 + 39.43 * (X(J) - X(J3o)) ^ 2 * T2(3) ^ 2) + BL3
  LINE -(X(J), L3(J)), 8
  AREA3 = AREA3 + L3(J)
NEXT J

LOCATE 23, 15
INPUT "Display the total spectrum on same screen ? (Y/N) ", C$
LOCATE 23, 15
PRINT "                                                    "
IF C$ = "y" OR C$ = "Y" THEN GOTO 210
CLS 1
GOSUB DISPLAY
VIEW PRINT 19 TO 25

210
  PSET (0, 0)
  FOR J = 1 TO (N1 + N2) * F
    LT(J) = L1(J) + L2(J) + L3(J)
    LINE -(X(J), LT(J)), 1
  NEXT J

  TOTALAREA = AREA1 + AREA2 + AREA3
```

```
  LOCATE 23, 10
  PRINT "A1 ="; INT(AREA1)
  LOCATE 23, 25
  PRINT "A2 ="; INT(AREA2)
  LOCATE 23, 40
  PRINT "A3 ="; INT(AREA3)
  LOCATE 23, 60
  PRINT "Total ="; INT(TOTALAREA)
  LOCATE 24, 25
  LINE INPUT "Another line simulstion? (Y/N) "; Y$
  IF Y$ = "y" OR Y$ = "Y" THEN GOTO 200
  CLS 2
RETURN

TWOGAUSS:
300
  CLS 0
  GOSUB DISPLAY
  VIEW PRINT 19 TO 25
  LOCATE 19, 10
  PRINT "Gauss: I(V) = Io*(T2)*EXP[-(1/2)*(2*3.14)^2*(V-Vo)^2*(T2)^2] +BL"

  LOCATE 20, 10: INPUT "Input I1o value :", I1o
  LOCATE 20, 40: INPUT "Input V1o value :", V1o
  LOCATE 21, 10: INPUT "Input T2(1) value :", T2(1)
  LOCATE 21, 40: INPUT "Input BL1 value :", BL1

  LOCATE 22, 10: INPUT "Input I2o value :", I2o
  LOCATE 22, 40: INPUT "Input V2o value :", V2o
  LOCATE 23, 10: INPUT "Input T2(2) value :", T2(2)
  LOCATE 23, 40: INPUT "Input BL2 value :", BL2
  CLS 2

  LOCATE 19, 10
  PRINT "Simulation: I(V) = Io*EXP[-(1/2)*(2*3.14)^2*(V-Vo)^2*(T2)^2] +BL"
  PRINT , "I1o="; I1o, "V1o="; V1o, "T2(1)="; T2(1), "BL1="; BL1
  PRINT , "I2o="; I2o, "V2o="; V2o, "T2(2)="; T2(2), "BL2="; BL2
  J1o = V1o * (N1 + N2) / (DIV * FPD)
  J2o = V2o * (N1 + N2) / (DIV * FPD)

  PSET (0, 0)
  AREA1 = 0
  FOR J = 1 TO (N1 + N2) * F
    G1(J) = I1o * EXP(-19.72 * (X(J) - X(J1o)) ^ 2 * T2(1) ^ 2) + BL1
    LINE -(X(J), G1(J)), 9
    AREA1 = AREA1 + G1(J)
  NEXT J

  PSET (0, 0)
  AREA2 = 0
  FOR J = 1 TO (N1 + N2) * F
    G2(J) = I2o * EXP(-19.72 * (X(J) - X(J2o)) ^ 2 * T2(2) ^ 2) + BL2
    LINE -(X(J), G2(J)), 13
    AREA2 = AREA2 + G2(J)
  NEXT J

  LOCATE 22, 15
  INPUT "Display the total spectrum on same screen ? (Y/N) ", C$
  LOCATE 22, 15
  PRINT "                                                    "
  IF C$ = "y" OR C$ = "Y" THEN GOTO 310
  CLS 1
  GOSUB DISPLAY
  VIEW PRINT 19 TO 25
```

```
310
  PSET (0, 0)
  FOR J = 1 TO (N1 + N2) * F
    G3(J) = G1(J) + G2(J)
    LINE -(X(J), G3(J)), 8
  NEXT J

  TOTALAREA = AREA1 + AREA2

  LOCATE 22, 10
  PRINT "Area1 ("; VGU$; FU$; ") = "; INT(AREA1)
  LOCATE 22, 43
  PRINT "Area2 ("; VGU$; FU$; ") = "; INT(AREA2)
  LOCATE 23, 29
  PRINT "Total area ("; VGU$; FU$; ") = "; INT(TOTALAREA)
  LOCATE 24, 25
  LINE INPUT "Another line simulstion? (Y/N) "; Y$
  IF Y$ = "y" OR Y$ = "Y" THEN GOTO 300
  CLS 2
RETURN

THREEGAUSS:
400
  CLS 0
  GOSUB DISPLAY
  VIEW PRINT 19 TO 25
  LOCATE 19, 10
  PRINT "Gauss: I(V) = Io*(T2)*EXP[-(1/2)*(2*3.14)^2*(V-Vo)^2*(T2)^2] +BL"

  LOCATE 20, 5: INPUT "I1o value :", I1o
  LOCATE 20, 25: INPUT "V1o value :", V1o
  LOCATE 20, 45: INPUT "T2(1) value :", T2(1)
  LOCATE 20, 65: INPUT "BL1 value :", BL1

  LOCATE 21, 5: INPUT "I2o value :", I2o
  LOCATE 21, 25: INPUT "V2o value :", V2o
  LOCATE 21, 45: INPUT "T2(2) value :", T2(2)
  LOCATE 21, 65: INPUT "BL2 value :", BL2

  LOCATE 22, 5: INPUT "I3o value :", I3o
  LOCATE 22, 25: INPUT "V3o value :", V3o
  LOCATE 22, 45: INPUT "T2(3) value :", T2(3)
  LOCATE 22, 65: INPUT "BL3 value :", BL3
  CLS 2

  LOCATE 19, 10
  PRINT "Simulation: I(V) = Io / [1+(2*3.14)^2*(V-Vo)^2*(T2)^2] + BL"
  PRINT , "I1o="; I1o, "V1o="; V1o, "T2(1)="; T2(1), "BL1="; BL1
  PRINT , "I2o="; I2o, "V2o="; V2o, "T2(2)="; T2(2), "BL2="; BL2
  PRINT , "I3o="; I3o, "V3o="; V3o, "T2(3)="; T2(3), "BL3="; BL3
  J1o = V1o * (N1 + N2) / (DIV * FPD)
  J2o = V2o * (N1 + N2) / (DIV * FPD)
  J3o = V3o * (N1 + N2) / (DIV * FPD)

  PSET (0, 0)
  AREA1 = 0
  FOR J = 1 TO (N1 + N2) * F
    G1(J) = I1o * EXP(-19.72 * (X(J) - X(J1o)) ^ 2 * T2(1) ^ 2) + BL1
    LINE -(X(J), G1(J)), 9
    AREA1 = AREA1 + G1(J)
  NEXT J

  PSET (0, 0)
  AREA2 = 0
  FOR J = 1 TO (N1 + N2) * F
```

```
    G2(J) = I2o * EXP(-19.72 * (X(J) - X(J2o)) ^ 2 * T2(2) ^ 2) + BL2
    LINE -(X(J), G2(J)), 13
    AREA2 = AREA2 + G2(J)
  NEXT J

  PSET (0, 0)
  AREA3 = 0
  FOR J = 1 TO (N1 + N2) * F
    G3(J) = I3o * EXP(-19.72 * (X(J) - X(J3o)) ^ 2 * T2(3) ^ 2) + BL3
    LINE -(X(J), G3(J)), 8
    AREA3 = AREA3 + G3(J)
  NEXT J

  LOCATE 23, 15
  INPUT "Display the total spectrum on same screen ? (Y/N) ", C$
  LOCATE 23, 15
  PRINT "                                                    "
  IF C$ = "y" OR C$ = "Y" THEN GOTO 410
  CLS 1
  GOSUB DISPLAY
  VIEW PRINT 19 TO 25

410
  PSET (0, 0)
  FOR J = 1 TO (N1 + N2) * F
    LT(J) = L1(J) + L2(J) + L3(J)
    LINE -(X(J), LT(J)), 1
  NEXT J

  TOTALAREA = AREA1 + AREA2 + AREA3

  LOCATE 23, 10
  PRINT "A1 ="; INT(AREA1)
  LOCATE 23, 25
  PRINT "A2 ="; INT(AREA2)
  LOCATE 23, 40
  PRINT "A3 ="; INT(AREA3)
  LOCATE 23, 60
  PRINT "Total ="; INT(TOTALAREA)
  LOCATE 24, 25
  LINE INPUT "Another line simulstion? (Y/N) "; Y$
  IF Y$ = "y" OR Y$ = "Y" THEN GOTO 400
  CLS 2
RETURN

MULTIPLE:
500
  CLS 0
  GOSUB DISPLAY
  VIEW PRINT 19 TO 25

  LOCATE 19, 5: INPUT "L1o :", L1o
  LOCATE 19, 25: INPUT "V1o :", V1o
  LOCATE 19, 45: INPUT "T2(1) :", T2(1)
  LOCATE 19, 65: INPUT "BL1 :", BL1

  LOCATE 20, 5: INPUT "L2o :", L2o
  LOCATE 20, 25: INPUT "V2o :", V2o
  LOCATE 20, 45: INPUT "T2(2) :", T2(2)
  LOCATE 20, 65: INPUT "BL2 :", BL2

  LOCATE 21, 5: INPUT "G1o :", G1o
  LOCATE 21, 25: INPUT "V3o :", V3o
  LOCATE 21, 45: INPUT "T2(3) :", T2(3)
  LOCATE 21, 65: INPUT "BL3 :", BL3
```

```
LOCATE 22, 5: INPUT "G2o :", G2o
LOCATE 22, 25: INPUT "V4o :", V4o
LOCATE 22, 45: INPUT "T2(4) :", T2(4)
LOCATE 22, 65: INPUT "BL4 :", BL4

CLS 2

PRINT , "L1o="; L1o, "V1o="; V1o, "T2(1)="; T2(1), "BL1="; BL1
PRINT , "L2o="; L2o, "V2o="; V2o, "T2(2)="; T2(2), "BL2="; BL2
PRINT , "G1o="; G1o, "V3o="; V1o, "T2(3)="; T2(3), "BL3="; BL3
PRINT , "G2o="; G2o, "V4o="; V2o, "T2(4)="; T2(4), "BL4="; BL4
J1o = V1o * (N1 + N2) / (DIV * FPD)
J2o = V2o * (N1 + N2) / (DIV * FPD)
J3o = V3o * (N1 + N2) / (DIV * FPD)
J4o = V4o * (N1 + N2) / (DIV * FPD)

PSET (0, 0)
AREA1 = 0
FOR J = 1 TO (N1 + N2) * F
  L1(J) = L1o * SQR(1 + 39.43 * (X(J) - X(J1o)) ^ 2 * T2(1) ^ 2) / (1 + 39.43 * (X(J) - X(J1o)) ^ 2 * T2(1) ^ 2) + BL1
  LINE -(X(J), L1(J)), 9
  AREA1 = AREA1 + L1(J)
NEXT J

PSET (0, 0)
AREA2 = 0
FOR J = 1 TO (N1 + N2) * F
  L2(J) = L2o * SQR(1 + 39.43 * (X(J) - X(J2o)) ^ 2 * T2(2) ^ 2) / (1 + 39.43 * (X(J) - X(J2o)) ^ 2 * T2(2) ^ 2) + BL2
  LINE -(X(J), L2(J)), 13
  AREA2 = AREA2 + L2(J)
NEXT J

PSET (0, 0)
AREA3 = 0
FOR J = 1 TO (N1 + N2) * F
  G1(J) = G1o * EXP(-19.72 * (X(J) - X(J3o)) ^ 2 * T2(3) ^ 2) + BL3
  LINE -(X(J), G1(J)), 9
  AREA3 = AREA3 + G1(J)
NEXT J

PSET (0, 0)
AREA4 = 0
FOR J = 1 TO (N1 + N2) * F
  G2(J) = G2o * EXP(-19.72 * (X(J) - X(J4o)) ^ 2 * T2(4) ^ 2) + BL4
  LINE -(X(J), G2(J)), 13
  AREA4 = AREA4 + G2(J)
NEXT J

LOCATE 23, 15
INPUT "Display the total spectrum on same screen ? (Y/N) ", C$
LOCATE 23, 15
PRINT "                                                    "
IF C$ = "y" OR C$ = "Y" THEN GOTO 510
CLS 1
GOSUB DISPLAY
VIEW PRINT 19 TO 25

510
  PSET (0, 0)
  FOR J = 1 TO (N1 + N2) * F
    L3(J) = L1(J) + L2(J) + G1(J) + G2(J)
    LINE -(X(J), L3(J)), 1
  NEXT J
```

```
  TOTALAREA = AREA1 + AREA2 + AREA3 + AREA4

  LOCATE 23, 5
  PRINT "A1="; INT(AREA1)
  LOCATE 23, 19
  PRINT "A2="; INT(AREA2)
  LOCATE 23, 33
  PRINT "A3="; INT(AREA3)
  LOCATE 23, 47
  PRINT "A4="; INT(AREA4)
  LOCATE 23, 61
  PRINT "Total A="; INT(TOTALAREA)
  LOCATE 24, 25
  LINE INPUT "Another line simulstion? (Y/N) "; Y$
  IF Y$ = "y" OR Y$ = "Y" THEN GOTO 500
  CLS 2
RETURN

NEWFILE:
  RUN 5
  'CLOSE
  'ERASE A$, X, Y, LVG, GV, L1, L2, L3, LT, G1, G2, G3, GT, T
  'KILL "FIRST": KILL "SECOND": KILL "DATA.PAR"
RETURN

QUIT:
  CLOSE
  ERASE A$, X, Y, LVG, GV, L1, L2, L3, LT, G1, G2, G3, GT, T
  KILL "FIRST": KILL "SECOND": KILL "DATA.PAR"
  END
RETURN

HANDLER:
BEEP
RESUME

SUB MARKS (FS, VS)
FOR I = 1 TO 9
LINE (0, I * VS / 10)-(FS / 100, I * VS / 10), 1      'LEFT
LINE (FS, I * VS / 10)-(FS - FS / 100, I * VS / 10), 1 'RIGHT
LINE (I * FS / 10, 0)-(I * FS / 10, VS / 50), 1       'BOTTOM
LINE (I * FS / 10, VS)-(I * FS / 10, VS - VS / 50), 1  'TOP
NEXT I
END SUB

SUB MENU
  VIEW PRINT 19 TO 25
  CLS 2
  LOCATE 19, 30
  PRINT "*** MAIN MENU ***"
  LOCATE 21, 10
  PRINT "F1--SCALE            F2--CURSOR            F3--2 LORENTZ"
  LOCATE 22, 10
  PRINT "F4--3 LORENTZ        F5--2 GAUSS           F6--3 GAUSS"
  LOCATE 23, 10
  PRINT "F7--MULTIPLE (2L+2G)   F8--NEWFILE         F9--QUIT"
  DO WHILE INKEY$ = ""
  LOOP
END SUB
```

References:

1. Microelectronic Polymers Ed. M.S. Htoo, Marcel Dekker, Inc., New York (1989)
2. S.D. Sentyria, ACS Symposium Series 346, (1986), Ch. 36.
3. A. Endo, M.Takada, K. Adachi, H. Takasago, T. Yada, and Y. Onishi, J. Electrochem. Soc. : Solid State Sci. & Tech., **134**, 2522 (1987)
4. D. S. Soane and Z. Martynenko, Polymers in Microelectronics, Elsevier, New York (1989)
5. C.E. Sroog, J Polymer Sci.: Macromolecular Reviews, **11**, 161 (1976)
6. G. Conte, L. D'ilario, and N. V. Pavel, J. Polym. Sci.: Polyme.Phys. **14**, 1553 (1976)
7. L.G. Lazaryan, D.Y. Tsvankin, B.M.Ginzburg, S. Tuichiev, L.N. Korzhavin, and S.Y. Frenkel, Vysokomol. Soyed. (A) **14**, 1194 (1972)
8. Y.P. Krasnov, A.Y. Sepanyan, Y.I. Mitchenko, Y.A. Tolkachev and N.V. Lukasheva, Vysokomol. Soyed. (A) **19**, 1566 (1977)
9. K.H. Gardner, J.R. Edman, J.E. Freida, S.C. Freilich and L.E. Manring, " Structure and morphology of PMDA-ODA films"
10. S. Isoda, H. Shimada, M. Kochi, and H. Kambe, J. Polym. Sci.: Polym. Phys. **19**, 1293 (1981)
11. N. Takahashi, D.Y. Yoon, and W. Parrish, Macromolecules, **17**, 2583 (1984)
12. M. Kochi, H. Shimada, and H. Kambe, J. Polym. Sci.: Polym. Phys. **22**, 1979 (1984)
13. T.P. Russell and H.R. Brown, J. Polym. Sci.: Polym. Phys. **25**, 1129 (1987)

14. T.P. Russell, H. Gugger, and J.D. Swalen, J. Polym. Sci.: Polym. Phys. 21, 1745 (1983)

15. R. DeIasi and J. Russel, J. Appl. Polym. Sci., 15, 2965 (1971)

16. K. Okamoto, K. Tanaka, O. Yokoshi, and H. Kita, J. Polym. Sci.: Polym. Phys. 27, 643 (1989)

17. E. Sacher and D.G. Sedor, J. Polym. Sci.: Polym. Phys. 12, 626 (1974)

18. E. Sacher, IEEE Trans Electr. Insul, EI-13 No 2, 94 (1978)

19. T.P. Russell, J. Polym. Sci.: Polym. Phys. 22, 1105 (1984)

20. T.P. Russell, Polym. Eng. & Sci. 24, No 5, 345 (1984)

21. J.F. Romanelli, J. M. Mayer, and E.J. Kramer, J. Polym. Sci.: Polym. Phys. 24, 263 (1986)

22. W.H. Hubbell, Jr., and Z.A. Munir, J. Polym. Sci.: Polym. Phys. 13, 493 (1975)

23. E. Sacher and J.R. Susko, J. Appl. Polym. Sci., 23, 2355 (1979)

24. E. Sacher and J.R. Susko, J. Appl. Polym. Sci., 26, 679 (1981)

25. D.D. Denton, J.B. Camou, and S.D. Senturia, ISA Conf. on Moisture and Humidity, 505 (1985)

26. D.K. Yang, W.J. Kores, and V.T. Stannett, J. Appl. Polym. Sci., 30, 1035 (1985)

27. D.K. Yang, W.J. Koros, and H.B. Hopfenberg, J. Appl. Polym. Sci., 31, 1619 (1986)

28. L. Iler, W.. Koros, K.D. Yang, and R. Yui, Polyimide, 1, ed. K.L. Mittal, Plenum Press, New York (1984), pp.443

29. N.G. McCrum, B.E. Read, and G. Williams, Anelastoc and Dielectric Effect in Polymeric Solid, John Wiley & Sons. New York (1967)

30. G. Willams, Polymer Science (Review) **59**, (1979)

31. A.R. Blythe, Electrical Properties of Polymers Cambridge University Press, Cambridge (1979)

32. L.E. Amborski, Ind. Eng. Chem., **2**, 189 (1963)

33. W.J. Wrasidlo, J. Macromol. Sci. -- Phys., B, **3**, 559 (1972)

34. W.J. Wrasidlo, J. Polym. Sci.: Polym. Phys., **11**, 2143 (1973)

35. D. Yang, J. Melcher, and G. Arlt, International Conf. on Properties & Applications of Dielectric Materials, 1985, **1**, pp. 434

36. J. Melcher, D. Yang, and G.Arlt, IEEE Trans. Electr. Insul., **24**, 31 (1989)

37. G. Xu, C.C. Grety, A.S. Nowick, S.Z. Li, Y.S. Pak, and S.G. Greenbaum, J. Appl. Phys., **66**, 5290 (1989)

38. F.Bloch, W.W. Hansen, and M. Pachard, Phys. Rev., **69**, 127 (1946)

39. E.M. Purcell, H.C. Torrey, and R.V. Pound, Phys. Rev., **69**, 37 (1946)

40. Ian C.P. Smith, NMR of Newly Accessible Nuclei, Vol. 2, Ed. P. Laszlo, Academic Press, New York (1983), Ch.1

41. H.W. Spiess, Advances in Polymer Science, Vol **66**, Springer-Verlag, Berlin Heidelberg, (1985)

42. Lynn W. Jelinski, High-Resolution NMR Spectroscopy of Synthetic Polymers in Bulk, Ed. Komoroski, VCH Publisher, New York (1986), Ch.10

43. H.J.C. Berendsen, J. Chem. Phys. **36**, 3297 (1962)

44. H.J.C. Berendsen and C. Migchelsen, Ann. N.Y. Acad. Sci., **125**, 365 (1965)

45. C. Migchelsen and H.J.C. Berendsen, J. Chem. Phys. **59**, 296 (1973)

46. R.E. Dehl, J. Chem. Phys. **48**, 831 (1968)

47. G. Chapman and K.A. Mclauchlan, Nature, 215, 391 (1967)

48. G.E. Chapman and K.A. Mclauchlan, Proc. Roy. Soc. B. 173, 223, (1969)

49. R.E. Dehl and C.A. Hoeve, J. Chem. Phys. 50, 3245 (1969)

50. B.M. Fung and M.M. Siegel, Biochem. Biophys. Acta. 278, 185 (1972)

51. B.M. Fung, J. Witschel. Jr., and L.L. McAmis, Boipolymers, 13, 1767 (1974)

52. T.C. Wong and T.T. Ang, J. Phys. Chem. 89, 4047 (1985)

53. S. Krishnamaurthy, D. McIntyre, E.R. Santee, Jr., and C.W. Wilson, J. Polym. Sci.: Polym. Phys. 11, 427 (1973)

54. M. Shporer and A.J. Vega, J. Polym. Sic.: Polym. Phys. 12, 645, (1974)

55. K. Matsumura, K. Hayamizu, T. Nakane, H. Yanagishita, and O. Yamamoto, J. Polym. Sci.: Polym. Phys. 25, 2149 (1987)

56. K. Matsumura, K. Hayamizu, T. Nakane, H. Yanagishita, and O. Yamamoto, J. Polym. Sci.: Polym. Phys. 26, 2215 (1988)

57. K. Matsumura, K. Hayamizu, and O. Yamamoto, J. Polym. Phys.: Polym. Phys. 27, 2407 (1989)

58. C.P. Slichter, Principles of Magnetic Resonance, 3rd Ed. Springer-Verlag, New York (1990)

59. M.L. Martin, G.J. Martin, and J.J. Delpuech, Practical NMR Spectroscopy, Heyden (1980)

60. B.C. Gerstein and C.R. Dybowski, Transient Techniques in NMR of Solid, Academic Press, Inc. New York (1985)

61. R.R. Ernst, G. Bodenhausen, and A Wokaun, Principles of Nuclear Magnetic Resonance in One and Two Dimensions, Clarendon Press, Oxford (1987)

62. A. Abragam, The Principles of Nuclear Magnetism, Clarendon Press, Oxford (1961)

63. A.D. Buckingham and K.A. McLauchlan, Progress in Nuclear Magnetic Resonance Spectroscopy, 12, Pergamon Press, New York (1967)

64. B. Halle and H. Wennerstrom, J. Chem. Phys. 75, 1928 (1981)

65. G.E. Pake, J. Chem. Phys. 16, 327 (1948)

66. H.S. Gutowsky and G.E. Pake, J. Chem. Phys. 18, 162 (1950)

67. R.T. Boere and R.G. Kidd Annual Reports on NMR Spectroscopy Ed. G.A. Webb Vol 13, Academic Press, New York (1982)

68. F.A. Bovey, Nuclear Magnetic Resonance Spectroscopy, 2nd Ed. Academic Press, Inc. New York (1988)

69. C.P. Poole, Jr. and H.A. Farach, Relaxation in Magnetic Resonance, Academic Press, Inc. New York (1971)

70. R.L. Vold, J.S. Waugh, M.P. Klein, and D.E. Phelps, J. Chem. Phys., 48, 3831 (1968)

71. E. Fukushima and S.B.W. Roeder Experimental Pulse NMR; A Nut and Bolts Approach Addison-Wesley Publishing Company (1981)

72. J.C. Hindman, A. Svirmickas, and M. Wood, J. Chem. Phys. 59, 1517 (1973)

73. J.C. Hindman, A.J. Zielen, A. Svirmickas, and M. Wood, J. Chem. Phys. 54, 621 (1971)

74. D.E. O'Reilly and E.M. Peterson, J. Chem. Phys. 55, 2155 (1971)

75. J.C. Hindman, A. Svirmickas, and M. Wood, J. Chem. Phys. 74, 1266 (1970)

76. J.C. Gore, M.S. Brown, J. Zhong, and I.M. Armitage, J. Magnetic. Resonance.

83, 246 (1989)

77. J.C. Hindman, A. Svirmickas, and M. Wood, J. Chem. Phys. 72, 4188 (1968)

78. B.Halle and H. Wennerstrom, J. Chem. Phys. 75, 1928 (1981)

79. C.R. Moylan, M.E. Best, and M.Ree, J. Polym. Sci.: Polym. Phys. 29, 87, (1991)

80. S.Z. Li, Y.S. Pak, K. Adamic and S.G. Greenbaum, B.S. Lim, G. Xu, and A.S. Nowick, to be published in J. Electrochemical Society.